MICROWAVE PROBE INVESTIGATION OF THE PULSED GLOW DISCHARGE

by

Colin W. Davidson

Thesis submitted for the degree of
Doctor of Philosophy
at the University of Edinburgh, August 1960.

List of Contents

Glossary of Symbols

a	broad waveguide dimension
B	magnetic flux density
b	narrow waveguide dimension
c	speed of light
D_a	ambipolar diffusion constant
E	electric field strength
e	magnitude of the charge of the electron
J	current density
j	$\sqrt{-1}$
k	Boltzmann's constant
M	atomic mass
m	mass of the electron
N	electron concentration (electrons/metre^3)
p	gas pressure (mm.Hg.)
Q_e	collision cross section for electrons
R	radius of discharge tube
T_e	electron temperature (^oK)
T_g	gas temperature (^oK)
t	time
v	velocity
x	distance from waveguide wall
x	distance from cathode (cm.)
y	normalised admittance
z	normalised impedance.
α	recombination coefficient for electrons
$\underset{\sim}{\epsilon_r} = \epsilon_r' - j\epsilon_r''$	relative dielectric constant
ϵ_o	dielectric constant of free space
λ_e	mean free path for electrons

λ_g guide wavelength

λ_o free space wavelength

μ_+ mobility of positive ions

ν collision frequency

$\underset{\sim}{\sigma} = \sigma' - j\sigma''$ complex microwave conductivity

ω angular frequency

Complex quantities and vectors are indicated thus, $\underset{\sim}{\epsilon}_r$ or $\underset{\sim}{E}$

Chapter 1

Introduction

Although the knowledge gained from research in the gas discharge field has formed the foundation for modern physics there are still many problems associated with gas discharges themselves which remain unsolved or are not completely understood. This is not surprising since the physical processes involved are complex and small quantities of impurities may have a marked effect on any results obtained. In addition the investigator has rather a limited number of research tools at his disposal.

Classical probe methods were until recently the most usual means of studying gas discharges. The voltage - current characteristics of metallic probes inserted into certain regions of a gas discharge can yield useful information about its properties (Langmuir and Mott-Smith, 1923). Such probe measurements give reliable results only when the ionisation density is high, as in the negative glow and positive column of a glow discharge, so that the current drawn by the probe has a negligible effect on the discharge. Large errors can be produced by contamination of the probe surface and by plasma oscillations in the discharge. However, according to Loeb (1955a), probe measurements can be expected to yield fairly accurate energy distributions and values of electron temperature, while under some conditions they yield local ion and electron concentrations to within perhaps half an order of magnitude.

Classical probe methods are applicable only to the steady state. Recently, however, Waymouth (1959) has developed a pulsed probe technique which has several advantages. The probe characteristic is obtained in about 10 µsec. so that changes in the discharge parameters occurring in perhaps 100 µsec. could be detected. A further advantage claimed for this particular method is that as the probe is normally maintained at a large negative potential the surface is cleaned by positive ion bombardment and contamination is thus avoided.

The development of modern microwave techniques has provided another powerful method for investigating the properties of ionised gases. Using the theory of the conductivity of ionised media, orginally developed in connection with the ionosphere, Biondi and Brown (1949) and others have developed microwave probe methods for the study of gas discharges. Such methods rely on the measurement of the microwave conductivity due to the free electrons in the gas and can yield no information about the positive ions.

The results obtained from probe measurements can usefully be supplemented by studies of the light intensity and spectroscopic studies of the discharge.

In recent years it has become almost conventional to determine the parameters associated with a gas discharge by measuring the effect of the ionised gas on the properties of a resonant microwave cavity, and most of the work has been concentrated on ionised plasmas produced by high power microwaves. However, microwave probe methods can also be usefully applied to the study of d.c. discharges. In particular the study of the pulsed glow discharge, which might find application in microwave circuits, has previously been rather neglected.

One obvious alternative to the use of a resonant cavity method for measurement of the discharge conductivity would be to mount the discharge tube directly across a section of rectangular waveguide so that it behaves as a dielectric post. This method was used by Prime (1952) to study discharges in mercury vapour and it has been used throughout the investigations described in this thesis. It has the advantage that conventional microwave impedance measuring equipment can be used to determine the discharge admittance and dielectric post theory can then be used to relate this admittance to the various discharge parameters.

The most convenient frequencies for this type of measurement are in the range 3KMc/s → 10KMc/s. (S and X-Band), as these frequencies are in common use and equipment is readily available. S-Band was chosen as being most suitable for the tests to be described in this thesis, as the longer wavelength leads to discharge tubes of reasonable dimensions: in addition the sensitivity of microwave probe measurements is greater in S-Band than in X-Band, and sensitivity is of great importance.

As the dynamic impedance of a glow discharge may be low, or even negative under some conditions, it was decided to feed d.c. discharges of this type from a high impedance source in order to obtain stable operation. Cold cathode discharges were to be studied under transient conditions, so for consistency of timing, the supply to the tubes was designed so that variable amplitude pulses could be superimposed on a small d.c. maintaining current. The variation in electron concentration and collision frequency in the region of the discharge within the waveguide system would then be reflected in a time variation of the position and amplitude of the standing wave pattern in the waveguide. By moving the discharge tube it would be possible to study the axial variation of the discharge parameters and in this way a complete picture of the behaviour of the discharge under transient conditions could be obtained. To simplify the problem of interpreting the results the measurements have been restricted to discharges in helium, which has already been widely studied by microwave methods.

Chapter 2.

Microwave Equipment

2.1. The Microwave System.

A diagram of the microwave system is given in Fig. 2.1.1. It is basically an S-Band microwave bench for the measurement of voltage standing wave ratio (v.s.w.r.), most of the components being in W.G. No.10.

A Heil tube oscillator, similar to the Type 0223 oscillator unit (Wayne Kerr Laboratories Limited), is the source of microwave power. The capacity coupled output probe is connected to an absorption wavemeter (Services Type W1633), while the inductive output probe is coupled to the waveguide system by a coaxial-to-waveguide transformer. A resonant iris has been mounted across the output flange of this transformer to reject any harmonics in the oscillator output.

The precision attenuator is normally set to about 30 dB., giving ample isolation between the oscillator and the rest of the system.

The standing wave indicator, which was supplied by S.E.R.L.,[1] is fabricated from 1/4" brass plate and has a residual standing wave ratio of the order of 0.99. At low microwave power levels the detector should have a square law characteristic (Torrey and Whitmer,

1. Services Electronics Research Laboratory, Baldock, Herts.

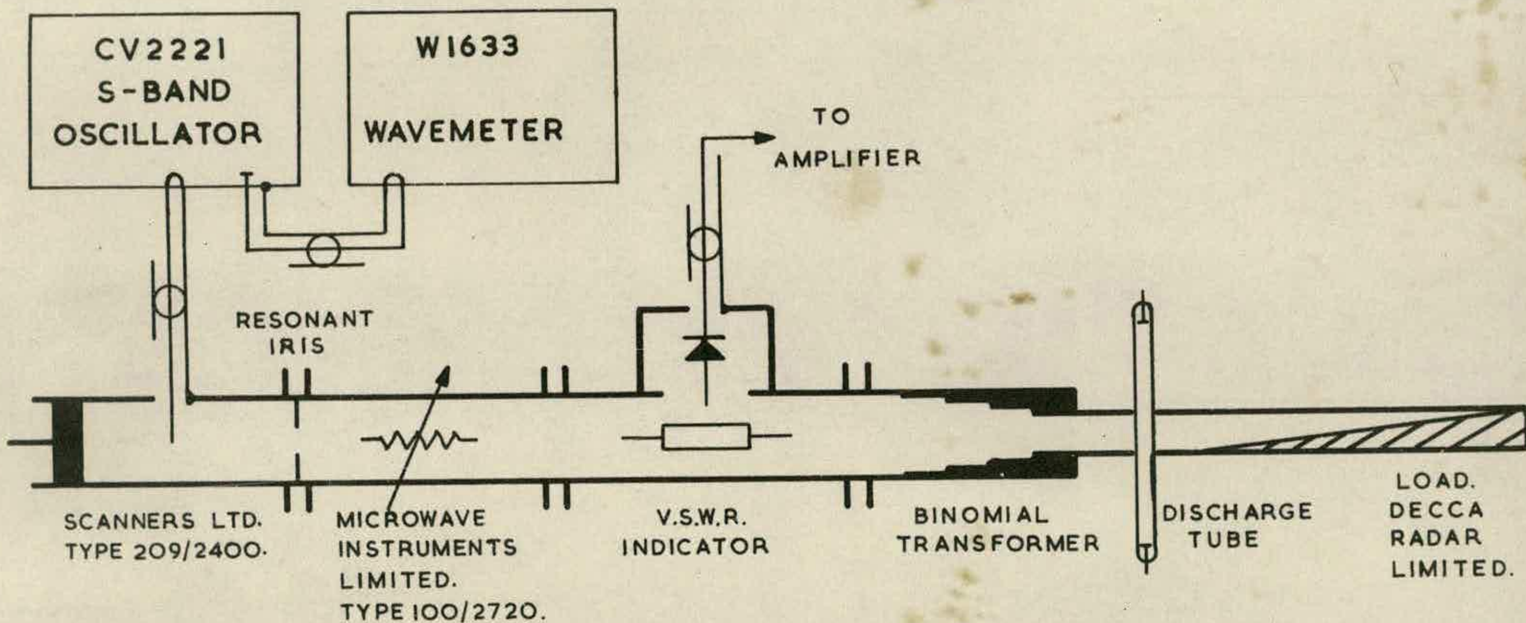

MICROWAVE SYSTEM

FIG. 2.1.1.

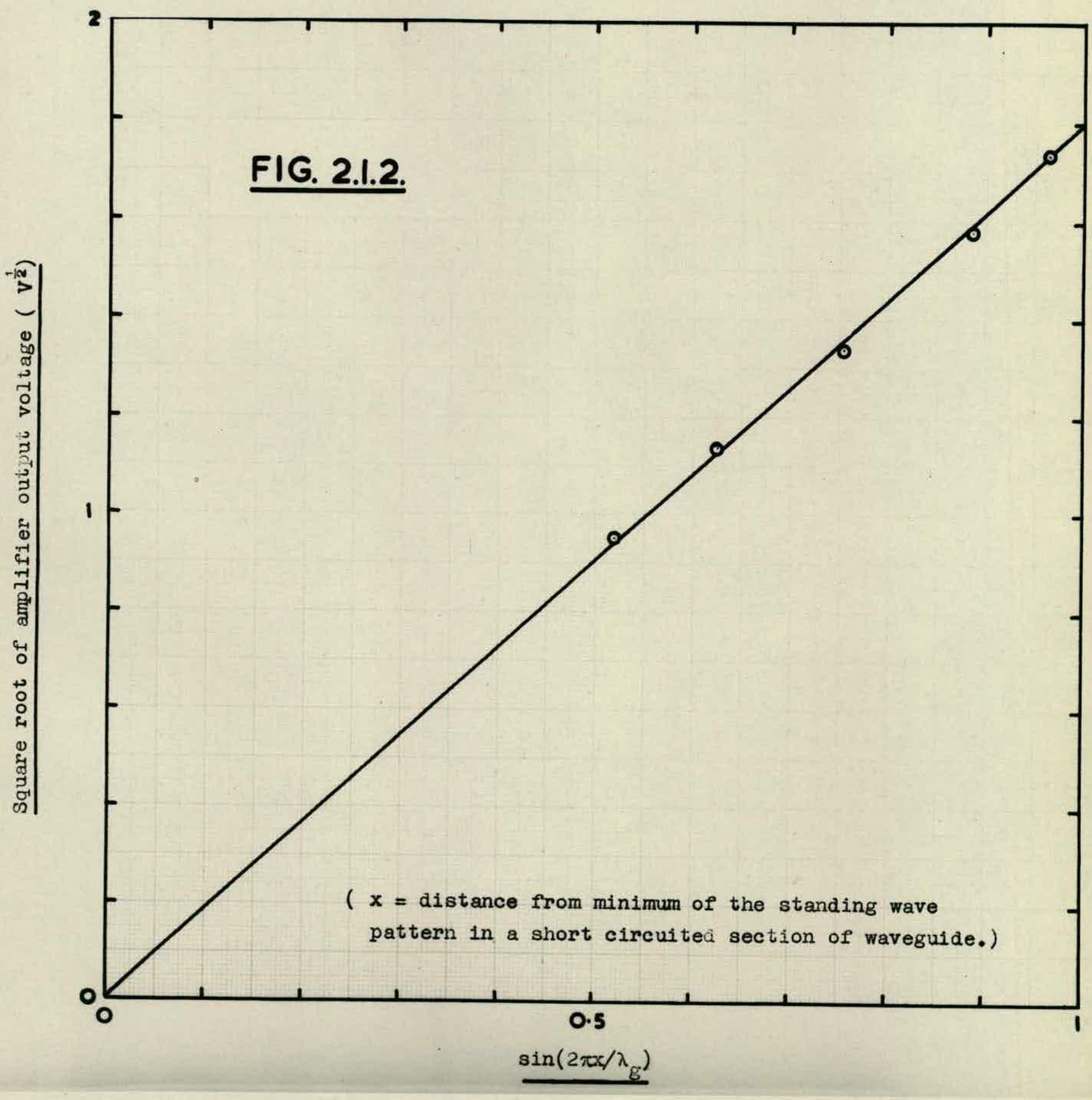
FIG. 2.1.2.
2
1
0
0
0·5
1
Square root of amplifier output voltage ($V^{\frac{1}{2}}$)
$\sin(2\pi x/\lambda_g)$
(x = distance from minimum of the standing wave
pattern in a short circuited section of waveguide.)

1948) and this has been confirmed experimentally (Fig.2.1.2.)

The discharge tube is mounted across a section of guide with a reduced height of 1 cm., in order to improve the axial resolution of the measurements, matching to the standard waveguide dimensions being achieved with the aid of a binomial impedance transformer. The discharge tube section is terminated with a matched wedge.

The waveguide flanges have been carefully aligned to avoid introducing discontinuities in the system and the residual standing wave ratio, measured before the hole for the discharge tube was machined, was approximately 0.98.

2.2. Microwave Oscillator

An S-Band Heil tube cavity oscillator (CV2221) is used as the source of microwave power. For normal operation this tube is used with a power supply designed to give constant mean power input. This was found to be unsuitable for pulse operation and has been replaced by a conventional stabilised supply delivering 220V d.c., which is low enough to ensure that the tube is not over-run for any value of screen grid voltage used. The screen grid voltage itself is held constant by a large capacitor.

The circuit diagram of the oscillator unit is given in Fig. 2.2.1. Provision has been made for

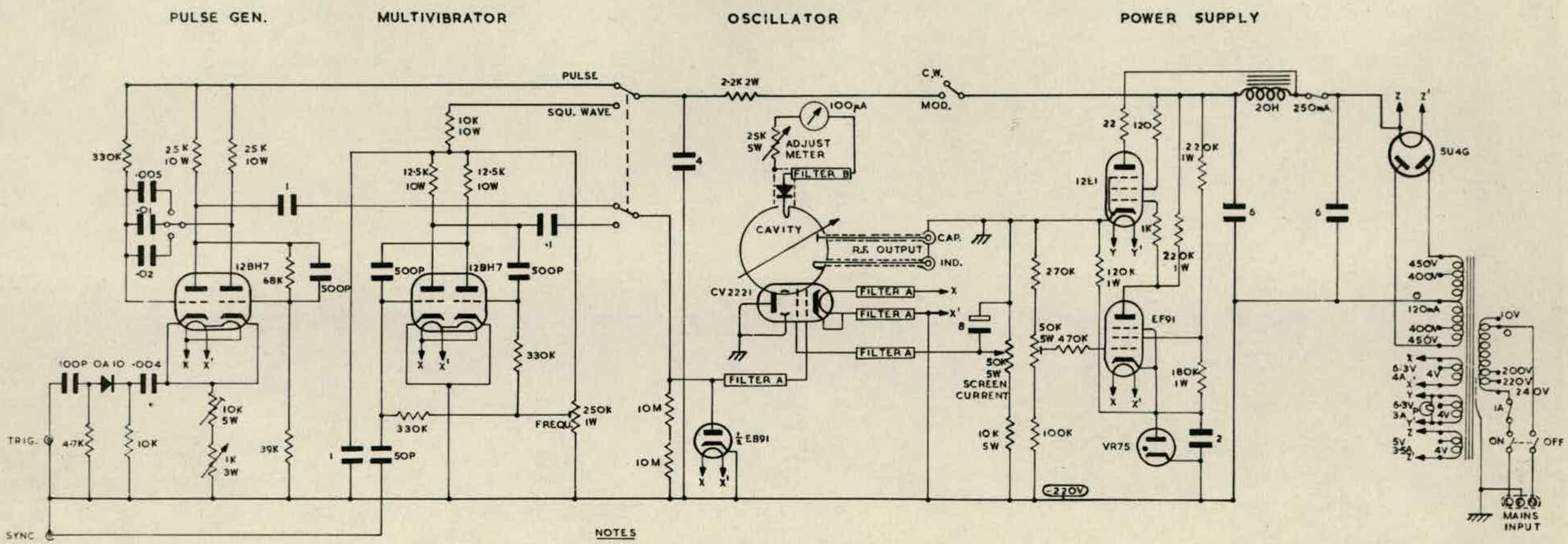

NOTES

1. ALL CAPACITOR VALUES ARE GIVEN IN μF. UNLESS OTHERWISE STATED.
2. ALL RESISTORS ARE ½W UNLESS OTHERWISE STATED.

FIG. 2.2.1.

pulse modulation (1,2 or 4 m.sec) or square wave modulation (3 Kc/s).

Positive pulses of amplitude greater than 20^{0}V are required to give satisfactory pulse operation of the oscillator and a rise time of less than 20 µsec. cannot easily be obtained.

Approximately 450V H.T. is available for the 12BH7 pulse generator which is triggered by the leading edge of the main pulse from the timing unit controlling the equipment (see Section 3.2). The series diode in the triggering circuit prevents spurious pulses being fed back to the triggering line and disturbing the other units connected to it. A diode clamp circuit is used on the oscillator grid so that the valve is normally cut-off and a large time constant is required for the coupling circuit for operation at low pulse repetition frequencies. The cathode resistor of the 12BH7 is variable and this provides a convenient method of adjusting the triggering sensitivity.

The 12BH7 multivibrator can be used to provide square wave modulation so that steady state v.s.w.r. measurements can be made with standard equipment.

2.3. Design of the Waveguide Transformer

The axial resolution which can be obtained when the discharge tube is mounted as a dielectric post in the waveguide is limited by the narrow waveguide dimension. For W.G. No.10 this is of the order of 3.5 cm. Since the negative glow region of a discharge in helium may have a similar length a considerable reduction in the narrow waveguide dimension is desirable. On the other hand, if the waveguide was too narrow there would be considerable microwave power loss along the axis of the discharge tube. As a compromise the narrow waveguide dimension has been reduced to 1 cm.

Some form of impedance matching is necessary between the narrow discharge tube section and the standard waveguide equipment. A simple quarter-wavelength matching section could be used, but this would have a very limited bandwidth. A better solution to this problem is the use of a multiple quarter-wavelength transformer of the binomial type (Southworth, 1950), which has a much greater bandwidth. In this design the reflection coefficients at the various transitions are made proportional to the coefficients of the binomial expansion $(1 + x)^{n-1}$, where n is the total number of transitions. The lumped admittances appearing at the transitions are negligible and as the waveguide impedance is directly proportional to the narrow dimension the appropriate dimensions can be readily calculated.

Although the binomial transformer is widely used it can be shown that a Chebyshev design would give a further bandwidth improvement (Levy, 1959).

In some preliminary experiments the transformer shown in Fig. 2.3.1. was used. It consists of a copper insert mounted in a section of No.10 waveguide with a 1:2:1: binomial transition to W.G. No. 10 at each end of the narrow discharge tube section. This transformer was checked for residual v.s.w.r. before machining the hole for the discharge tube and it was found to be ~ 0.97. However, this might have been due to partial cancellation of reflections from the two transitions. Because of this fact, and also the unbalanced nature of the transformer, a single symmetrical 1:3:3:1 transition was made and a special matched load used to terminate the discharge tube section, thus avoiding the second transition to W.G. No.10 (Figures 2.3.2. and 2.3.3.).

The transformer and discharge tube section were fabricated from 1/4" brass plate and silver plated after assembly. The matched load (Decca Radar Limited) takes the form of a tapered wedge of loaded resin and gives a v.s.w.r. ~ 0.99. The residual v.s.w.r. of this transformer was ~ 0.98 at 3000 Mc/s.

In order to simplify impedance measurements the discharge tube is mounted $3\lambda g/2$ from the flange at the normal operating frequency (3000 Mc/s.)

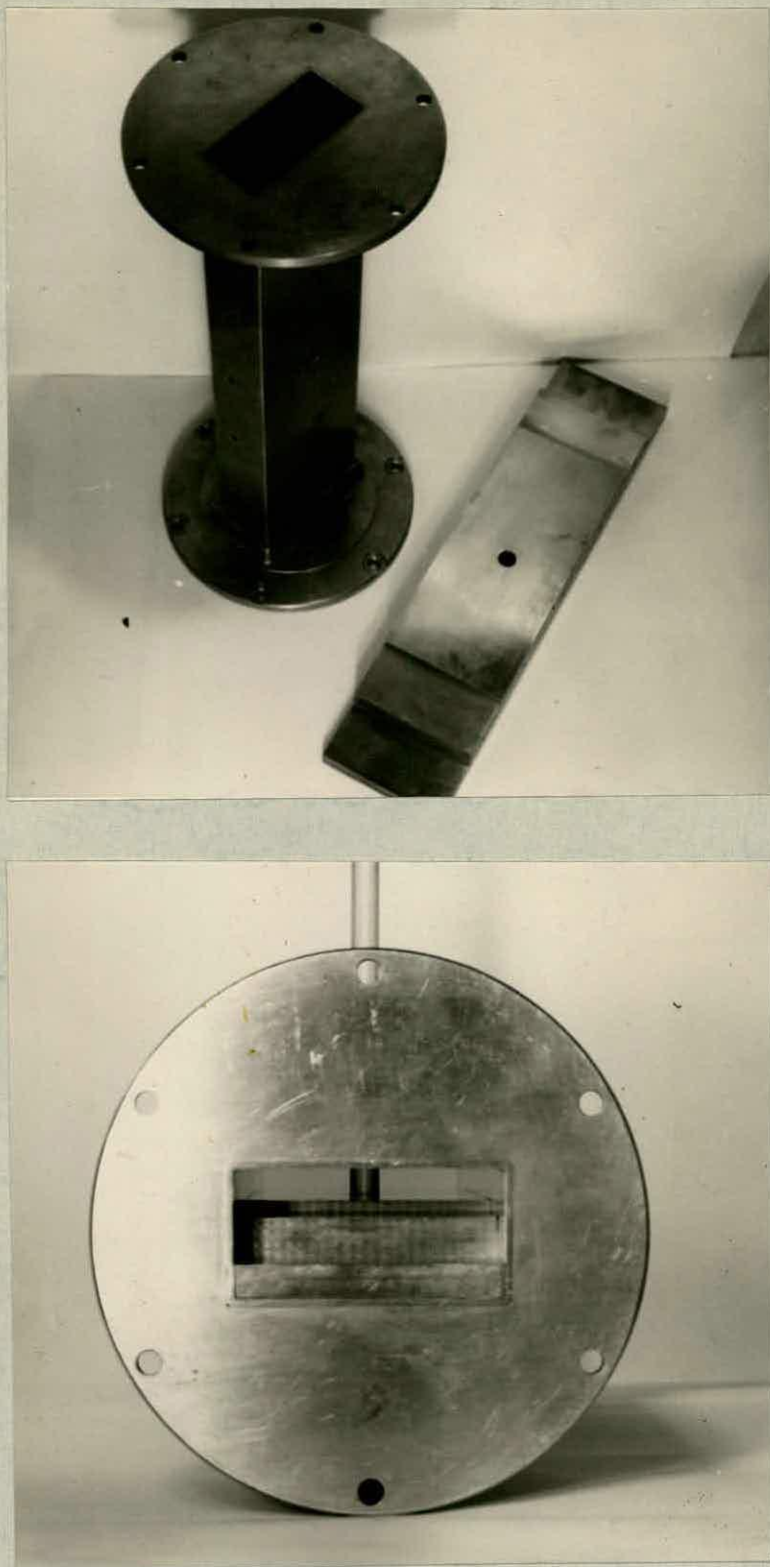

Figure 2.3.1.

Photographs of an experimental binomial transformer.

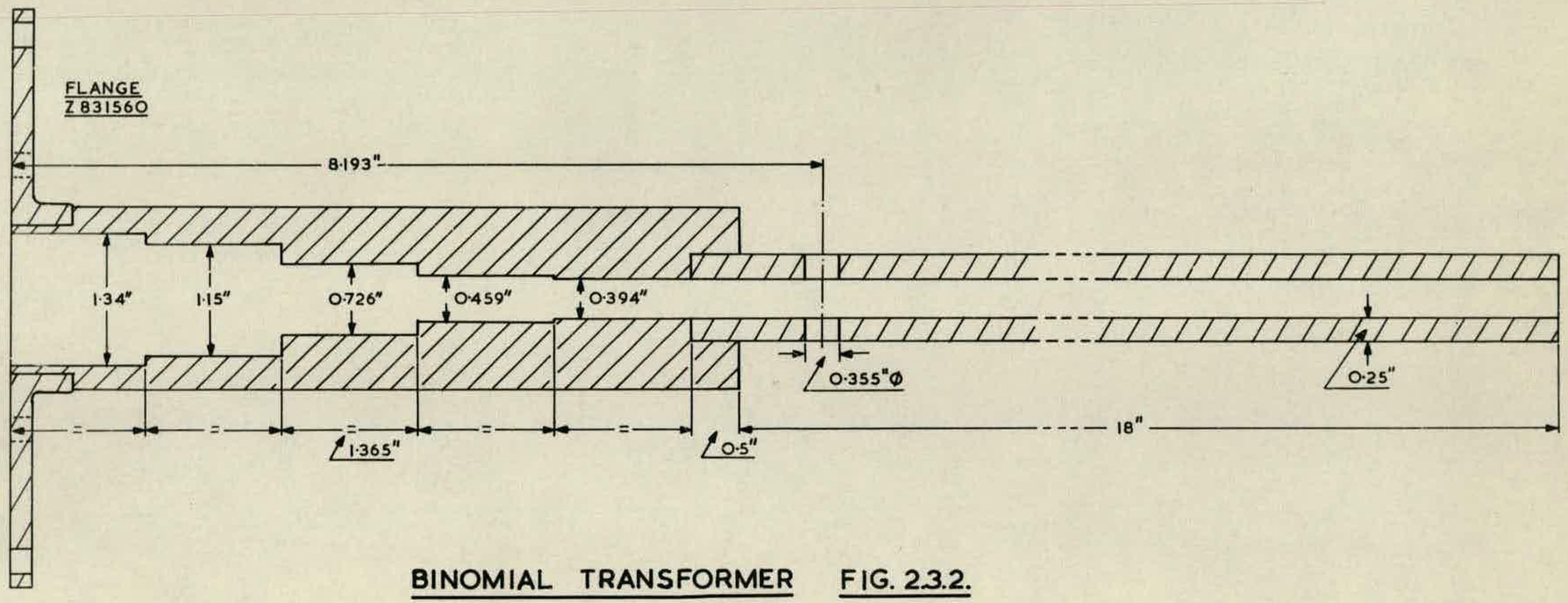

BINOMIAL TRANSFORMER FIG. 2.3.2.

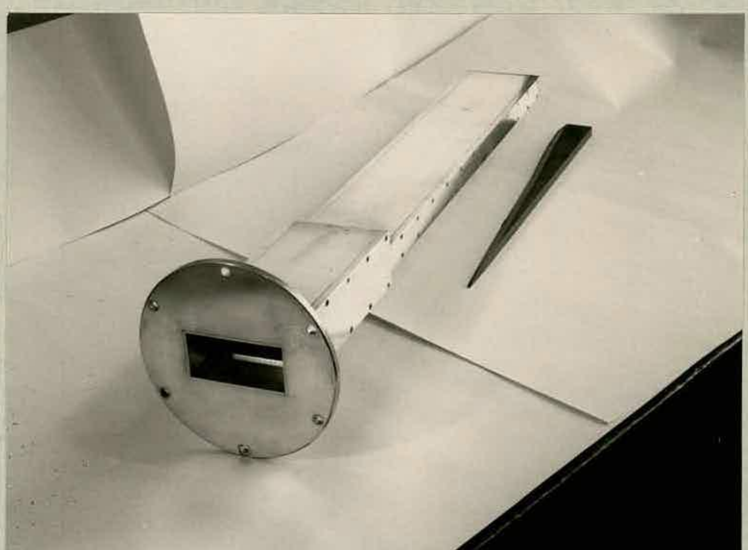

Figure 2.3.3.

Photograph of the

binomial transformer.

CHAPTER 3

Instrumentation

3.1. The Complete System

In order to study the microwave properties of a pulsed discharge using the dielectric post method it is necessary to measure the v.s.w.r. in the microwave system as a function of time. A block diagram of the system used in these experiments is given in Fig. 3.1.1. and Fig. 3.1.2. is a photograph of the equipment.

In the case of a steady discharge, when the v.s.w.r. produced in the waveguide is constant, a C.W. microwave oscillator can be used to feed the waveguide system and the output from the v.s.w.r. probe is a d.c. signal. However, in the case of a pulsed discharge the probe output is modulated by the time variation of the standing wave pattern due to changes in the discharge admittance.

The v.s.w.r. at any instant is a measure of the discharge admittance and can be obtained by a sampling process, or by recording the probe output, for a large number of probe positions, so that a permanent record of the time variation of the v.s.w.r. pattern is obtained. The probe output is typically of the order of 1 mV. and must be amplified before the v.s.w.r. can be measured conveniently. A bandwidth of at least 1 Mc/s is desirable so that changes which occur over a period of microseconds will be recorded.

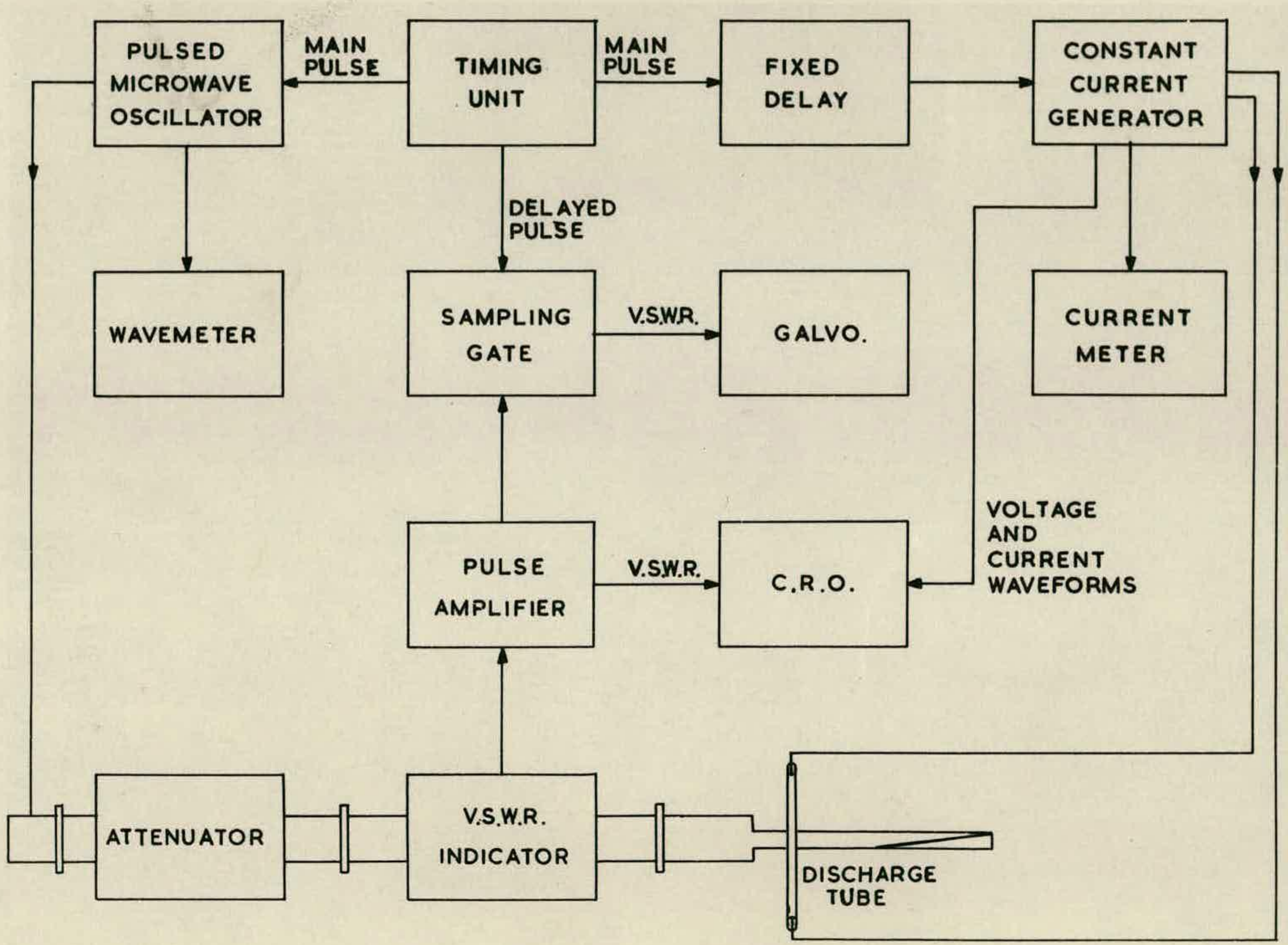
PULSED MICROWAVE OSCILLATOR
MAIN PULSE
TIMING UNIT
MAIN PULSE
FIXED DELAY
CONSTANT CURRENT GENERATOR
DELAYED PULSE
WAVEMETER
SAMPLING GATE
V.S.W.R.
GALVO.
CURRENT METER
PULSE AMPLIFIER
V.S.W.R.
C.R.O.
VOLTAGE AND CURRENT WAVEFORMS
ATTENUATOR
V.S.W.R. INDICATOR
DISCHARGE TUBE

FIG. 3.1.1.

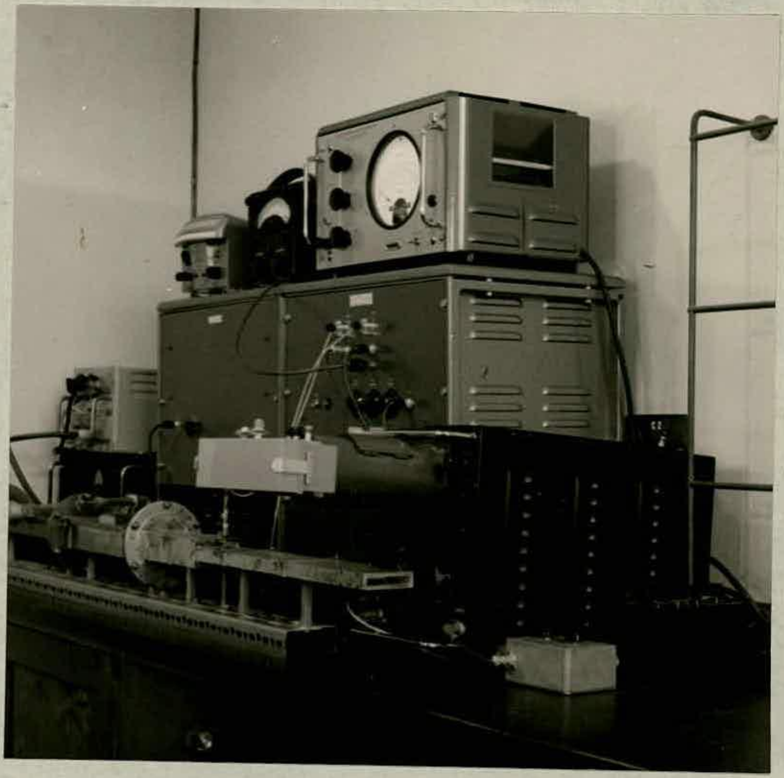

Fig. 3.1.2.

In order to avoid the difficulties associated with a high gain d.c. amplifier the microwave oscillator is switched on for 1 m.sec. each time the discharge tube is pulsed. For a low pulse repetition frequency (p.r.f.) the d.c. component of the probe output signal is then negligible and an a.c. coupled amplifier with good low frequency response can be used.

The system operates at a p.r.f. of 12.5 per sec. The microwave oscillator is pulsed on and after a fixed delay of approximately 25 μ.sec, (which allows the oscillator amplitude to become stable) the discharge tube is pulsed. A delayed pulse train is also availabe and this can be used to sample the v.s.w.r. at a given time after the application of the pulse to the discharge tube. Alternatively the amplified probe signal can be recorded with the aid of an oscilloscope and camera.

A more detailed description of the various units and their operation is given in the following sections.

3.2. Timing Unit

The transistorised timing unit was designed by Scott (1956). It provides pulse repetition frequencies of 12.5, 25, or 50 per. sec. using a 100Kc/s. quartz crystal as a frequency standard.

A p.r.f. of 12.5 per. sec. has been used in order to prolong the useful life of the discharge tubes.

The main output from the unit triggers the microwave oscillator, the discharge tube pulse generator and the oscilloscope. It consists of 40V. positive pulses 15 μsec. long.

In addition a second output channel provides pulses which are delayed with respect to the main output by an amount variable from 0 → 1800 μsec. with an accuracy of better than 1 μsec. These delayed pulses are used to operate a gate circuit which samples the v.s.w.r. probe signal and the v.s.w.r. can therefore be measured at any selected time after the discharge tube is pulsed.

The unit also provides 10 μsec. and 40 μsec. time markers which can be used to apply brightness modulation to the oscilloscope so that an accurate time scale is available.

3.3. Constant Current Pulse Generator

Rectangular current pulses superimposed on a small d.c. maintaining current are fed to the discharge tube from a pulsed power unit. (Fig. 3.3.1).

Basically the unit consists of a 5.3 KV d.c. supply with an 11E3 tetrode and feedback amplifier to give a high output impedance.

It was considered desirable to have one end of the discharge tube at earth potential. Since the

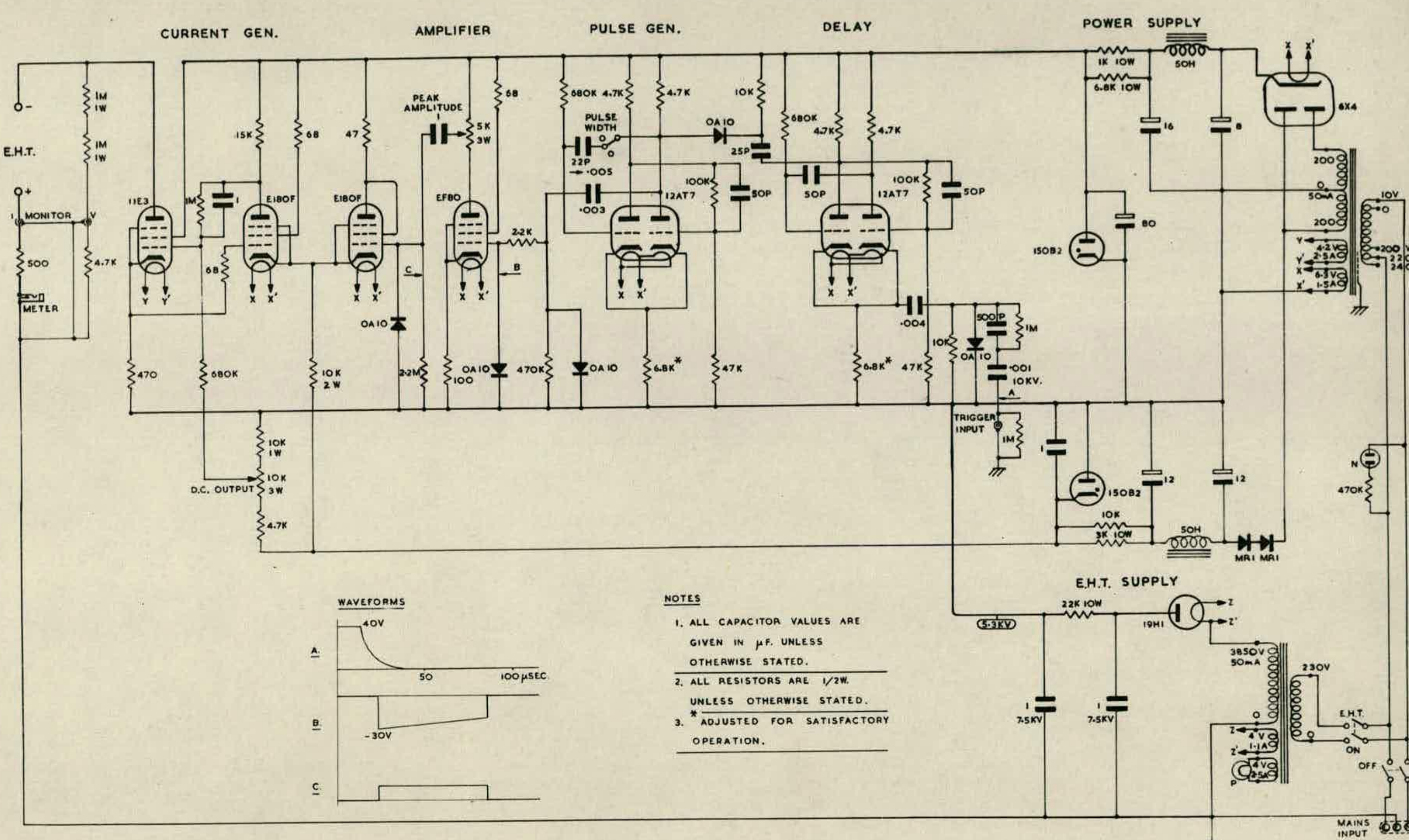
CURRENT GEN.
AMPLIFIER
PULSE GEN.
DELAY
POWER SUPPLY
E.H.T.
MONITOR
METER
PEAK AMPLITUDE
PULSE WIDTH
D.C. OUTPUT
TRIGGER INPUT
E.H.T. SUPPLY
MAINS INPUT
11E3
E180F
EF80
12AT7
6X4
150B2
19H1
OA10
MR1
WAVEFORMS
40V
50
100 μSEC.
-30V
NOTES
1. ALL CAPACITOR VALUES ARE GIVEN IN μF. UNLESS OTHERWISE STATED.
2. ALL RESISTORS ARE 1/2W. UNLESS OTHERWISE STATED.
3. * ADJUSTED FOR SATISFACTORY OPERATION.

FIG. 3.3.1.

discharge tube is connected as the anode load of the tetrode the output stage and the associated pulse generator and trigger circuits are connected directly to the negative supply and isolated from earth. A special oil filled transformer insulated for 6.5KV. supplies the H.T. for these circuits and for simplicity a neon stabilised supply is used.

The pulse generator is triggered by the trailing edge of the main pulse from the time unit (which also triggers the microwave oscillator), after a delay of 10 μsec. This produces a total delay of 25 μsec. which is sufficient to allow the microwave oscillator to reach a steady state. Pulse widths in the range 5 μsec. to 750 μsec. can be selected. An EF80 variable gain amplifier shapes the pulse generator output waveform and also provides a means of altering the amplitude of the current pulses fed to the discharge tube. The 11E3 and one of the E180F pentodes form a high gain feedback loop which can be represented by the equivalent circuit of Fig. 3.3.2. The effective output impedance of this circuit is given by,

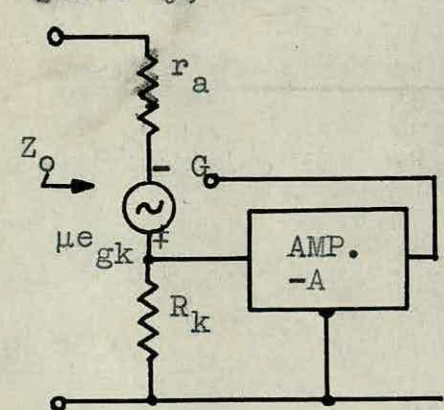

$$Z_o = r_a + R_k(1 + \mu + A\mu). \quad 3.3.1$$

so that $Z_o \sim A\mu R_k \quad . \; . \; . \; 3.3.2.$

Fig. 3.3.2.

Current pulses are provided by altering the voltage level of the feedback loop with pulses injected by the second E180F pentode, while the d.c. maintaining current can be controlled by varying the bias on the series valve.

The maximum value of R_k which can be used is limited by the permissable change in voltage levels under pulse conditions and this depends upon the d.c. supply voltage available for the amplifier. The gain A, which can be obtained in practice is also limited since it is not possible for reasons of stability to include more than one stage of amplification in the feedback loop.

The output impedance of the circuit varies with the operating conditions, but for steady currents of a few milliamperes it is of the order of 1MΩ rising to about 2MΩ under dynamic conditions.

This must be compared with the output impedance of the 11E3 which is about 150KΩ .

The 11E3 has given satisfactory operation in this circuit for long periods although it is not intended for continuous operation at such a high voltage. It will deliver rectangular pulses of 50 mA. into a 100KΩ resistive load with a rise time of 2 μsec. (Fig. 3.3.2a), although the mean output should not be more than about 2 mA. to avoid exceeding the anode dissipation. When using discharge tubes filled with helium at 5 mm. Hg. pressure the pulse shape deteriorates for amplitudes greater than 5 mA. due to

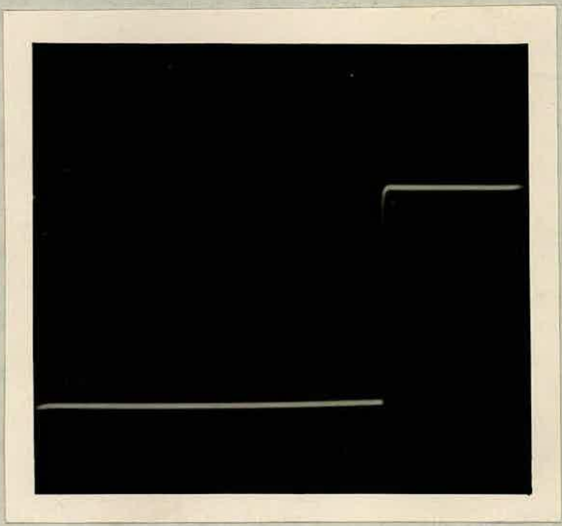

Fig. 3.3.2a.

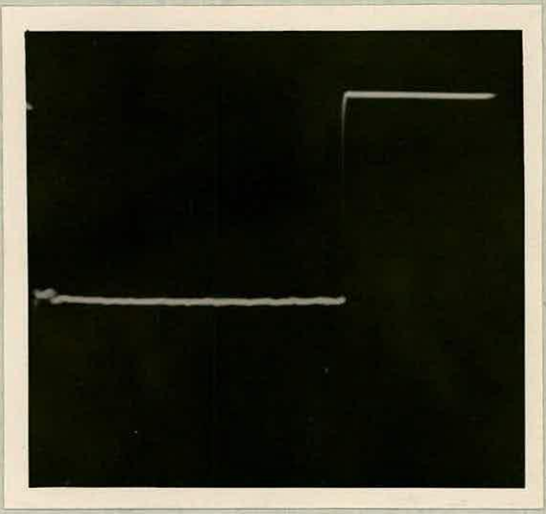

Fig. 3.3.2b.

the high voltage required across the tube. At higher pressures a rise time of the order of 5 μsec. can be obtained for 20 mA. pulses (Fig. 3.3.3b).

Monitoring points are provided for the output voltage and current waveforms.

3.4. Pulse Amplifier and Sampling Unit

The output from the v.s.w.r. probe is a train of 1 m.sec. pulses of about 1 mV amplitude which are modulated by the varying standing wave pattern in the waveguide when the discharge tube is pulsed. For a p.r.f. of 12.5 per sec. the d.c. component of the signal is of the order of 1% of the pulse amplitude and can be neglected. An a.c. amplifier can therefore be used (Fig. 3.4.1.)

The amplifier consists of two feedback units, each using 1 - E180F and 1 - 12AT7. The gain of each unit is approximately 33 so that the overall gain is 10^3. The bandwidth extends from 1 c/s to 1 Mc/s. which is sufficient to ensure that changes in v.s.w.r. occurring in a period of a few microseconds can be detected. A conventional series stabilised supply delivers 200V d.c. with a ripple content of 1 mV. to the amplifier. Unstabilised d.c. has been used to supply the valve heaters to reduce 50 c/s noise to a minimum.

The output from the amplifier can be fed directly to the oscilloscope which is triggered by the timing

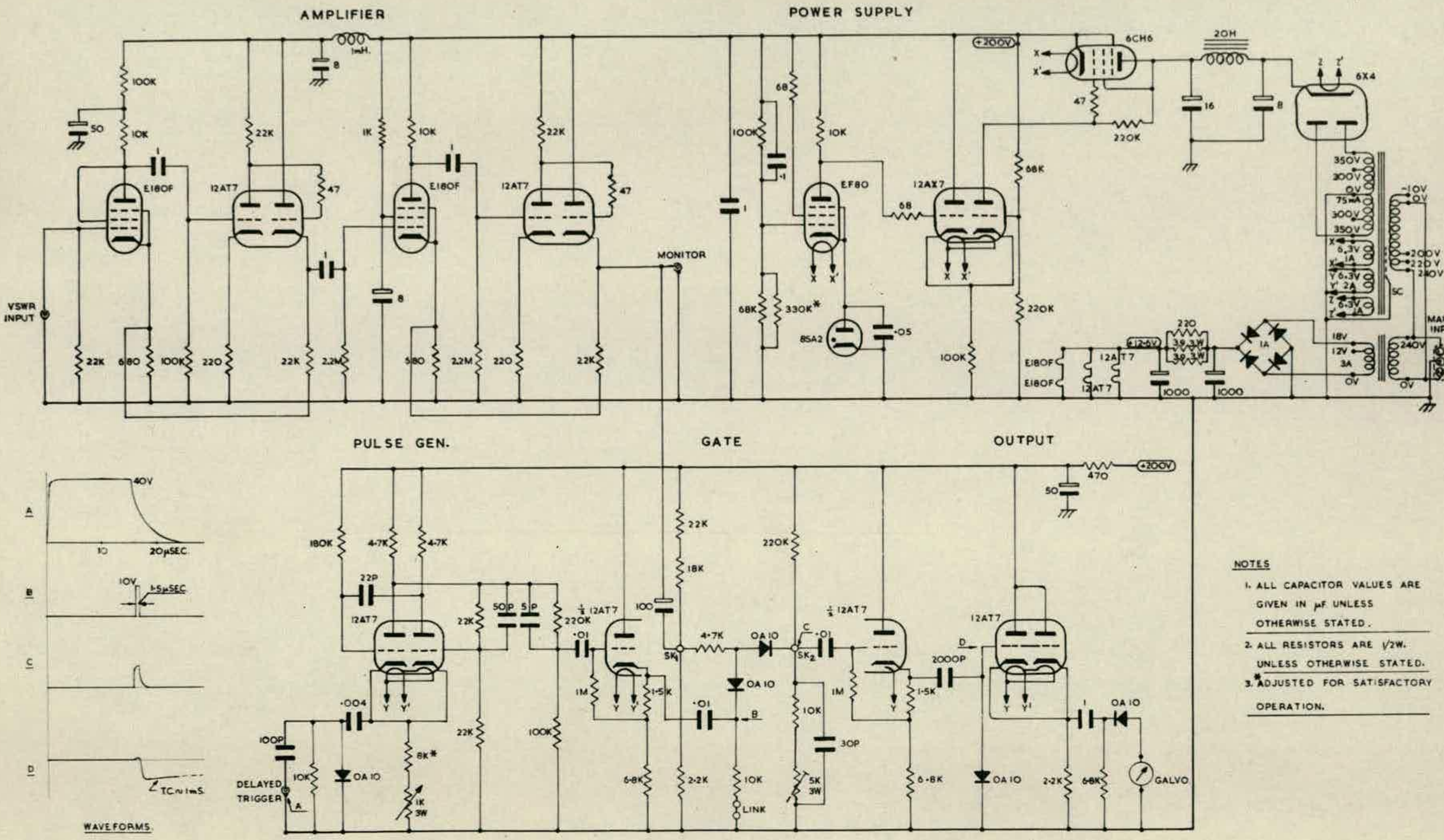

FIG. 3.4.1.

NOTES

1. ALL CAPACITOR VALUES ARE GIVEN IN μF UNLESS OTHERWISE STATED.
2. ALL RESISTORS ARE 1/2W. UNLESS OTHERWISE STATED.
3. * ADJUSTED FOR SATISFACTORY OPERATION.

unit. A photograph of the display obtained for one position of the v.s.w.r. probe is shown in Fig.3.4.2. (brightness modulation by 40 μsec. time markers).

The initial part of the display corresponds to the rise in standing wave ratio as the discharge is pulsed. At the end of the current pulse the v.s.w.r. falls as recombination occurs. Finally the microwave oscillator is switched off and the probe output falls to zero.

By recording this display for a large number of positions of the v.s.w.r. probe (Fig. 3.4.3.) and enlarging the photographs obtained (Fig.3.4.2.) the v.s.w.r. pattern at any time during the current pulse can be measured. The first two photographs in Fig. 3.4.3. show the discharge tube current and voltage waveforms. The next fifteen show the probe output throughout the period of the current pulse for probe positions spaced 0.5 cm. apart. The last set are similar but show only the recombination period.

A typical set of v.s.w.r. patterns for the recombination period are shown in Fig. 3.4.4. (time measured from the end of the current pulse). This method of recording the results has been used almost exclusively as the results can be obtained quickly and a permanent record is available for future examination.

Alternatively the v.s.w.r. can be measured more directly with the aid of the sampling unit, which is

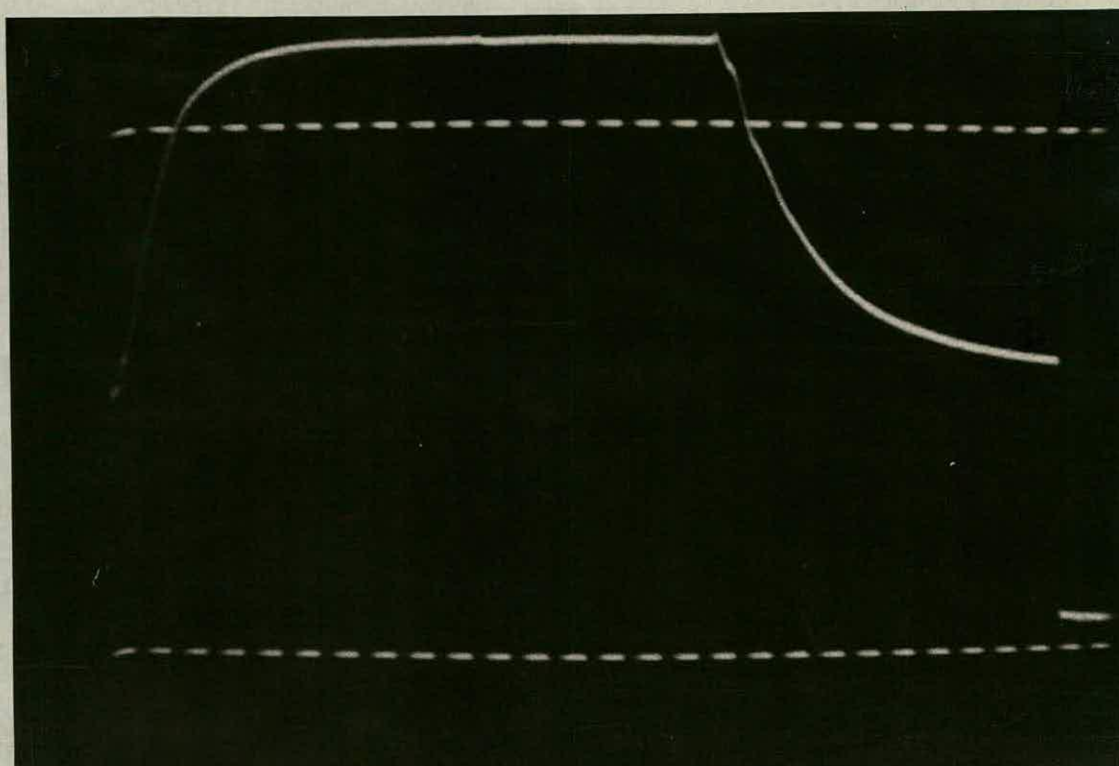

Figure 3.4.2.

(Brightness modulation by 40 μsec time markers)

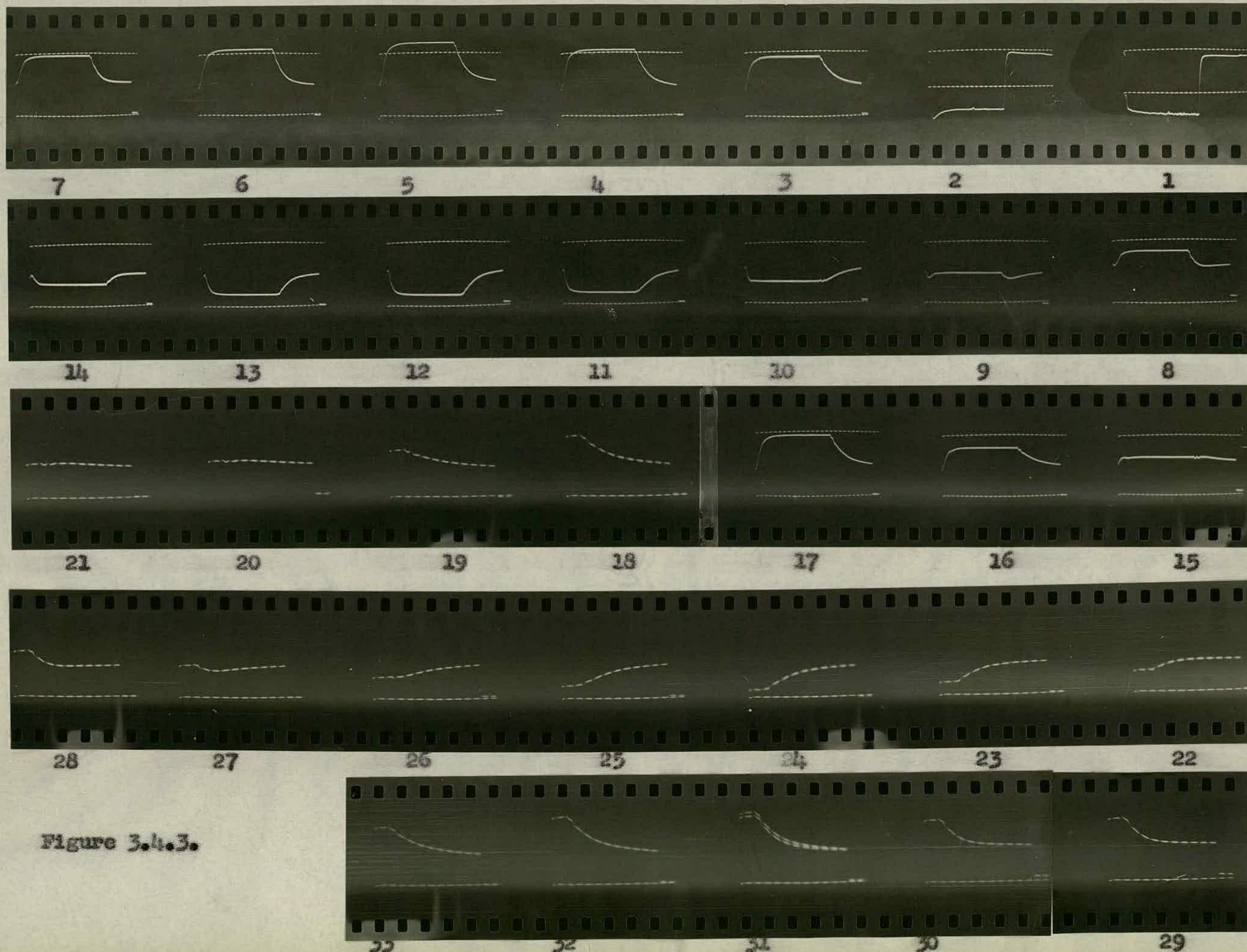

7 6 5 4 3 2 1
14 13 12 11 10 9 8
21 20 19 18 17 16 15
28 27 26 25 24 23 22
32 31 30 29

Figure 3.4.3.

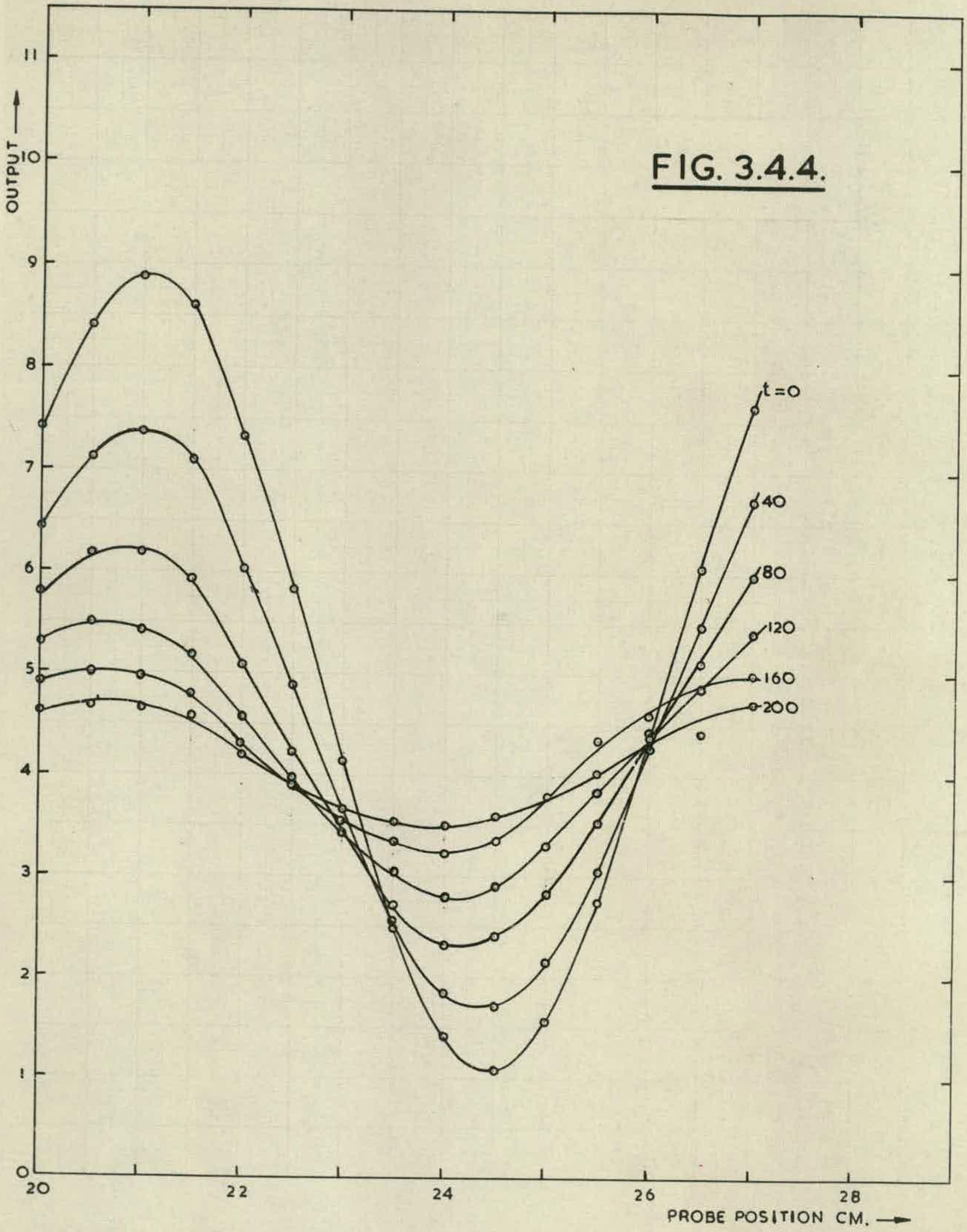
OUTPUT
0
1
2
3
4
5
6
7
8
9
10
11
20
22
24
26
28
PROBE POSITION CM.
t=0
40
80
120
160
200

FIG. 3.4.4.

also shown in Fig. 3.4.1. The amplifier output is fed to a series diode gate which can be opened by a 1.5 µsec. pulse generator. The pulse generator is triggered by the trailing edge of the delayed pulse from the timing unit, so that the diode gate can be used to sample the amplifier output at any preset time after the discharge tube is pulsed. Adjustment of the diode gate is carried out by removing the short circuiting link shown in the diagram and setting the potentiometer so that the d.c. potential between the input and output terminals is zero. Provided that the amplifier output voltage does not exceed 4V. no output is obtained from the gate until it is opened by the 1.5 µsec. pulse generator.

The gate output (1.5 µsec. pulses with a p.r.f. of 12.5 per sec) is passed to a pulse stretching circuit before being rectified and passed to a galvanometer. The galvanometer records the average output current which for this circuit is proportional to the square of the input voltage (Fig. 3.4.5.) (The v.s.w.r. indicator also has a square law characteristic.)

The v.s.w.r. at a given time in the cycle of operation can be obtained simply by setting the required delay on the timing unit and recording the maximum and minimum of the standing wave pattern as the probe is moved along the waveguide.

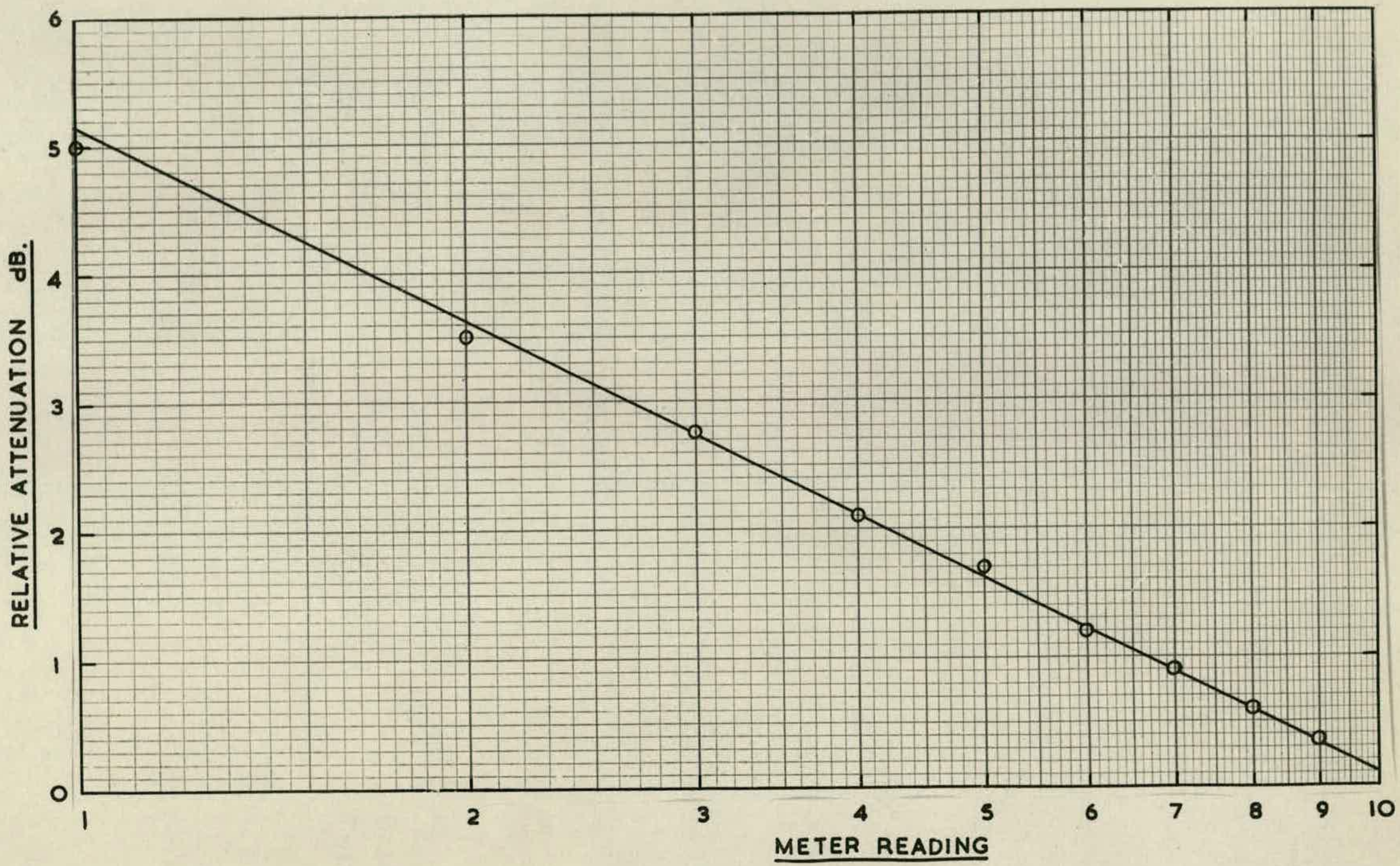

RELATIVE ATTENUATION dB.
6
5
4
3
2
1
0
1
2
3
4
5
6
7
8
9
10
METER READING

FIG. 3.4.5.

CHAPTER 4

The Gas Discharge Tubes

4.1. Discharge Tube Design

In order to determine suitable dimensions for the discharge tubes some experimental tubes of 2 cm. diameter and 40 cm. in length were made. It was found that the striking and maintaining voltages of these tubes were rather large for the range of gas pressure which was of interest. In addition the diameter was too large to allow accurate microwave measurements to be made as the tube diameter was a large fraction of the waveguide width so that considerable leakage of microwave power was possible. However, the experience gained from these tubes led to the final design described below.

The discharge tubes used in the experiments were made from precision bore pyrex which was externally ground to a close tolerance so that the cross sectional area would be constant. The pyrex tube used was 7.5 mm. bore x 9 mm. external diameter and an electrode spacing of 20 cm. was found to be satisfactory.

Skolnik and Puckett (1955) have suggested that molybdenum electrodes are better than tungsten as far as electrical noise and sputtering are concerned. For this reason molybdenum electrodes have been used, although some tubes with tungsten electrodes have also been made to compare the sputtering rates of these materials.

The molybdenum electrodes were made from a 6 mm. diameter disc of 16 gauge sheet mounted on one end of a short length of 1.5 mm. diameter rod. To obtain a plane electrode surface the rod is forced into a hole bored in the centre of one face of the disc. This gives a rigid mechanical construction without the necessity for brazing. The tungsten electrodes are of similar construction, but due to the difficulties of machining tungsten the supporting rod passes through the disc and is ground off to give a plane electrode surface.

The electrodes were electrolytically cleaned before being sealed into the tubes using C11 - C9 - pyrex metal-to-glass seals for the molybdenum and C9 - pyrex seals for the tungsten.

It was found that the discharge tended to strike behind the cathode thus altering the characteristics of the discharge. To reduce this tendency a short length of 6 mm. diameter pyrex tube has been fitted over the electrode supports with one end in close contact with the back of the electrode. This is quite effective, although the discharge still strikes behind the cathode for pulse currents greater than 10 → 20mA. depending on the gas pressure. A photograph showing details of the electrode structure and the metal-to-glass seals is given in Fig. 4.1.1.

In order to obtain satisfactory gas purity it was found necessary to use sealed tubes with a barium getter in the exhaust arm, which is placed behind one of the electrodes to avoid disturbing the discharge. One of

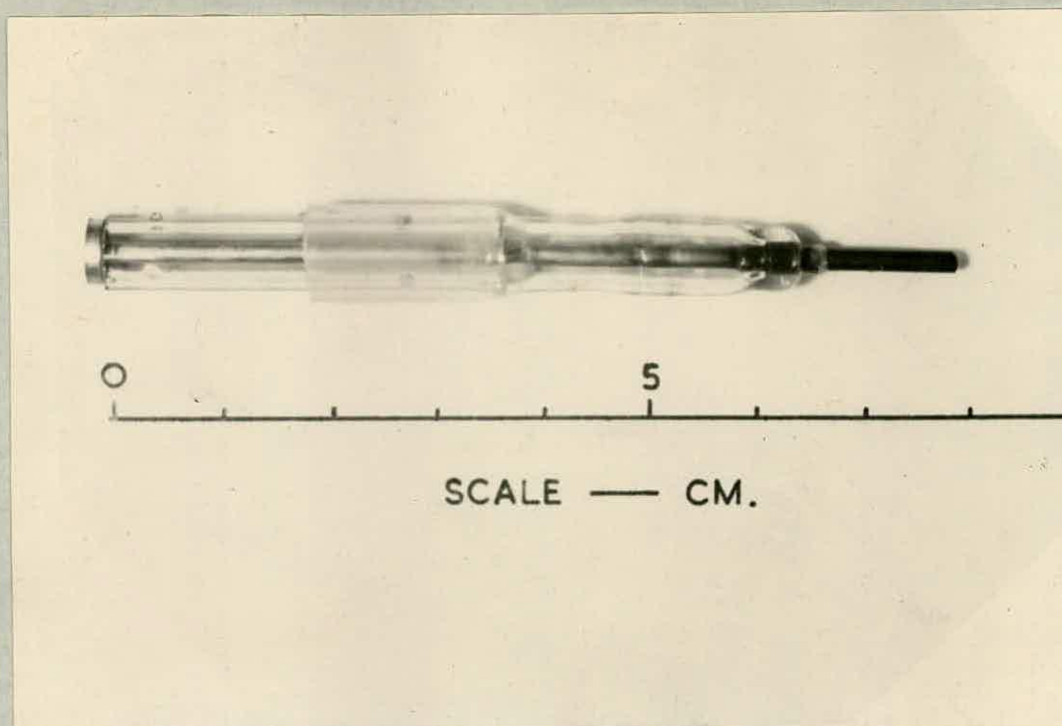

Fig. 4.1.1.

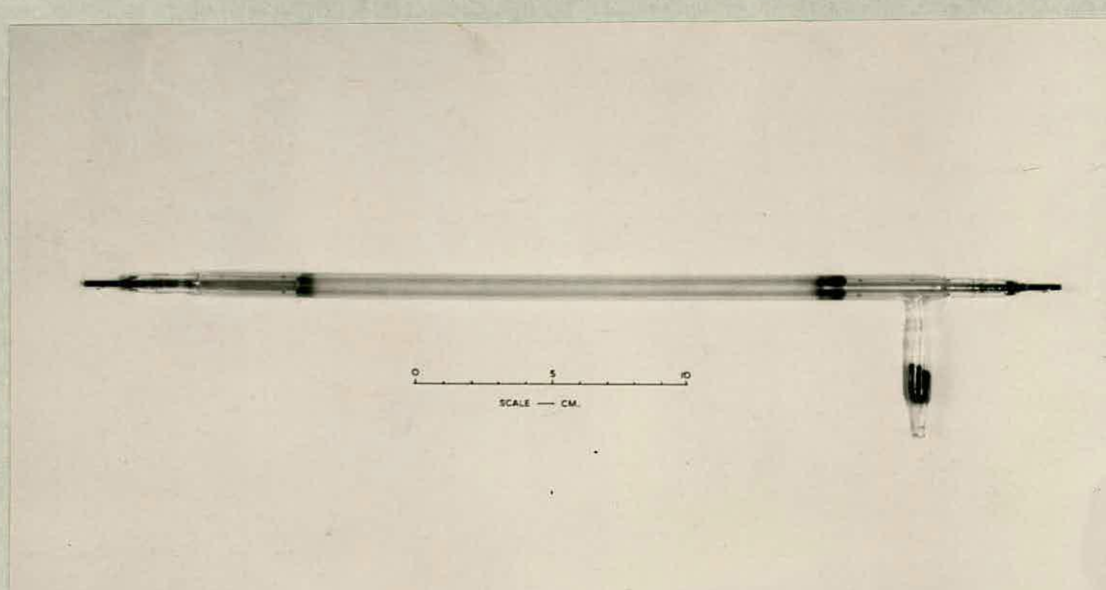

Fig. 4.1.2.

these tubes is shown in Fig. 4.1.2.

Details of the assembly procedure for making the discharge tubes are given in Appendix A.

4.2. The Vacuum System

The vacuum system used to fill the discharge tubes is shown in Fig. 4.2.1.

The system is pumped by an oil filled rotary backing pump type S.R.2.[1] and a two stage silicone oil diffusion pump type 102[2] with a water cooled baffle to prevent the oil diffusing into the vacuum system. The pumps are protected against failure of the mains or cooling water supplies. The limiting vacuum which the pumps can produce is of the order of 5×10^{-6} mm. Hg.

The use of a mercury diffusion pump was avoided as this would lead to mercury as an impurity in the discharge tubes.

The main manifold of the vacuum system (See Fig. 4.2.1.) is a length of 25 mm. pyrex tube, which is connected to the diffusion pump by a neoprene rubber seal and an industrial type coupling. A cold trap is connected between the main system and the ionisation gauge (Type IG - 2AH[2]) and discharge tube. An electrically heated oven can be lowered over the tube to outgas this part of the system. Spectroscopically pure helium is supplied from the gas bottle[3] and the

1. Metropolitan-Vickers Co., Ltd., Manchester.
2. W. Edwards and Co., Ltd., London
3. British Oxygen Co., Ltd., Wembley.

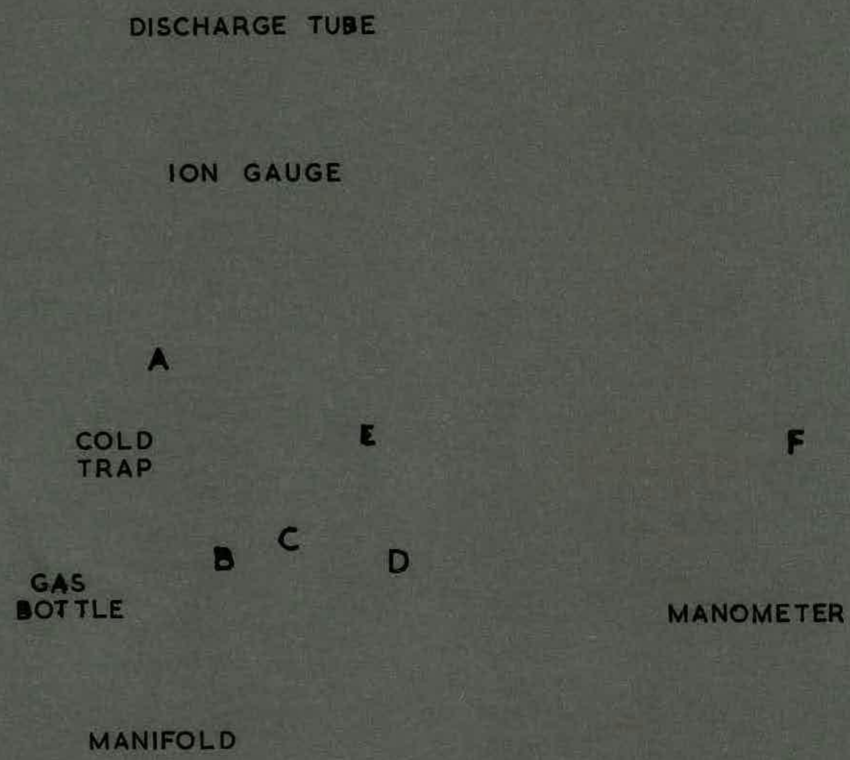
DISCHARGE TUBE
ION GAUGE
A
COLD
TRAP
E
F
B
C
D
GAS
BOTTLE
MANOMETER
MANIFOLD

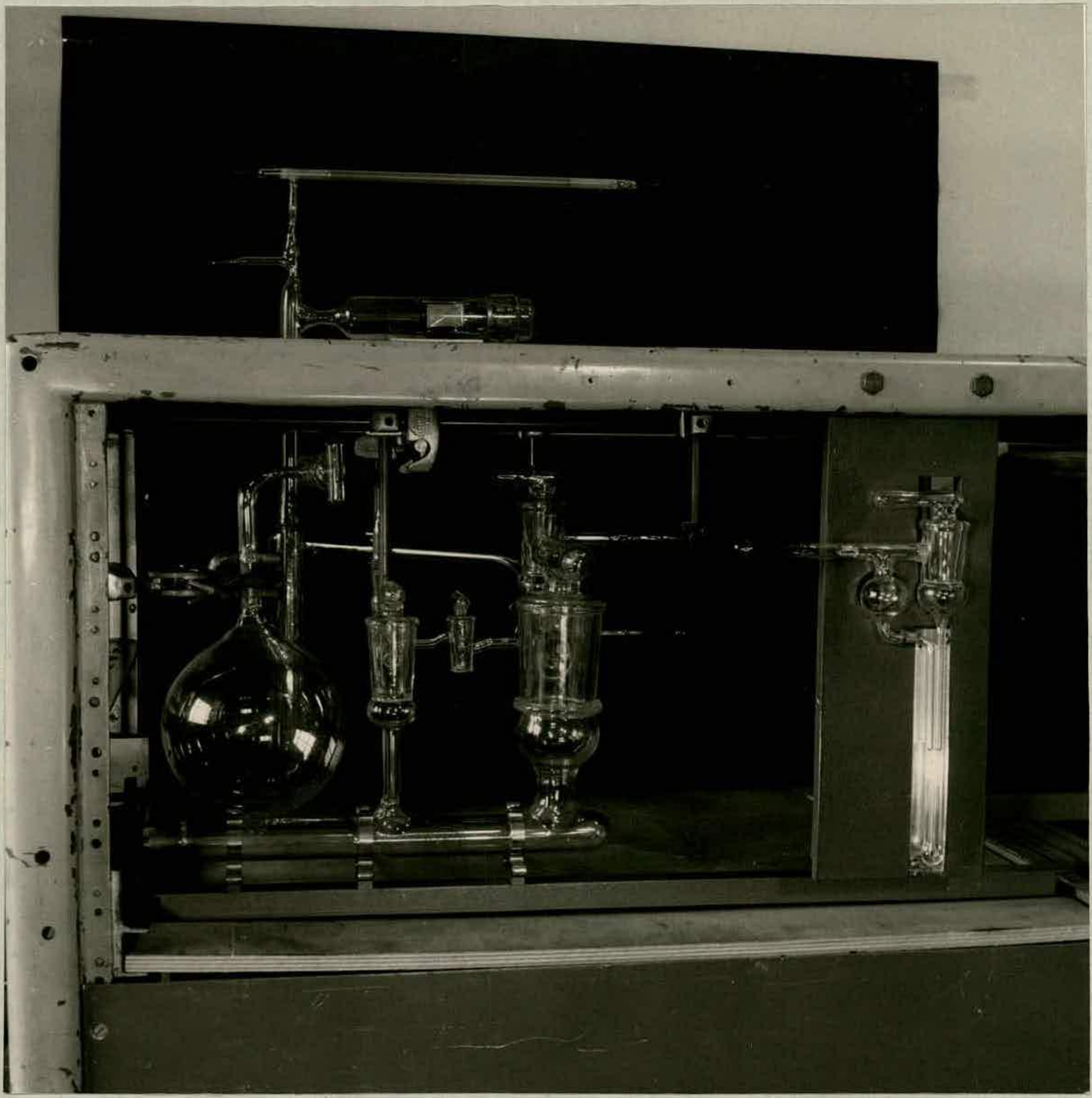

Fig. 4.2.1.

gas pressure can be measured with the oil manometer. Using silicon oil type DC703[1] a magnification factor of 12.47, compared with mercury, is obtained. A mirror scale is fitted to reduce errors due to parallax and the pressure can be read with an error of the order of 0.03 mm.Hg.

The procedure used to evacuate and fill the discharge tubes to the required pressure was as follows:

All taps, except tap A, were opened and the system evacuated. The glass was then outgassed as far as possible using an air-gas flame. A liquid air flask was placed over the cold trap and the ionisation gauge and discharge tube further outgassed by heating to 400°C. for about one hour using an electrically heated oven. This reduced the residual pressure to less than 10^{-5} mm. Hg. After the system had cooled all the taps were closed and tap A opened momentarily to fill the part of the system adjacent to the gas bottle. The capillary tap C was then opened to flush the system with helium, the pressure being indicated on the manometer. This gas was pumped off and the system refilled to a pressure of $5 \rightarrow 10$ mm. Hg. and a d.c. discharge of about 1 mA run in the tube for 15 minutes in each direction to outgas the surface of electrodes.

Finally the system was again evacuated and filled to the required pressure and the tube sealed off. The getter was then fired using an induction heater.

---

1. W. Edwards and Co., Ltd., London.

It would have been an advantage if it had been possible to heat the electrodes in a hydrogen furnace before assembly of the tubes and also to outgas them with an induction heater before tubes were sealed. However, suitable facilities for this were not available at the time and the procedure described has proved satisfactory.

4.3. The Problem of Gas Purity

One of the main difficulties associated with gas discharges is the problem of maintaining the gas in a pure state. Desorption of the glass and outgassing and sputtering of the electrodes can yield large volumes of impurities. From this point of view a tube sealed permanently to the vacuum system would be ideal as it could readily be filled with pure gas. However, this method would lead to mechanical difficulties as either the discharge tube or the waveguide system must be moved in order to scan along the length of the tube.

A more convenient alternative is the use of a tube fitted with a high vacuum tap, or of course the tube could be sealed off permanently, although this latter method gives rise to some uncertainty about the gas pressure after the tube has been in use for some time.

To find a solution to the problem of maintaining the gas in a suitable pure state some experiments were carried out using both sealed tubes fitted with barium getters, and a tube fitted with a high vacuum tap so that it could be refilled. Measurements of the striking voltage and static characteristic were made as well as studies of the general appearance of the discharge and spectrographic examination.

The static characteristics of the tubes filled with helium at 10 mm. Hg. pressure are illustrated in Fig. 4.3.1. Curve A refers to an unsealed tube fitted with a high vacuum tap, while B and C are for a sealed tube before and after firing the getter. One disadvantage of the tube fitted with a tap is that it is not possible to heat it to high temperatures due to the presence of grease. As a result it cannot be outgassed thoroughly.

The difference in the static characteristic of the tubes is obvious, the striking and maintaining voltage of the unsealed tube are much lower than for the sealed tubes. The effect of the getter in the sealed tubes is quite small, as might be expected, since these characteristics were taken shortly after sealing off the tubes.

In addition to these differences in electrical characteristics the discharges have a very different appearance. The gettered tubes have a salmon-pink positive column with one or two diffuse striations at the negative end and the negative glow region is almost white. The unsealed tube tends to have a blue positive column with distinct striations which become more marked as the tube ages. Also, the negative glow region is much shorter than in the case of the sealed tube. This is illustrated in Fig. 4.3.3. and Fig.

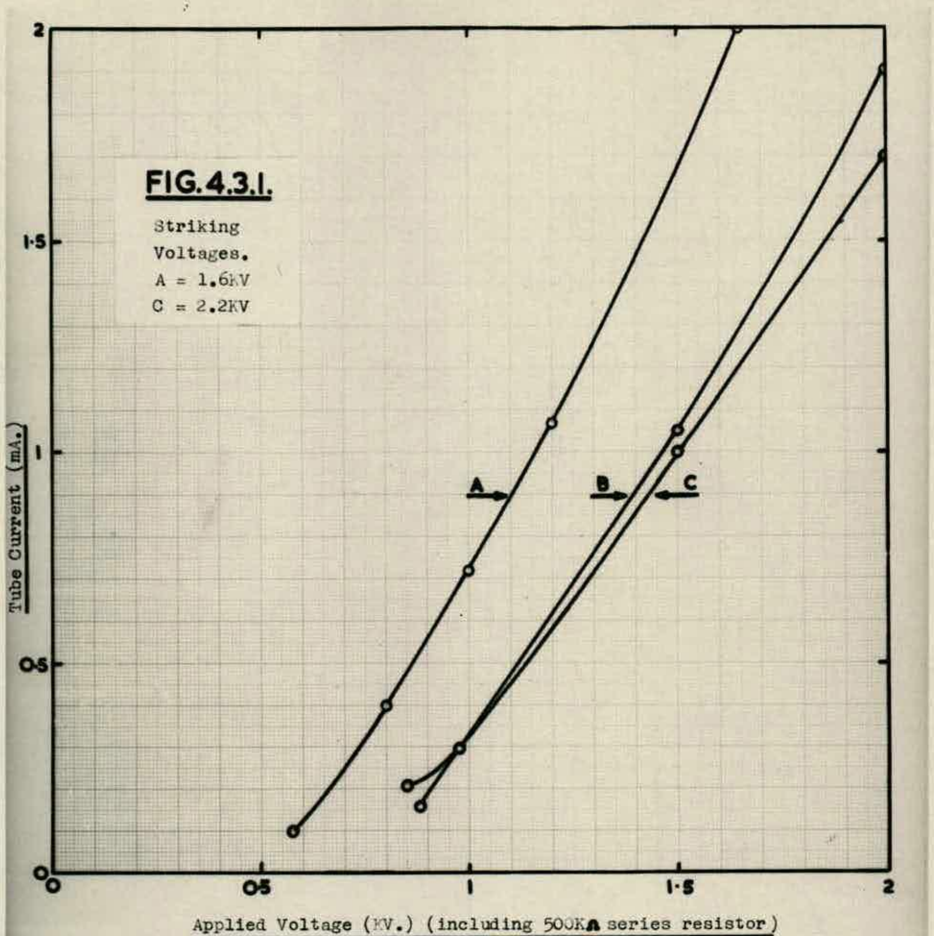
FIG. 4.3.1.
Striking
Voltages.
A = 1.6KV
C = 2.2KV
A
B
C
Tube Current (mA.)
0
0·5
1
1·5
2
Applied Voltage (KV.) (including 500KΩ series resistor)

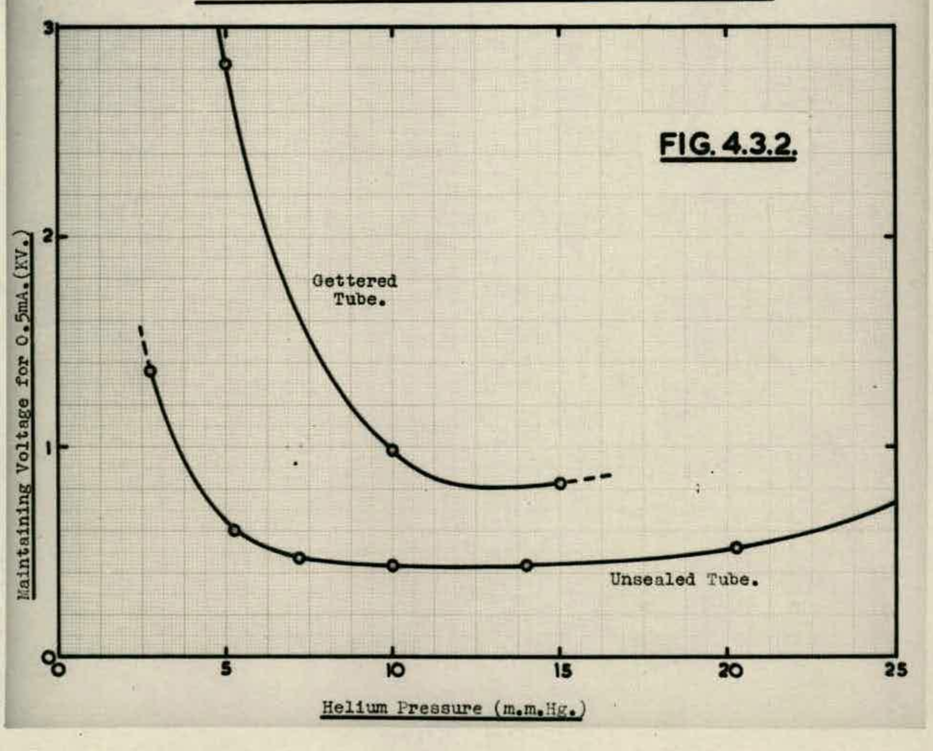
FIG. 4.3.2.
Gettered
Tube.
Unsealed Tube.
Maintaining Voltage for 0.5mA. (KV.)
0
1
2
3
5
10
15
20
25
Helium Pressure (m.m.Hg.)

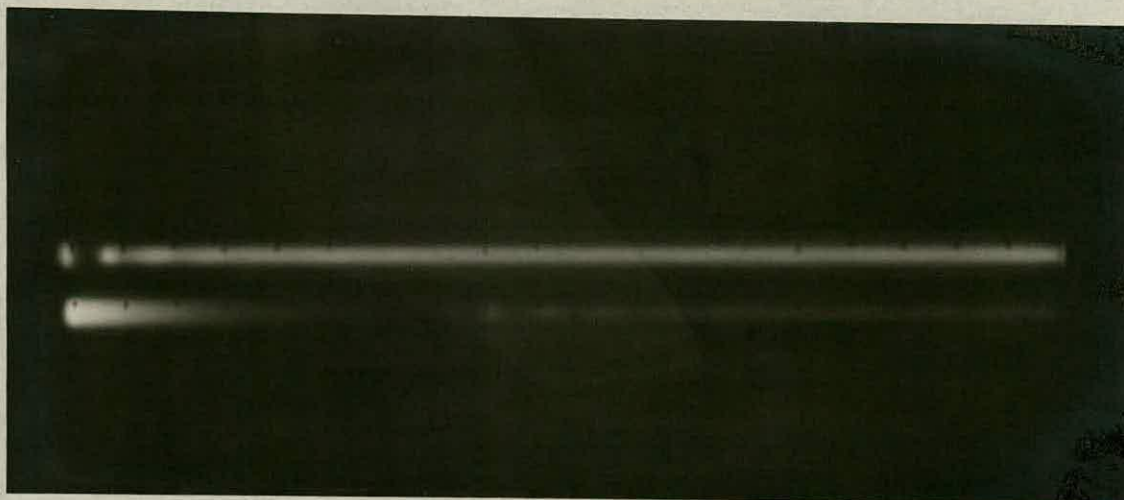

Figure 4.3.3.

(Top discharge for 500 μA d.c.
Bottom discharge for 10 mA pulses)

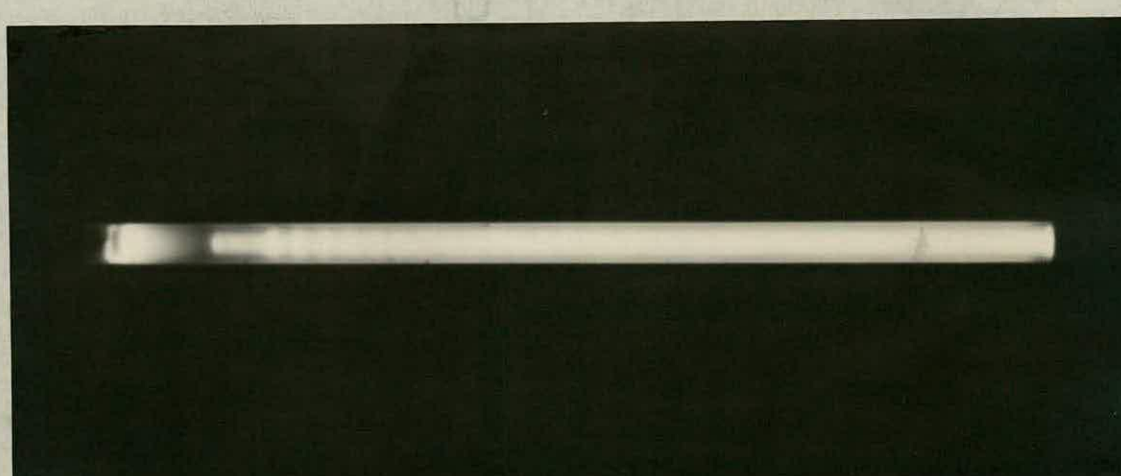

Figure 4.3.4.

(Discharge for 300 μA d.c. with 30 mA pulses)

4.3.4. which are photographs of pulsed discharges in sealed an unsealed tubes respectively.

The voltage required to maintain a given current in the tube and the striking voltage are also reduced considerably by the presence of impurities. Fig. 4.3.2. gives a comparison between the maintaining voltages for sealed and unsealed tubes for a wide range of pressure.

In an effort to determine the degree of gas purity some spectrographic measurements of the light from the discharge have been made. Using a quartz spectrograph[1] with 50 micron slit and an exposure of 3 minutes on HP3 plates[2] the spectra shown in Fig. 4.3.5. were obtained. (Considerable detail is lost in the printing process). They all refer to 6 mA pulses in helium at 10 mm. Hg. pressure. (Scale units are Å x 100).

The top spectrum is for an unsealed tube with impurities present. The second and third are for a gettered tube of the type used in the experiments. In the positive column only lines of atomic helium are obtained, while in the negative glow a large number of molybdenum lines are also present. The only lines which cannot be identified as belonging to either helium or molybdenum (the cathode material) are the lines of a faint triplet at about 3677 Å.

It was estimated that the unsealed tube contained about 1% carbon monoxide and hydrogen, which are

---

1. Hilger and Watts Limited, London
2. Ilford Limited, Ilford, Essex.

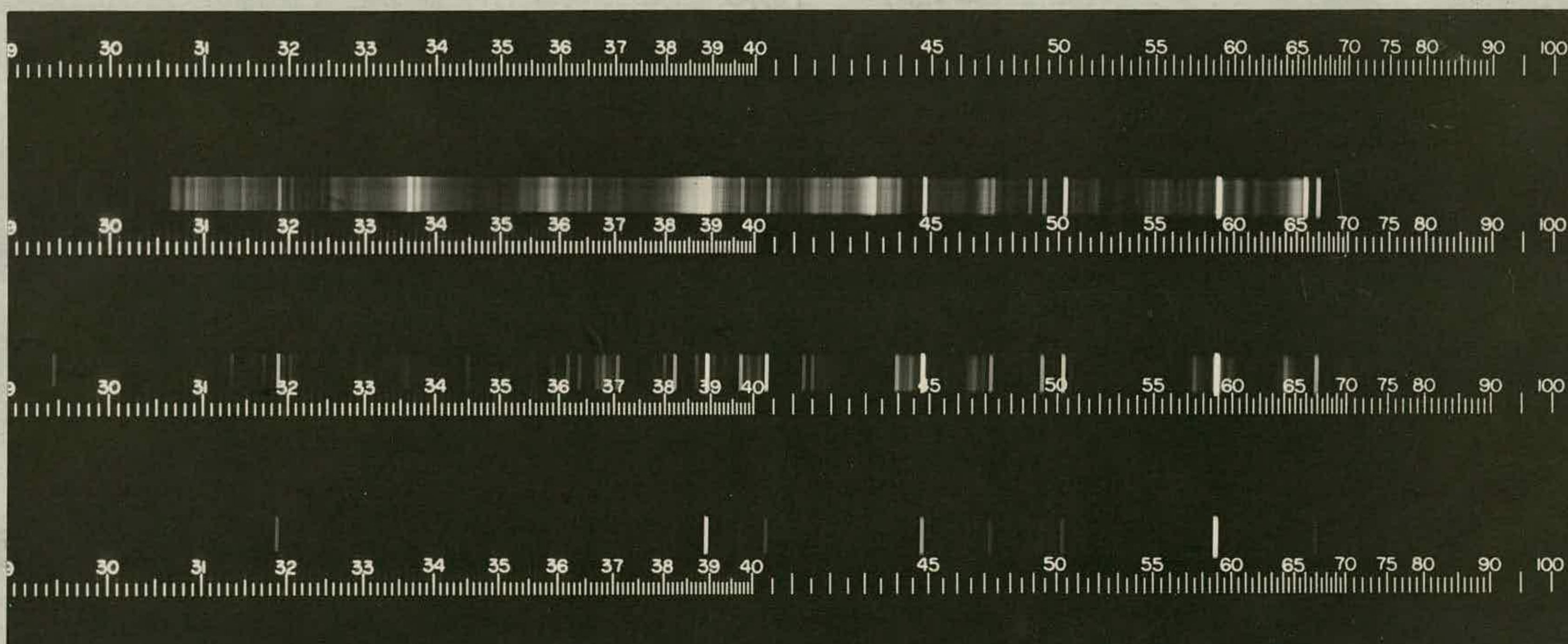
30 31 32 33 34 35 36 37 38 39 40 45 50 55 60 65 70 75 80 90 100
30 31 32 33 34 35 36 37 38 39 40 45 50 55 60 65 70 75 80 90 100
30 31 32 33 34 35 36 37 38 39 40 45 50 55 60 65 70 75 80 90 100
30 31 32 33 34 35 36 37 38 39 40 45 50 55 60 65 70 75 80 90 100

Figure 4.3.5.

characteristic of coal gas, and were probably absorbed by the electrodes when making the tube. On the other hand the sealed tubes with getters contain no detectable quantity of impurities even after considerable use and this type of tube was therefore adopted for the experiments.

As an example, one of these gettered tubes had a striking voltage of 2.2KV shortly after the getter was fired. After several hours of operation under pulsed conditions (during which cathode sputtering occured) the striking voltage altered to 2.4KV and only minor changes in the dynamic characteristics were noted.

It appears from these results that one of the simplest indications of the presence of impurities is the colour of the discharge and the appearance of stationery striations in the positive column, although as mentioned later moving striations are present even in pure gas.

CHAPTER 5

Relations between the complex dielectric constant of a discharge and the discharge parameters

5.1. Simple Lorentz Result

The problem of determining the effective dielectric constant or conductivity of an ionised gas arose originally in connection with the study of the effects of the ionosphere on radio propagation (Eccles, 1912). In this connection the problem is usually treated using the concept of collision frequency.

When an electromagnetic wave is incident on an ionised region the equation of motion for free electrons is,

$$m\frac{d\underset{\sim}{v}}{dt} = -e\left(\underset{\sim}{E} + \underset{\sim}{v} \times \underset{\sim}{B}\right) \qquad 5.1.1.$$

The motion of the relatively massive ions can be neglected, and since $v \ll c$ the force due to the magnetic field is also negligible.

Following Lorentz we introduce a term to account for losses due to collisions, so that equation 5.1.1. becomes

$$m\frac{d\underset{\sim}{v}}{dt} + g(\underset{\sim}{v}) = -e\underset{\sim}{E} \qquad 5.1.2.$$

The loss term, $g(\underset{\sim}{v})$, must have dimensions of rate of change of momentum and can be replaced by $\nu(m\underset{\sim}{v})$ where ν is the average frequency of collisions in which the total momentum is dissipated.

So that,

$$m\frac{d\underset{\sim}{v}}{dt} + \nu(m\underset{\sim}{v}) = -eE \qquad 5.1.3.$$

Assuming that v is harmonic with E, solution of equation 5.1.3. gives

$$\underset{\sim}{v} = \frac{-e\underset{\sim}{E}}{m(\nu + j\omega)} \qquad 5.1.4.$$

The corresponding current density is,

$$J = -Nev = \frac{Ne^2E}{m(\nu+j\omega)} = \underset{\sim}{\sigma} E \qquad 5.1.5.$$

so that the complex conductivity of the ionised region is

$$\underset{\sim}{\sigma} = \sigma' - j\sigma'' = \frac{Ne^2}{m}\left[\frac{\nu}{(\omega^2+\nu^2)} + j\frac{\omega}{(\omega^2+\nu^2)}\right] \qquad 5.1.6.$$

and since

$$\underset{\sim}{\epsilon_r} = \epsilon_r' - j\epsilon_r'' = \left[\left(1 + \frac{\sigma''}{\omega\epsilon_0}\right) - j\frac{\sigma'}{\omega\epsilon_0}\right] \qquad 5.1.7.$$

the complex dielectric constant is given by

$$\underset{\sim}{\epsilon_r} = \left[\left(1 - \frac{Ne^2}{m\epsilon_0(\omega^2+\nu^2)}\right) - j\frac{Ne^2\nu}{m\omega\epsilon_0(\omega^2+\nu^2)}\right] \qquad 5.1.8.$$

For a microwave frequency of 3000 Mc/s, and $\nu \sim \omega$, ϵ_r' becomes negative for electron concentrations greater than about 10^{16} electrons/metre^3.

5.2. The Isothermal Plasma

The disadvantage of the simple result of equation 5.1.8. is that it fails to take into account the distribution in energy of the electrons and therefore cannot give a proper average over all electron velocities.

Margenau (1946) has studied the case of an ionised gas in which the initial electron velocity distribution is modified by the application of a low power microwave probing signal.

If there exists an electron concentration N in the region considered and $f(v_x, v_y, v_z)\,dv_x\,dv_y\,dv_z$ have velocity components about v_x, v_y, v_z then the velocity distribution function f satisfies the Boltzmann transfer equation. (Chapman and Cowling, 1952),

viz.
$$\frac{\underset{\sim}{F}}{m}\frac{\partial f}{\partial \underset{\sim}{v}} + \underset{\sim}{v}\frac{\partial f}{\partial \underset{\sim}{r}} + \frac{\partial f}{\partial t} = \left(\frac{\partial f}{\partial t}\right)_e \qquad 5.2.1.$$

where $\underset{\sim}{F}$ denotes the force applied to an electron at (r,t) and $\left(\frac{\partial f}{\partial t}\right)_e$ represents the rate at which the velocity distribution is being altered by encounters with gas atoms.

For a uniform electron distribution $\frac{\partial f}{\partial \underset{\sim}{r}} = 0$

We can consider the force F to be simply

$$\underset{\sim}{F} = -e\underset{\sim}{E} \quad (v \ll c),$$

and specify that $\underset{\sim}{E} = E_x$

Equation 5.2.1. then becomes,

$$\frac{\partial f}{\partial t} - \frac{eE}{m}\frac{\partial f}{\partial v_x} = \left(\frac{\partial f}{\partial t}\right)_e \qquad 5.2.2.$$

Inserting $E = \hat{E}\cos\omega t$, $\gamma = \frac{e\hat{E}}{m}$, we have,

$$\frac{\partial f}{\partial t} - \gamma\cos\omega t\,\frac{\partial f}{\partial v_x} = \left(\frac{\partial f}{\partial t}\right)_e \qquad 5.2.3.$$

The velocity distribution function can be expanded in terms of the isotropic velocity distribution function $f_0(v)$ and terms involving γv_x Thus,

$$f(\underset{\sim}{v}) = f_0(v) + \gamma v_x\left[f_1(v)\cos\omega t + g_1(v)\sin\omega t\right] \qquad 5.2.4.$$

and higher order terms which we will neglect.
Where the losses are due to encounters with gas atoms at temperature T_g Chapman and Cowling give,

$$\left(\frac{\partial f_0}{\partial t}\right)_e = \frac{1}{v^2}\frac{\partial}{\partial v}\left[\frac{v^3}{M\lambda_e}\left(mvf_0 + kT_g\frac{\partial}{\partial v}f_0\right)\right] \qquad 5.2.5.$$

$$\frac{\partial}{\partial t}\left(v_x f_1\right)_e = -\frac{v_x v}{\lambda_e}f_1 \qquad 5.2.6.$$

$$\frac{\partial}{\partial t}\left(v_x g_1\right)_e = -\frac{v_x v}{\lambda_e}g_1 \qquad 5.2.7.$$

where λ_e is the mean free path for electrons and is considered to be constant.

Substituting the results of equations 5.2.4. - 5.2.7. in the Boltzmann transfer equation, equation 5.2.3. we have

$$\left[-\gamma v_x f_1 \omega \sin\omega t + \gamma v_x g_1 \omega \cos\omega t\right]$$

$$-\gamma \cos\omega t\left[\frac{v_x}{v}\frac{\partial f_0}{\partial v} + \gamma f_1 \cos\omega t + \gamma g_1 \sin\omega t\right.$$

$$\left. + \frac{\gamma v_x^2}{v}\frac{\partial f_1}{\partial v}\cos\omega t + \frac{\gamma v_x^2}{v}\frac{\partial g_1}{\partial v}\sin\omega t\right]$$

$$= \frac{1}{v^2}\frac{\partial}{\partial v}\left[\frac{v^3}{M\lambda_e}\left(mvf_0 + kT_g\frac{\partial}{\partial v}f_0\right)\right]$$

$$-\frac{\gamma v_x v}{\lambda_e} f_1 \cos\omega t - \frac{\gamma v_x v}{\lambda_e} g_1 \sin\omega t \qquad 5.2.8.$$

(Since $\frac{\partial f_0}{\partial v_x} = \frac{v_x}{v}\frac{\partial f_0}{\partial v}$)

This must be satisfied for all values of v_x. We can therefore equate terms odd in v_x and obtain.

$$-f_1 \omega \sin\omega t + g_1 \omega \cos\omega t - \frac{\cos\omega t}{v}\frac{\partial f_0}{\partial v}$$

$$= -\cos\omega t \frac{v}{\lambda_e} f_1 - \sin\omega t \frac{v}{\lambda_e} g_1 \qquad 5.2.9.$$

equating sine and cosine terms we obtain

$$g_1 = \frac{\omega\lambda_e}{v} f_1 \qquad 5.2.10$$

$$f_1 = \frac{\lambda_e}{v^2 + \omega^2\lambda_e^2}\frac{\partial f_0}{\partial v} \qquad 5.2.11$$

Equating terms even in v_x in equation 5.2.8. yields,

$$-\gamma^2 f_1 \cos^2\omega t - \gamma^2 g_1 \sin\omega t \cos\omega t - \gamma^2 \frac{v_x^2}{v}\frac{\partial f_1}{\partial v}\cos^2\omega t$$

$$-\gamma^2 \frac{v_x^2}{v}\frac{\partial g_1}{\partial v}\sin\omega t \cos\omega t$$

$$= \frac{1}{v^2}\frac{\partial}{\partial v}\left[\frac{v^3}{M\lambda_e}\left(mvf_0 + kT_g\frac{\partial}{\partial v}f_0\right)\right] \qquad 5.2.12$$

Averaging over all directions and replacing v_x^2 by its average value $\frac{v^2}{3}$ we have

$$\frac{\gamma^2}{6}\frac{\partial}{\partial v}(v^3 f_1) = \frac{1}{v^2}\frac{\partial}{\partial v}\left[\frac{v^3}{M\lambda e}\left(mv f_0 + kT_g \frac{\partial}{\partial v} f_0\right)\right] \quad 5.2.14.$$

Inserting f_1 from equation 5.2.11. and solving for f_0 leads to

$$f_0 = Ae^{-x}\left[1 + \frac{x}{x_1 + \alpha}\right]^{\alpha} \quad 5.2.15.$$

where $x = \frac{mv^2}{2kT_g}$, $x_1 = \frac{m(\omega\lambda e)^2}{2kT_g}$, $\alpha = \frac{M}{12m}\left(\frac{eE\lambda e}{kT_g}\right)^2$

The constant A can be determined by integrating in the velocity space, since the electron concentration is given by

$$N = \int f(\underset{\sim}{v})\, d\underset{\sim}{v} = 4\pi\int_0^\infty f_0(v)\, v^2 dv \quad 5.2.16.$$

For the particular case $x_1 \gg \alpha$ (i.e. $E^2 \ll \frac{6(m\omega)^2 kT_g}{Me^2}$) Margenau has shown that f_0 is Maxwellian and is given by

$$f_0 = A \exp\left[\frac{-x_1}{x_1 + \alpha} x\right] \quad 5.2.17.$$

Corresponding to a temperature

$$T_e = T_g\left(1 + \frac{\alpha}{x_1}\right) \quad 5.2.18.$$

The current density produced by the microwaves is given by

$$J = -Ne\bar{v}_x = -e\gamma\int v_x^2 (f_1 \cos\omega t + g_1 \sin\omega t)\, d\underset{\sim}{v} \quad 5.2.19.$$

On substituting the values of f_1 and g_1 given by equations 5.2.10. and 5.2.11. for Maxwellian, the corresponding complex conductivity becomes:

$$\underset{\sim}{\sigma} = \frac{4}{3}\frac{Ne^2\lambda_e}{(2\pi mkT_g)^{1/2}}\left[K_2(x_1) - jx_1^{1/2}K_{3/2}(x_1)\right] \qquad 5.2.20.$$

where

$$K_n(x_1) = \int_0^\infty \frac{x^n e^{-x}}{x_1 + x}\,dx$$

(The functions $(1/n!)\,K_n(x_1)$ have been tabulated by Dingle et al (1956) for a wide range of the argument.)

For the particular case $x_1 \to \infty$ (i.e. small collision frequency) equation 5.2.20. reduces to,

$$\underset{\sim}{\sigma} = \frac{16}{3}\frac{Ne^2}{m\omega^2\lambda_e}\left(\frac{kT_g}{2\pi m}\right)^{1/2} - j\frac{Ne^2}{m\omega} \qquad 5.2.21.$$

The imaginary part of equation 5.2.21. is identical to the imaginary part of equation 5.1.6. for $\nu \ll \omega$

Comparing the real parts, we must have

$$\frac{Ne^2\nu}{m\omega^2} = \frac{16}{3}\cdot\frac{Ne^2}{m\omega^2}\cdot\frac{1}{\lambda_e}\left(\frac{kT_g}{2\pi m}\right)^{1/2} \qquad 5.2.22.$$

so that

$$\nu = \frac{16}{3}\cdot\frac{1}{\lambda_e}\left(\frac{kT_g}{2\pi m}\right)^{1/2} \qquad 5.2.23.$$

However, the number of encounters per second is given by

$\nu_e = \dfrac{\text{mean thermal velocity}}{\text{mean free path}}$, which for a

Maxwellian velocity distribution is

$$\nu_e = \frac{4}{\lambda_e}\left(\frac{kT_g}{2\pi m}\right)^{1/2} \qquad 5.2.24.$$

so that the apparent collision frequency ν in an isothermal plasma $(T_e \sim T_g)$ is of the same order as the frequency of encounters with gas atoms, ν_e

Equation 5.2.20. is rather limited in application. Because of the restriction $x_1 \gg \alpha$ it applies only to a Maxwellian velocity distribution and as shown by equation 5.2.18. the electrons are in thermal equilibrium with the gas atoms.

If the above restriction is not satisfied

$$E^2 \nless \frac{6(m\omega)^2 kT_g}{M e^2}$$

and the electron temperature will be greater than the gas temperature due to the energy absorbed from the microwaves. This can be used as a criterion to determine if the microwave probing signal is disturbing the discharge being studied.

5.3. The general case for any specified distribution function.

In the analysis outlined in the last section only two processes were considered to contribute to the energy of the electrons, the absorption of microwave power and collisions with the gas atoms. For low microwave power levels the results obtained therefore refer to the case of electrons in thermal equilibrium with the gas atoms. However, in a practical case there may well be some other source of energy (e.g. a steady electric field) so that the electron temperature may be greater than the gas temperature and in fact the electron velocity distribution function may not be Maxwellian.

Margenau (1958) has extended the analysis to allow for any distribution function and any relation between collision frequency and electron velocity.

He has shown that in the general case the complex conductivity is given by

$$\underset{\sim}{\sigma} = \frac{Ne^2}{m}\left[I_1 - jI_2\right] \qquad 5.3.1.$$

where $$I_1 = \frac{4\pi}{3}\int_0^\infty f_{00}(v)\frac{\partial}{\partial v}\left(\frac{\nu v^3}{\omega^2+\nu^2}\right)dv \qquad 5.3.2.$$

$$I_2 = \frac{4\pi}{3}\omega\int_0^\infty f_{00}(v)\frac{\partial}{\partial v}\left(\frac{v^3}{\omega^2+\nu^2}\right)dv \qquad 5.3.3.$$

provided that $$4\pi\int_0^\infty f_{00}(v)\,v^2\,dv = 1$$

$f_{00}(v)$ is the isotropic distribution function due to all sources of energy excluding the microwaves.

If ν is independent of v equations 5.3.2. and 5.3.3. lead to the simple Lorentz result for any arbitrary distribution function.

It is more realistic to consider the case of constant mean free path, then $\nu \propto v$ For electrons having a Maxwellian velocity distribution function corresponding to a temperature T_e.,

$$f_{00} = \left(\frac{m}{2\pi k T_e}\right)^{3/2} \exp\left(-mv^2/2kT_e\right) \qquad 5.3.4.$$

Fang (1959) has expressed the corresponding values of I_1 and I_2 in terms of the functions tabulated by Dingle et al (1956). However, in terms of the functions used in equation 5.2.20. the complex conductivity is

$$\underset{\sim}{\sigma} = \frac{4Ne^2}{3\pi^{1/2}m}\frac{1}{\nu_0}\left[K_2(x_2) - j x_2^{1/2} K_{3/2}(x_2)\right] \qquad 5.3.5.$$

where $x_2 = \left(\frac{\omega}{\nu_0}\right)^2$ and ν_0 is the collision frequency corresponding to $v = v_0 = \left(\frac{2kT_e}{m}\right)^{1/2}$

But since $\nu_0 = \frac{v_0}{\lambda_e} = \left(\frac{2kT_e}{m}\right)^{1/2} \cdot \frac{1}{\lambda_e}$

equation 5.3.5. becomes

$$\underset{\sim}{\sigma} = \frac{4}{3}\frac{Ne^2\lambda_e}{(2\pi m k T_e)^{1/2}}\left[K_2(x_2) - j x_2^{1/2} K_{3/2}(x_2)\right] \qquad 5.3.6.$$

where $x_2 = \frac{m(\omega\lambda_e)^2}{2kT_e}$

Equation 5.3.6. is almost identical to equation 5.2.20. but T_e replaces T_g. We see therefore that equation 5.2.20. can be applied to electrons of any temperature provided that the excess electron energy is not due to the effects of the microwaves.

For electrons uniformly distributed in energy up to some maximum value corresponding to a velocity v_1 and collision frequency ν_1, Margenau has shown that the Lorentz result is applicable if ν is replaced by ν_1

If all the electrons have the same energy, then

$$\underset{\sim}{\sigma} = \frac{Ne^2}{m(\omega^2+\nu^2)^2}\left[\left(\tfrac{4}{3}\omega^2 + \tfrac{2}{3}\nu^2\right)\nu - j\omega\left(\omega^2+\tfrac{1}{3}\nu^2\right)\right] \quad 5.3.7.$$

5.4. Comparison of the various results.

Since the distribution function is generally unknown in practice, and for some regions of a d.c. discharge it is certainly not Maxwellian (Pringle and Farvis, (1955)), it is convenient to use the simple Lorentz result for the complex conductivity.

It is therefore necessary to estimate the errors which might arise from this assumption when the electron velocity distribution function has the various forms considered above.

The Maxwellian case has been considered previously by Margenau and Stillinger (1959) and Fang (1959).

The values of ωI_1 and ωI_2 corresponding to equations 5.1.6., 5.3.6. and 5.3.7. are plotted as a function of $\left(\frac{\omega}{\nu}\right)$ in Figures 5.4.1. and 5.4.2. respectively.

It can be seen that these functions are relatively insensitive to the form of the velocity distribution function. Microwave measurements therefore yield little information about the velocity distribution function. For $\omega \sim \nu$ the values of ωI_1 given by equations 5.3.6. and 5.3.7. differ from the Lorentz result only by about 10%. The error is much greater for extreme values of $\left(\frac{\omega}{\nu}\right)$. In the case of ωI_2 the difference is approximately 30% for $\omega \sim \nu$ and decreases rapidly as $\left(\frac{\omega}{\nu}\right)$ increases.

In practice the real and imaginary parts of the conductivity are measured, while the electron concentration, velocity distribution function, and collision frequency are unknown. However, referring to equation 5.1.6. we see that, if the Lorentz result is applicable $\frac{\sigma''}{\sigma'} = \frac{I_2}{I_1} = \left(\frac{\omega}{\nu}\right)$

The electron concentration can then be conveniently determined from the imaginary part of the conductivity since this can be more accurately measured.

For $\omega \sim \nu$ this has the effect of reducing the error in the calculation of electron concentration. For example, if all electrons have the same energy and $I_2/I_1 = 2$ the correct value of $\left(\frac{\omega}{\nu}\right)$ is approximately 2.75 (See Fig. 5.4.3.) while equation

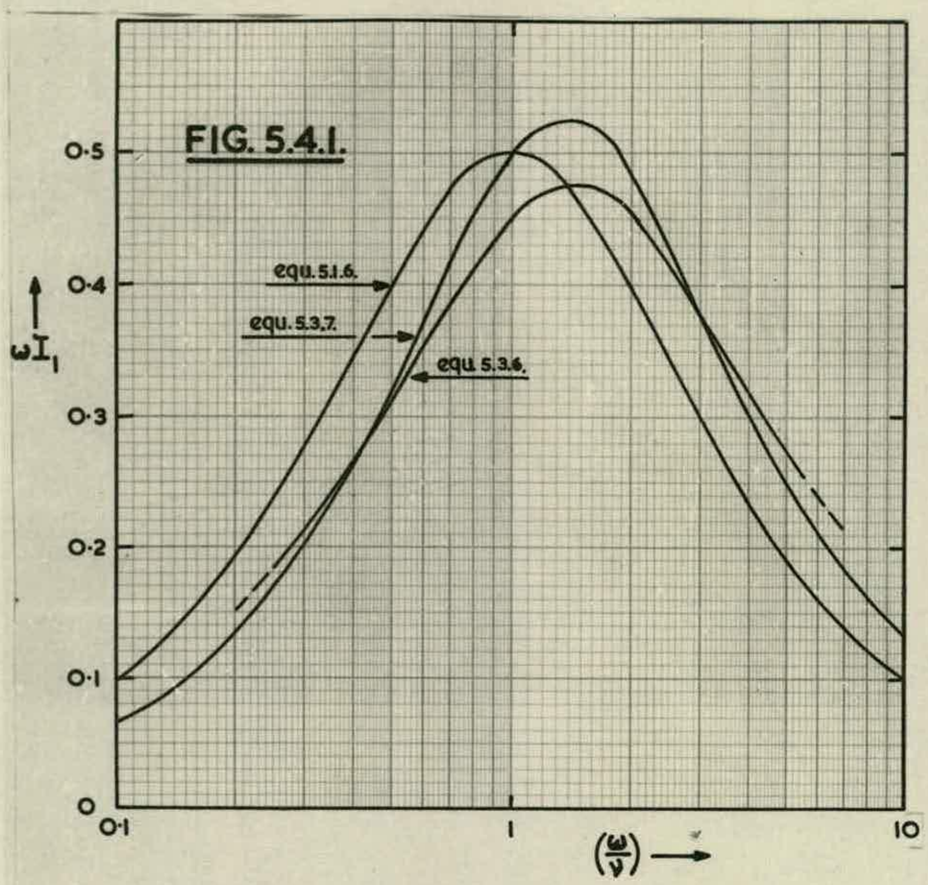
FIG. 5.4.1.
equ. 5.1.6.
equ. 5.3.7.
equ. 5.3.6.
ωI₁
0·5
0·4
0·3
0·2
0·1
0
0·1
1
10
(ω/ν)

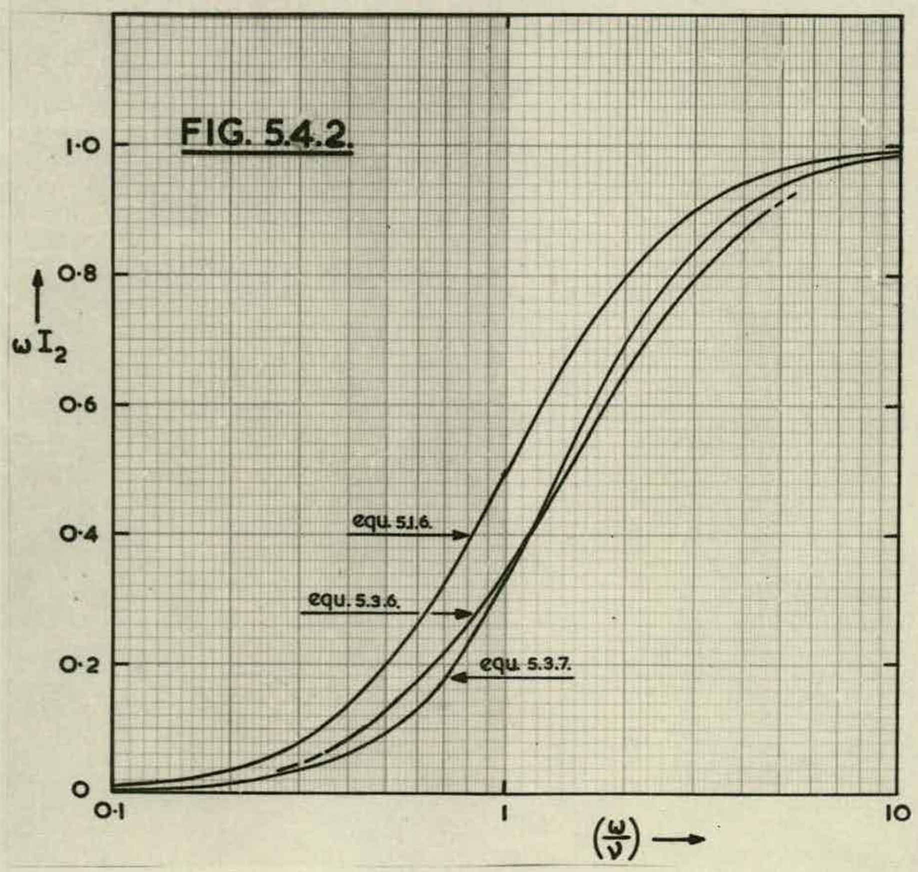
FIG. 5.4.2.
equ. 5.1.6.
equ. 5.3.6.
equ. 5.3.7.
ωI₂
1·0
0·8
0·6
0·4
0·2
0
0·1
1
10
(ω/ν)

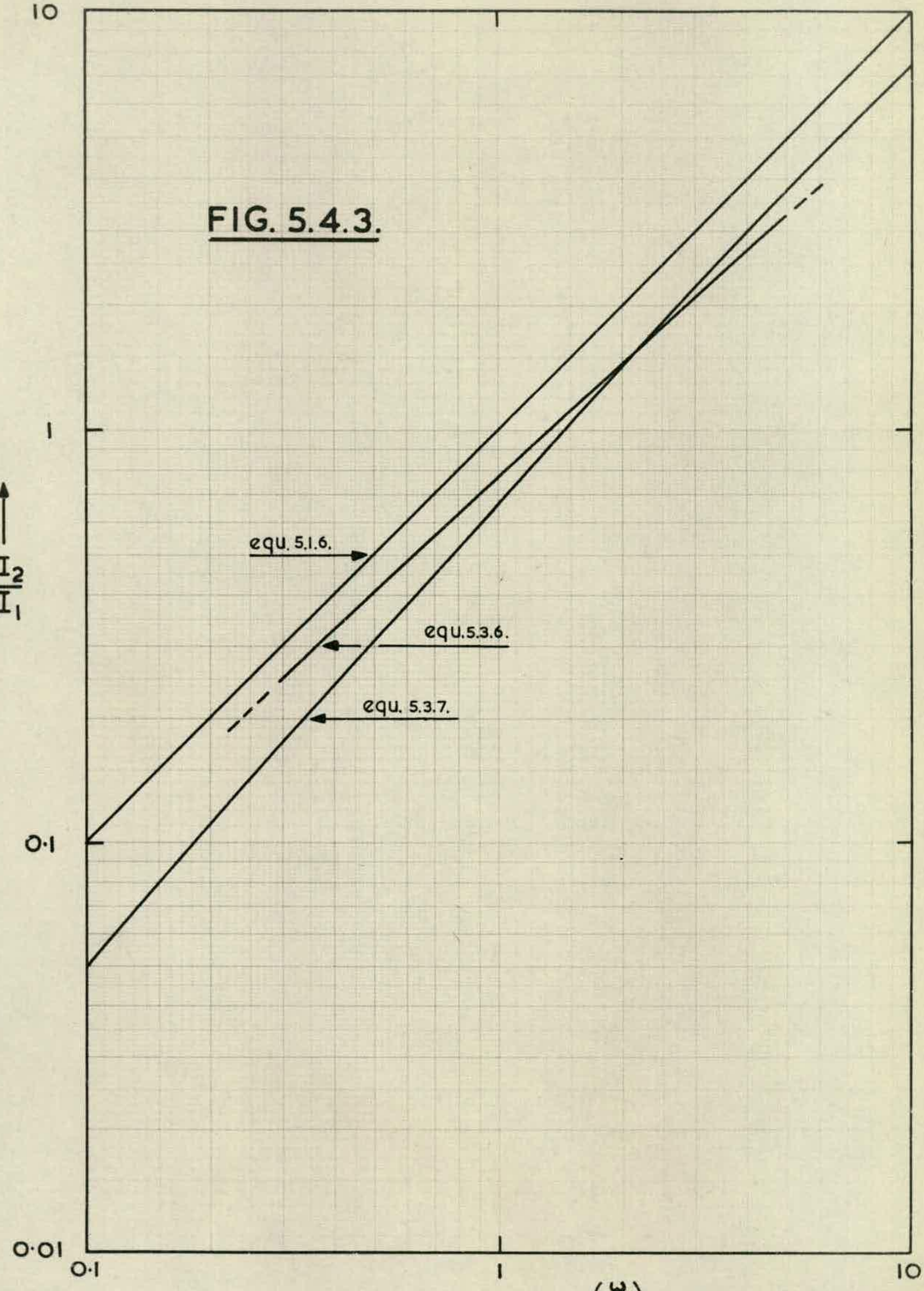
FIG. 5.4.3.
10
1
0·1
0·01
0·1
1
10
$\frac{I_2}{I_1}$
$\left(\frac{\omega}{\nu}\right)$
equ. 5.1.6.
equ. 5.3.6.
equ. 5.3.7.

5.1.6. gives a value of 2. From figure 5.4.2. the correct value of ωI_2 is 0.81 and the Lorentz result gives 0.80.

It has been shown above that equation 5.1.6. is applicable for any electron velocity distribution function if ν is independent of v. However, the collision cross section for helium is constant for electron energies up to a few electron volts (Hirshfield and Brown, 1958) so that $\nu \propto v$
In this case, even when all electrons have the same energy the use of equation 5.1.6. leads to an error of only approximately 25% in $\left(\frac{\omega}{\nu}\right)$, for $\left(\frac{\omega}{\nu}\right)$ in the range 1 $\rightarrow$ 10 (which is the range appropriate to these experiments) while the error in the calculated electron concentration is negligible.

During the latter stages of recombination in an isolated discharge the electron velocity distribution function will tend to be Maxwellian and equation 5.3.6. will apply. However, if the distribution function is unknown the Lorentz formula will yield reliable values for the electron concentration while the calculated values of collision frequency may be 20% to 30% high in some extreme cases.

CHAPTER 6

Dielectric Post Theory

The method used in these experiments to obtain values for the discharge parameters relies on the measurement of the microwave admittance of the discharge considered as a dielectric post across the waveguide. The results discussed in Chapter 5 give the discharge parameters N, ν and T_e in terms of the complex dielectric constant or conductivity of the discharge. A relation between the microwave admittance and the dielectric constant of the discharge is therefore required before the discharge parameters can be calculated.

6.1. An Approximate Equation

In similar experiments on a d.c. discharge Prime (1952) has used a result due to Frank (1943), which is also given by Montgomery et al (1948) and Moreno(1948).

Frank's result was obtained for a centred dielectric post using the method of images, which reduces the problem to that of an infinite grating of parallel dielectric rods. For a post of small diameter the equivalent circuit is a simple shunt admittance across the waveguide.

According to Frank the shunt admittance is given by

$$\frac{1}{\underset{\sim}{y}} = j\,\frac{a}{2\lambda_g}\left[\log_e\frac{\lambda_0}{R} - f\left(\frac{a}{\lambda_0}\right) - \frac{1}{2\underset{\sim}{\epsilon_r}}\left(\frac{\lambda_0}{\pi R}\right)^2 - 1{\cdot}47\right] \quad 6.1.1.$$

so that the complex dielectric constant is given by,

$$\underset{\sim}{\epsilon_r} = \frac{\frac{1}{2}\left(\frac{\lambda_o}{\pi R}\right)^2}{\left[\log_e \frac{\lambda_o}{R} - f\left(\frac{a}{\lambda_o}\right) - 1.47 - j\frac{2\lambda_g}{a\underset{\sim}{y}}\right]} \qquad 6.1.2.$$

The function $f\left(\frac{a}{\lambda_o}\right)$ is almost linear and can be represented by,

$$f\left(\frac{a}{\lambda_o}\right) = -1.775\frac{a}{\lambda_o} + 2.214 \qquad 6.1.3.$$

Substituting this result in equation 6.1.2. yields,

$$\underset{\sim}{\epsilon_r} = \frac{\frac{1}{2}\left(\frac{\lambda_o}{\pi R}\right)^2}{\left[\log_e \frac{\lambda_o}{R} + 1.775\frac{a}{\lambda_o} - j\frac{2\lambda_g}{a\underset{\sim}{y}} - 3.684\right]} \qquad 6.1.4.$$

For a 7.5 mm. diameter post in W.G. No.10 at λ_o = 10 cm equation 6.1.4. reduces to the simple equation,

$$\underset{\sim}{\epsilon_r} = \frac{40.7\underset{\sim}{y}}{\underset{\sim}{y} + j4.35} \qquad 6.1.5.$$

Frank states that equation 6.1.1. is valid provided that $\left(\frac{2\pi R}{\lambda_o}\right)^2 \ll 1$. However, Montgomery gives equation 6.1.1. along with the restriction $\left|\underset{\sim}{\epsilon_r}\right|\left(\frac{2\pi R}{\lambda_o}\right)^2 \ll 1$. Prime has assumed that the restriction given by Frank is sufficient. For the discharge tubes used in this case (R = 3.75 mm., λ_o = 10 cm.), $\left(\frac{2\pi R}{\lambda_o}\right)$ = 0.055 so that this restriction would be satisfied, but since $\left|\underset{\sim}{\epsilon_r}\right|$ may be of the order of 10 for reasonable electron concentrations the more severe restriction given by Montgomery would be violated.

Frank (1959) has suggested that the range of application of equation 6.1.1. could be investigated by measuring the microwave admittance of dielectric posts of known dielectric constant. Unfortunately most common materials have a dielectric constant of the order of 3, with the exception of water. Some of the hydrocarbons have dielectric constants of 10 to 20 but they all have marked absorption in the microwave region and reliable values for their dielectric constants are not available.

Experimental results obtained for distilled water ($\epsilon_r = 77$, Marcuvitz (1951a.)) and perspex ($\epsilon_r = 2.24$) gave values of $\underset{\sim}{\epsilon_r} = 67 - j63$ and $\underset{\sim}{\epsilon_r} = 1.6 - j0.2$ respectively, after substitution in equation 6.1.4. This indicates that the error is much greater for a large dielectric constant (although this may be partly due to leakage through the holes in the waveguide walls) and it seems that the restriction given by Frank is insufficient.

Further, if there is no dielectric post so that $\underset{\sim}{y} = 0$, then from equation 6.1.4. $\underset{\sim}{\epsilon_r} = 0$. In fact we should find $\underset{\sim}{\epsilon_r} = 1$. Alternatively, if $\underset{\sim}{\epsilon_r}$ is assumed to be unity we find $\underset{\sim}{y}$ finite. Prime has argued that this admittance is due to the displacement current produced in the post when $\underset{\sim}{\epsilon_r} = 1$. This argument must be false since a dielectric post with $\underset{\sim}{\epsilon_r} = 1$ produces no discontinuity in the waveguide and no admittance could be measured experimentally.

Equation 6.1.1. cannot be applied to the present problem as the restriction $|\underset{\sim}{\epsilon_r}|\left(\frac{2\pi R}{\lambda_0}\right)^2 \ll 1$ would not be satisfied, but it seems that there may also be some doubt regarding the general validity of this result.

6.2. The General Equation.

The problem of a conducting post in a rectangular waveguide can be solved by replacing the post by a suitable current system in the position of the post axis (Lewin, 1951). The current distribution must be chosen so that the fields produced at the surface of the post by these currents and the incident wave satisfy the boundary conditions. The principal mode produced in the waveguide by this assumed current distribution can then be calculated and combined with the incident wave to give the transmission and reflection coefficients for the post. A suitable equivalent circuit can then be deduced.

It may be possible to extend this method of solution to cover the case of a dielectric post although the boundary conditions are not so simple as for the perfectly conducting post and the solution would be more difficult.

An alternative approach is the direct solution of the field equations satisfying the boundary conditions for a dielectric post in a rectangular waveguide. This latter method has been used by Schwinger (Marcuvitz 1951.b.).

The results, which are given below, are for a post of radius R placed a distance x from the waveguide wall and parallel to the electric field in the waveguide. The equivalent circuit takes the form of a T-network with normalised shunt arm impedance z_a and normalised series arm impedances z_b. Where z_a and z_b are given by,

$$z_a + \frac{1}{2} z_b = -j\frac{a}{2\lambda_g} \operatorname{cosec}^2\left(\frac{\pi x}{a}\right) \times$$

$$\left[\frac{J_0(\beta)}{J_0(\alpha)} \frac{1}{\beta J_0(\alpha) J_1(\beta) - \alpha J_0(\beta) J_1(\alpha)} - S_0 + \frac{\alpha^2}{4}\right] \quad 6.2.1.$$

$$z_b = \frac{-j\dfrac{2a}{\lambda_g}\left(\dfrac{2\pi R}{a}\right)^2 \sin^2\dfrac{\pi x}{a}}{\left[\alpha^2 \dfrac{J_1(\beta)}{J_0(\alpha)} \dfrac{1}{\alpha J_0(\alpha) J_1(\beta) - \beta J_0(\beta) J_1(\alpha)} - 2\right]} \quad 6.2.2.$$

where $\alpha = \dfrac{2\pi R}{\lambda_0}$, $\beta = \alpha\sqrt{\underset{\sim}{\epsilon_r}}$

and $$S_0 = \log_e\left(\frac{4a}{2\pi R}\sin^2\frac{\pi x}{a}\right) - 2\sin^2\frac{\pi x}{a}$$

$$+ 2\sum_{n=2}^{\infty} \sin^2\left(\frac{n\pi x}{a}\right)\left[\frac{1}{\sqrt{n^2 - \left(\frac{2a}{\lambda_0}\right)^2}} - \frac{1}{n}\right]$$

For a small diameter post $\left(\frac{2R}{a}\right) < 0.1$ say, or $\underset{\sim}{\epsilon_r}$ close to unity, z_b is negligible, so that the equivalent circuit reduces to a simple shunt admittance. For a centred post $(x = a/2)$ this is,

$$\frac{1}{\underset{\sim}{y}} = z_a = -j\frac{a}{2\lambda_g}\left[\frac{J_0(\beta)}{J_0(\alpha)}\cdot\frac{1}{\beta J_0(\alpha)J_1(\beta) - \alpha J_0(\beta)J_1(\alpha)} - S_0 + \frac{\alpha^2}{4}\right] \quad 6.2.4.$$

where
$$S_0 = \log_e\left(\frac{4a}{2\pi R}\right) - 2 + 2\sum_{\substack{n=2 \\ n \text{ odd}}}^{\infty}\left[\frac{1}{\sqrt{\frac{1}{n} - \left(\frac{2a}{\lambda_0}\right)^2}} - \frac{1}{n}\right]$$

Rearranging equation 6.2.4. we obtain,

$$\beta\frac{J_1(\beta)}{J_0(\beta)} = \frac{1}{J_0^2(\alpha)}\cdot\frac{1}{\left[S_0 - \frac{\alpha^2}{4} + j\frac{2\lambda_g}{a\underset{\sim}{y}}\right]} + \alpha\frac{J_1(\alpha)}{J_0(\alpha)} \quad 6.2.5.$$

Substituting the constants for a 7.5 mm. diameter discharge in W.G. No.10 at λ_0 = 10 cm. (see Appendix B) we obtain,

$$\beta\frac{J_1(\beta)}{J_0(\beta)} = \frac{0.26733}{0.16035 + j/\underset{\sim}{y}} + 0.02795 \quad 6.2.6$$

Now if $\alpha, \beta \ll 1$ we can approximate the Bessel functions by the first term of the series expansions and equation 6.2.6. reduces to

$$\frac{\beta^2}{2} = \frac{\alpha^2}{2}\underset{\sim}{\epsilon_r} = \frac{0.26733}{0.16035 + j/\underset{\sim}{y}} + 0.02795$$

or,

$$(\underset{\sim}{\epsilon_r} - 1) = \frac{60\underset{\sim}{y}}{\underset{\sim}{y} + j6.35} \quad 6.2.7$$

This is of similar form to equation 6.1.5. derived from Frank's result. However, if $\underset{\sim}{\epsilon_r} = 1$ in equation 6.2.7. $\underset{\sim}{y} = 0$ as we might expect.

Unfortunately, equation 6.2.4. gives the microwave admittance for a post of known dielectric constant. In fact the dielectric constant is the unknown in this case and a solution to equation 6.2.6. must be obtained for known values of the admittance.

6.3. Solution of the general equation.

Equation 6.2.6. cannot be solved directly. However, if a suitable range of values for the real and imaginary parts of β is chosen and the corresponding values of admittance are calculated using equation 6.2.6. then the dielectric constant corresponding to any measured admittance can be obtained by interpolating between these results. The microwave admittance corresponding to any chosen value of complex dielectric constant can be readily calculated with the aid of a digital computer.

In practice the imaginary part of the dielectric constant is always negative, while the real part may be positive or negative depending on the electron concentration. Thus $\underset{\sim}{\epsilon_r}$ always lies in the third or fourth quadrant of the complex plane,
and so β will always lie in the second quadrant, so that the real part of β is always negative and the imaginary part is positive. Thus $\beta = (-l + jm)$

Assuming that $l > m$ and expanding the left hand side of equation 6.2.6. about ℓ using Taylor's theorem (see Appendix B),

$$\beta \frac{J_1(\beta)}{J_0(\beta)} = \ell J - jm\left[\ell + \ell J^2\right]$$

$$- \frac{m^2}{2}\left[1 + 2\ell J - J^2 + 2\ell J^3\right]$$

$$+ j\frac{m^3}{6}\left[2\ell - 2J + \left(8\ell + \frac{2}{\ell}\right)J^2 - 6J^3 + 6\ell J^4\right]$$

$$+ \frac{m^4}{24}\left[\left(16\ell + \frac{6}{\ell}\right)J - \left(28 + \frac{6}{\ell^2}\right)J^2 + \left(40\ell + \frac{22}{\ell}\right)J^3\right.$$

$$\left. - 36J^4 + 24\ell J^5\right] + \cdots = A + jB$$

6.3.1.

where $J \equiv \frac{J_1(\ell)}{J_0(\ell)}$

so that

$$A = \ell J - \frac{m^2}{2}\left[1 + 2\ell J - J^2 + 2\ell J^3\right] + \cdots$$

6.3.2.

$$B = -m\left[\ell + \ell J^2\right]$$

$$- \frac{m^3}{6}\left[2\ell - 2J + \left(8\ell + \frac{2}{\ell}\right)J^2 - 6J^3 + 6\ell J^4\right] + \cdots$$

6.3.3.

If $l < m$ substitution of jm for l and $-jl$ for m will give the corresponding expansion about m

Since $J_0(jm) = I_0(m)$ and $J_1(jm) = j\,I_1(m)$, where $I_0(m)$ and $I_1(m)$ are modified Bessel functions of imaginary argument (Watson, 1952), equations 6.3.2. and 6.3.3. become,

$$A = -mI + \frac{l^2}{2}\left[1 - 2mI + I^2 + 2mI^3\right] + \cdots \qquad 6.3.4.$$

$$B = -l\left[m - mI\right] - \frac{l^3}{6}\left[2m - 2I - \left(8m - \frac{2}{m}\right)I^2 + 6I^3 + 6mI^4\right] + \cdots \qquad 6.3.5.$$

where $I \equiv \dfrac{I_1(m)}{I_0(m)}$

The imaginary part of the dielectric constant is normally small so that $|\epsilon_r'| > |\epsilon_r''|$, so that $m > l$ and equations 6.3.4. and 6.3.5. must be used. If the collision frequency is high or the electron concentration is low so that $l > m$ equations 6.3.2. and 6.3.3. will apply.

Preliminary experiments indicated that the electron concentration was unlikely to exceed 10^{18} electrons/metre^3, while the collision frequency was of the order of 10^{10}/sec. Then equation 5.1.6. gives

$$\epsilon_r' = \left[1 - \frac{Ne^2}{m\epsilon_0(\omega^2 + \nu^2)} \right] \sim -10$$

and

$$\epsilon_r'' = \frac{Ne^2\nu}{m\omega\epsilon_0(\omega^2+\nu^2)} \sim 3$$

so that $\underset{\sim}{\epsilon_r} \sim (-10 - j3)$
and $\beta = \alpha\sqrt{\underset{\sim}{\epsilon_r}} = (-0.15 + j\,0.75)$

In the computation values of ℓ have been taken in the range $0 \rightarrow 0.2$ in steps of 0.05 and values of m in the range $0 \rightarrow 1$ in steps of 0.01 and 0.02.

An autocode programme has been prepared for the Pegasus digital computer to calculate the admittance corresponding to each value of ℓ and m in the ranges given above. A copy of the programme together with the tabulated results is given in Appendix B.

The series expansions given in equations 6.3.2. - 6.3.5. converge rapidly and a preliminary programme check showed that terms of higher order than ℓ^4 or m^4 can be neglected. The Bessel functions are calculated from the appropriate series expansions, four or five terms being sufficient. In order to simplify the programme both forms of the series expansion for $\beta \dfrac{J_1(\beta)}{J_\alpha(\beta)}$ have been computed

and the corresponding values of $\underset{\sim}{y}$ given by equation 6.2.6. tabulated. The appropriate solution for $\ell > m$ or $m > \ell$ being selected by inspection.

The relevant results are plotted in Fig. 6.3.1. For large values of m the real part of the admittance is determined largely by the value of ℓ, while m controls the imaginary part. The locus for $\ell = \alpha = 0.236$ would of course pass through the origin, corresponding to $\underset{\sim}{\epsilon_r} = (1 + j0)$

The corresponding plot of $\underset{\sim}{\epsilon_r}$ against $\underset{\sim}{y}$ obtained from Fig. 6.3.1. by interpolation, is given in Fig. 6.3.2., which can be used to give the complex dielectric constant directly from the measured microwave admittance. As might be expected the real part of the dielectric constant tends to control the susceptance and the imaginary part the conductance.

The interpolation required to obtain the results of Fig. 6.3.2. could be avoided if the values of ℓ and m corresponding to any given value of $\underset{\sim}{\epsilon_r}$ were calculated as part of the programme and then substituted in Equation 6.2.6., but at the time of these calculations this was considered an unnecessary complication.

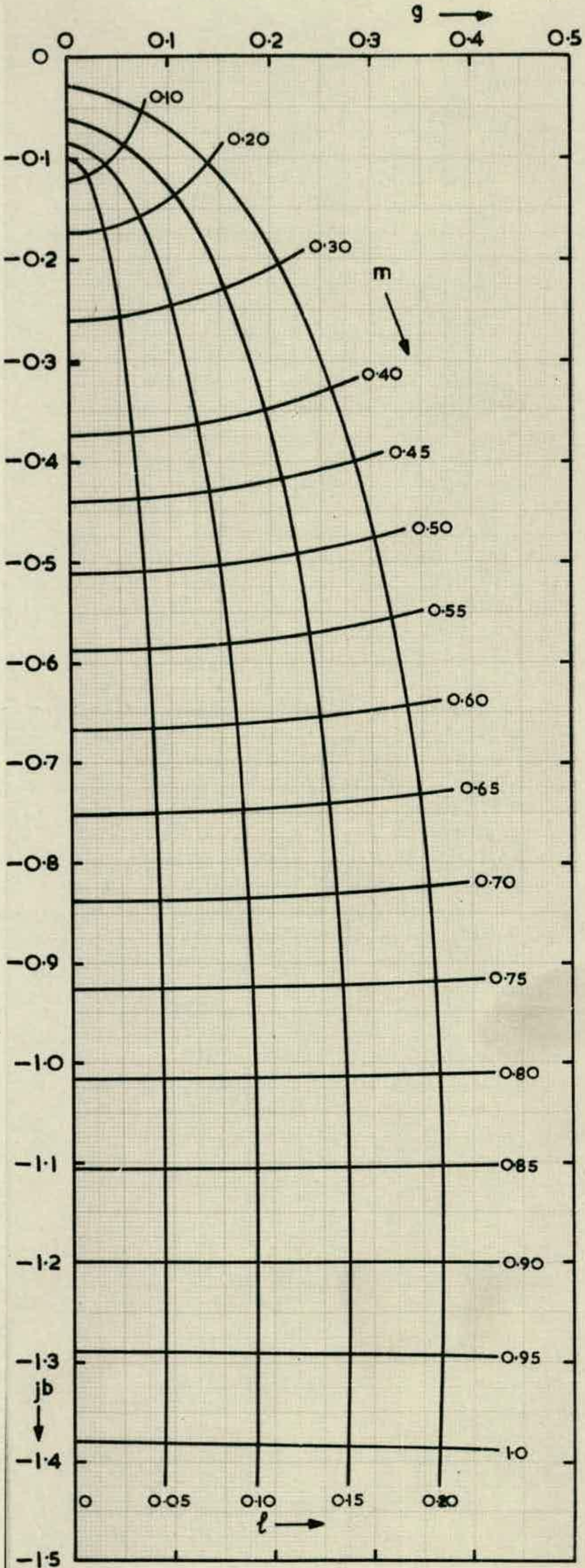

g
0
0·1
0·2
0·3
0·4
0·5
0
−0·1
−0·2
−0·3
−0·4
−0·5
−0·6
−0·7
−0·8
−0·9
−1·0
−1·1
−1·2
−1·3
−1·4
−1·5
jb
m
0·10
0·20
0·30
0·40
0·45
0·50
0·55
0·60
0·65
0·70
0·75
0·80
0·85
0·90
0·95
1·0
0
0·05
0·10
0·15
0·20
l

FIG. 6.3.I.

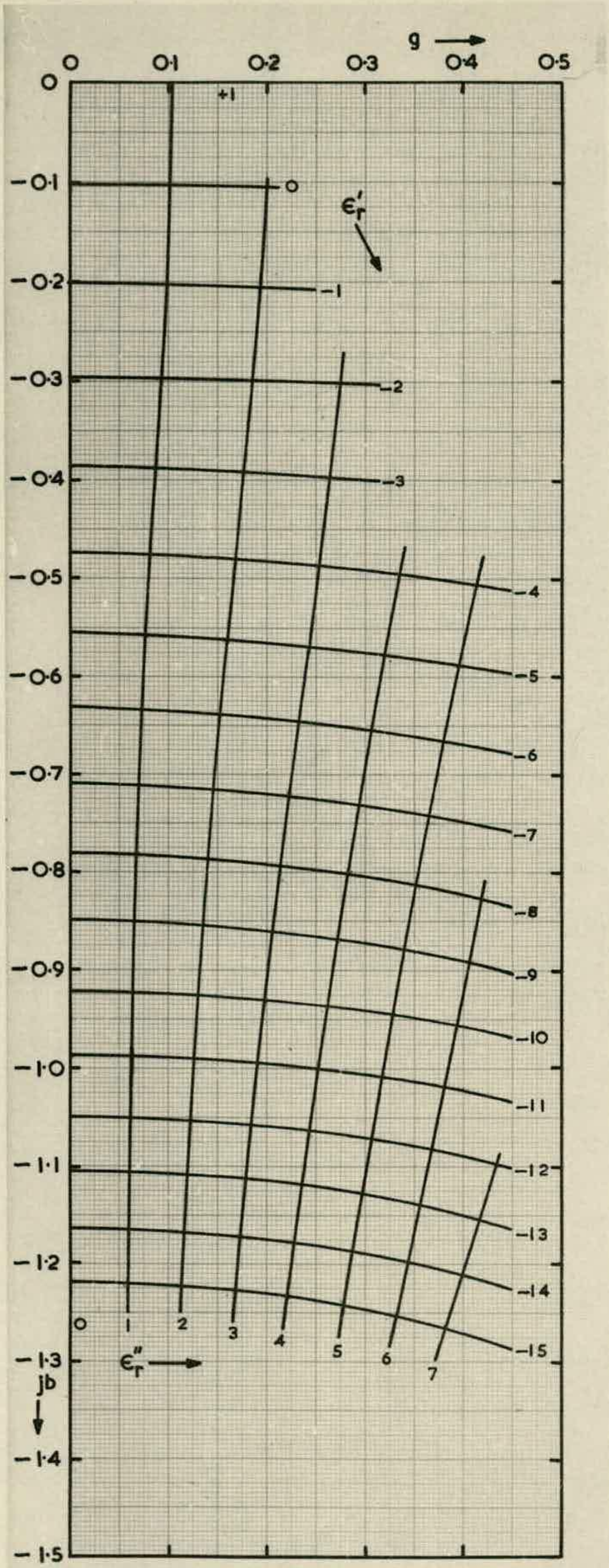
g
0
0·1
0·2
0·3
0·4
0·5
0
−0·1
−0·2
−0·3
−0·4
−0·5
−0·6
−0·7
−0·8
−0·9
−1·0
−1·1
−1·2
−1·3
jb
−1·4
−1·5
ϵ_r'
+1
0
−1
−2
−3
−4
−5
−6
−7
−8
−9
−10
−11
−12
−13
−14
−15
ϵ_r''
0
1
2
3
4
5
6
7

FIG. 6.3.2.

Chapter 7

The Experimental Results

7.1. Accuracy of the microwave measurements

The accuracy with which the microwave admittance of the discharge can be measured is limited by the residual v.s.w.r. in the system. In practice the residual v.s.w.r. was approximately 0.98, which could lead to an error in the normalised conductance or susceptance of the order of $\pm$ 0.02. Referring to Fig. 6.3.2. the corresponding error in ϵ_r' or ϵ_r'' is of the order of $\pm$ 0.2.

The v.s.w.r. is obtained from results similar to those shown in Fig. 3.4.4. The magnitude of the v.s.w.r. can be obtained with negligible error, but there may be an error in the measured position of the minimum. In these experiments the admittance measured represents the admittance of the discharge itself plus the admittance of the pyrex tube and matched waveguide system. The normalised susceptance varies over the range $0 \rightarrow -1$, while the conductance varies from $0 \rightarrow 0.5$, and the pyrex tube has an admittance of $\underset{\sim}{y} = 1.00 + j0.125$.

In this region of the admittance chart an error in the position of the minimum has little effect on the susceptance, but leads to an error in the conductance. For example, an error of 0.05 cm. ($\sim 0.0035\lambda$) in the position of the minimum would lead to an error in the conductance of the order of 0.01, equivalent to an error of 0.1 in ϵ_r''

Errors introduced in reading the admittance chart or determining $\underset{\sim}{\epsilon_r}$ from Fig. 6.3.2. will be small compared with the errors discussed above, so that the error in ϵ_r' and ϵ_r'' should not be much greater than $\pm$ 0.2. For reasonable values of electron concentration and collision frequency this might correspond to an error of the order of 10%.

The v.s.w.r. produced by the pyrex tube in W.G. No.10 is approximately 0.86, while the tube mounted in the binomial transformer gives a value of 0.88. The normalised admittance should of course be unchanged. Allowing for the residual v.s.w.r. of 0.98 this result is satisfactory.

As a check on the accuracy which could be obtained a measurement was made using a section of discharge tube filled with perspex ($\underset{\sim}{\epsilon_r}$ = 2.22 + j0). The measured admittance was $\underset{\sim}{y}$ = -0.01 + j0.140. Positive values of susceptance are not plotted in Fig. 6.3.2., but referring to the table of computed values in Appendix B we obtain the value of = 2.31 - j0.09, which is within the limits of error discussed above.

Referring to equations 5.1.6. and 5.1.7.,

$$\frac{\nu}{\omega} = \frac{\epsilon_r''}{1 - \epsilon_r'} \qquad 7.1.1.$$

Values of collision frequency calculated using this result may therefore be in error by about 20%. However, the real part of equation 5.1.8. leads

$$N = (1 - \epsilon_r')\frac{m\epsilon_0\omega^2}{e^2}\left(1 + \left(\frac{\nu}{\omega}\right)^2\right) \qquad 7.1.2.$$

In these experiments $\frac{\nu}{\omega} < 1$ so that the accuracy of the calculated values of electron concentration is limited by the error in ϵ_r'

The electron temperature can be obtained from equation 5.3.6., since

$$\frac{\sigma''}{\sigma'} = \frac{1 - \epsilon_r'}{\epsilon_r''} = \frac{x_2^{\frac{1}{2}} K_{3/2}(x_2)}{K_2(x_2)} \rightarrow \frac{3\sqrt{\pi}}{8} x_2^{\frac{1}{2}} \text{ for } x_2 \gg 1 \qquad 7.1.3.$$

where $x_2 = \dfrac{m(\omega\lambda_e)^2}{2kT_e}$

$\frac{\sigma''}{\sigma'}$ is plotted as a function of x_2 in Fig. 7.1.1. In this case the accuracy will be of the same order as that obtained for the values of collision frequency, although for large values of $\frac{\sigma''}{\sigma'}$ the error will be doubled.

Values of electron temperature deduced from the microwave measurements must be treated cautiously since the term electron temperature is only strictly applicable to the case of a Maxwellian velocity distribution function. In fact the distribution function in the negative glow region of a discharge is not normally Maxwellian, although it may tend to be so during the recombination period at the end of the current pulse.

As well as the errors introduced by the limited accuracy of the microwave equipment it must be remembered that values of electron concentration obtained are average values over the cross section and a 1 cm. length of the discharge tube. On the other

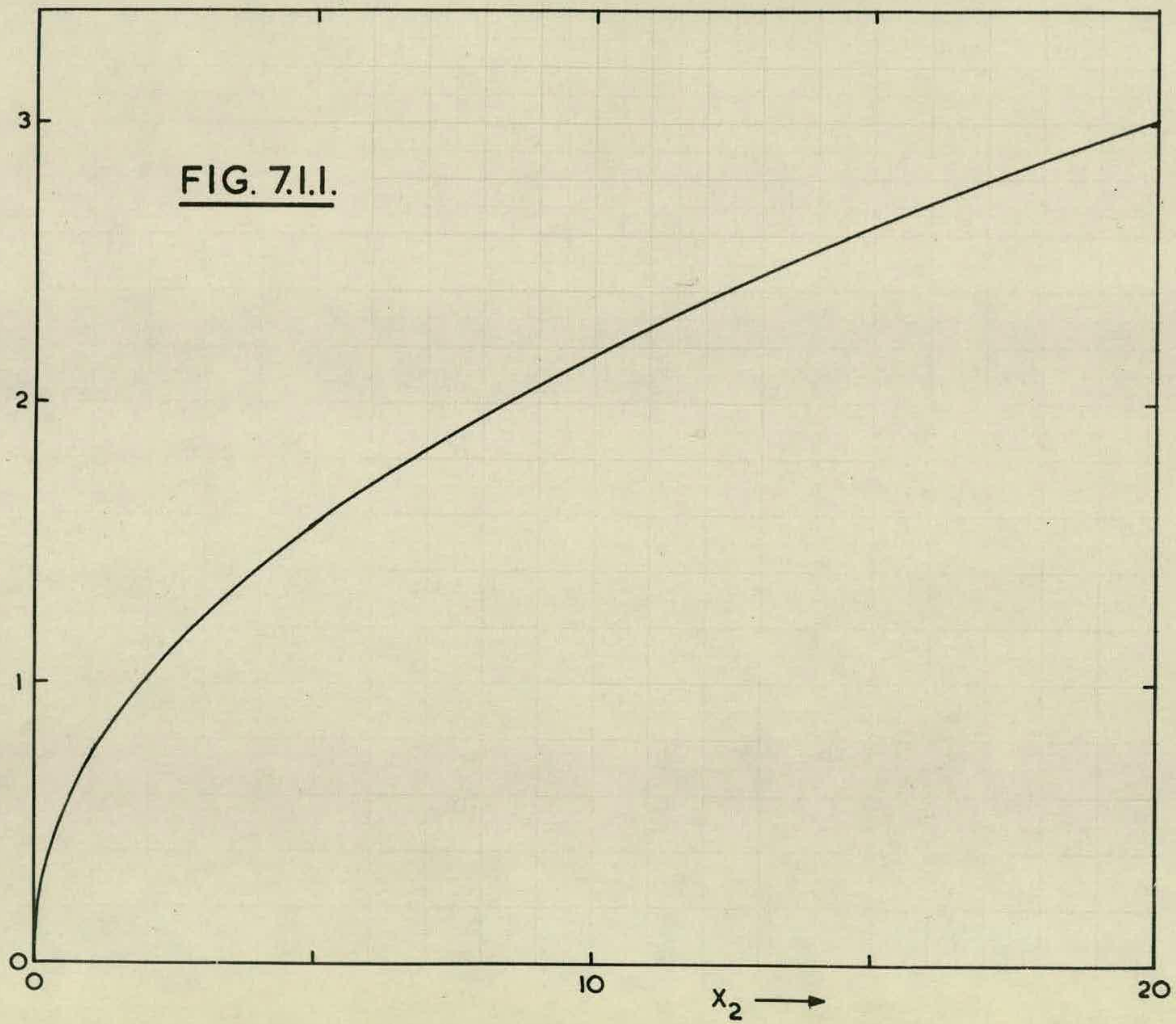

FIG. 7.1.1.

hand the values of recombination coefficient determined from the decay of the electron density may not be greatly affected by this averaging process since the recombination coefficient will tend to be constant throughout the region.

It has been shown in section 5.2. that the microwave probing signal may disturb the discharge and increase the electron temperature if the power level used is too high. In order that this effect may be made negligible the microwave field strength must satisfy the condition $E \ll \sqrt{\frac{6(m\omega)^2 k T_g}{M e^2}}$

which gives $E \ll 200 V/m.$ for helium at $300^{\circ}K$. In fact the microwave power level was less than - 30dB. with respect to 0.1W., corresponding to $E < 10$ V/m., so that this condition is satisfied. This has been confirmed by measuring the admittance of the discharge for two microwave power levels. As no difference could be detected it can be assumed that the microwave signal has a negligible effect on the properties of the discharge.

Another possible source of error is leakage of microwave power through the holes in the waveguide walls. Quarter wavelength copper sleeves were fitted over the discharge tube just outside the waveguide, but no difference in the v.s.w.r. in the waveguide system could be detected. It has therefore been assumed that leakage along the axis of the discharge tube is also negligible.

We can therefore conclude that the values of electron concentration calculated may be subject to errors of about 10%. Calculated values of collision frequency and electron temperature are not likely to be so accurate due to the error in ϵ_r'' and the fact that the velocity distribution function is unknown.

7.2. The Experimental Measurements

Microwave measurements have been made in the negative glow region of pulsed discharges in helium for gas pressures in the range 5 → 15 mm.Hg. Gettered tubes of the type described in chapter 4 were used, details of the various tubes being as follows.

Tube 1 Gas pressure = 5 mm. Hg., Molybdenum electrodes
Tube 2 Gas pressure = 10 mm.Hg., Molybdenum electrodes
Tube 3 Gas pressure = 15 mm.Hg., Molybdenum electrodes
Tube 4 Gas pressure = 10 mm.Hg., Tungsten electrodes

The tubes were operated with a d.c. maintaining current of approximately 250µA and rectangular current pulses of a few milliamps were superimposed. The pulses being approximately 640 µsec long with a p.r.f. of 12.5 per second.

Typical voltage and current waveforms are shown in Figure 7.2.1. which refers to tube 4 for a peak current of 6 mA. In (a) the current waveform is shown along with a zero and 4 mA calibration (brightness modulation by 40 µ sec time markers), while (b) shows

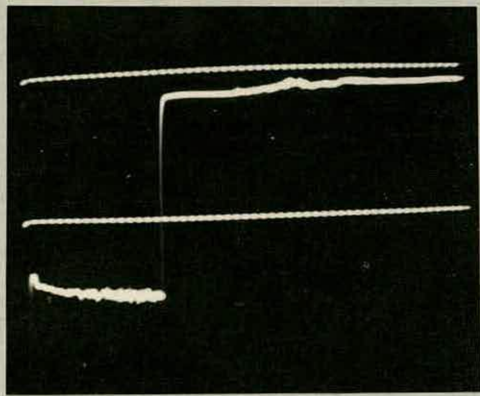

(a.)

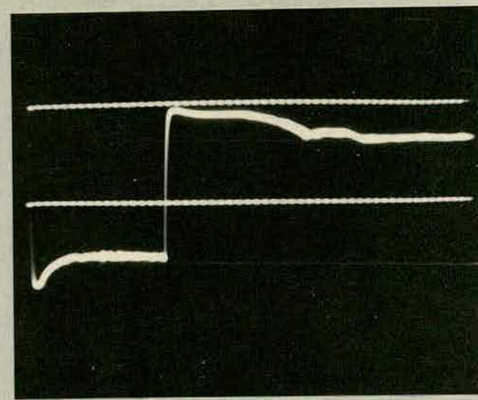

(d.)

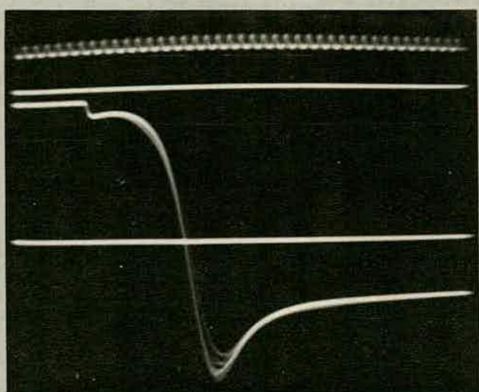

(b.)

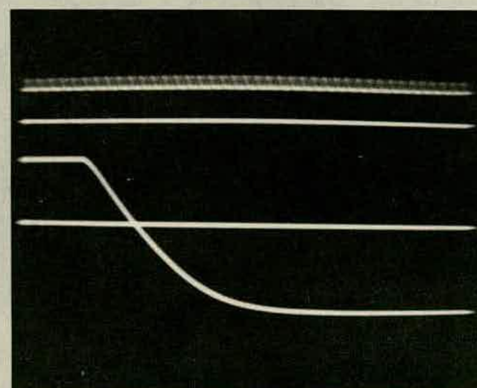

(e.)

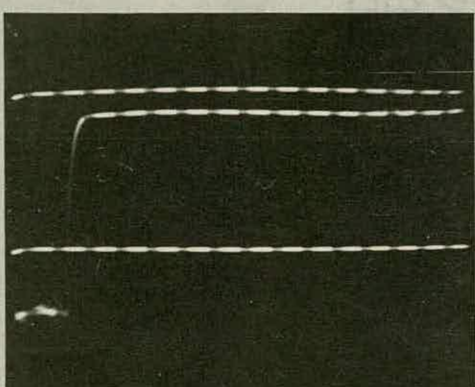

(c.)

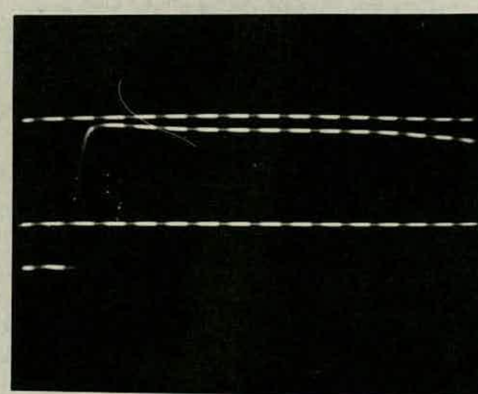

(f.)

Figure 7.2.1.

Typical Voltage and Current Waveforms.

the leading edge of the pulse (1 μsec. markers) and (c) shows the trailing edge. Figures 7.2.1. (d), (e) and (f) are the corresponding voltage waveforms along with a zero and 1.73 KV calibration.

The microwave measurements have been supplemented by measurements of the light output from the discharge. Using a double slit system to sample the intensity over a $^1/8"$ length of the tube several volts output can be obtained from a 931-A photomultiplier tube with an H.T. voltage of 750 → 1000V and a load resistor of 10KΩ . The slit system can be scanned along the tube to study the axial variation of light intensity, which is illustrated in Figure 7.2.2. (brightness modulation by 10 μsec markers).

In the negative glow the intensity variation is of the form shown in Figure 7.2.2.a (reduced gain). In the positive column the mean intensity varies along the axis of the tube due to the presence of stationary striations (See Fig.4.3.2.), but large amplitude oscillations of the type observed by Donahue and Dieke (1951) are also present. These oscillations are quite stable at the negative end of the positive column and advance in phase towards the anode, but they become unstable near the anode end of the tube (Figure 7.2.2.g). The period of these oscillations appears to be directly proportional to gas pressure. At 10 mm.Hg. pressure the oscillations

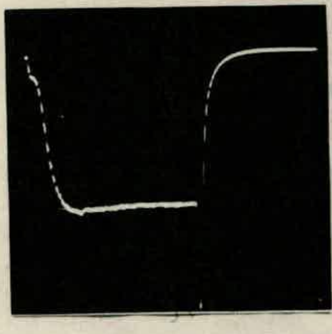

(a) x = 2cm. Gain = 0.1
Negative Glow.

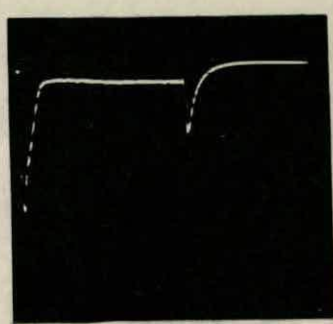

(b) x = 8 cm. Gain = 1
Dark Space.

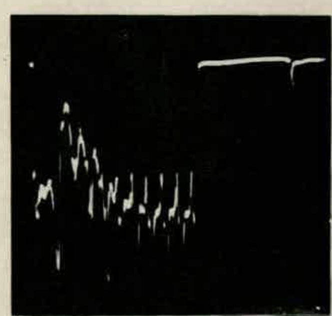

(c) x = 9.7 cm.
First Striation.

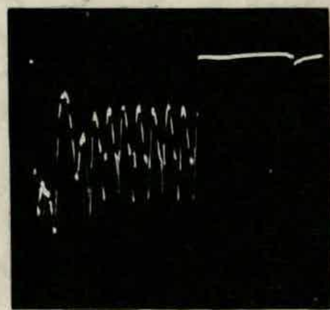

(d) x = 10 cm.
First Minimum.

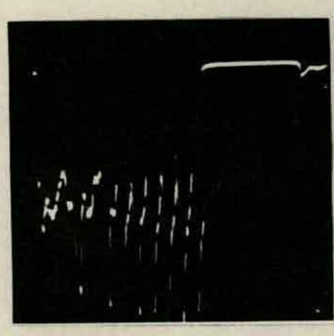

(e) x = 10.7 cm.
Second Striation.

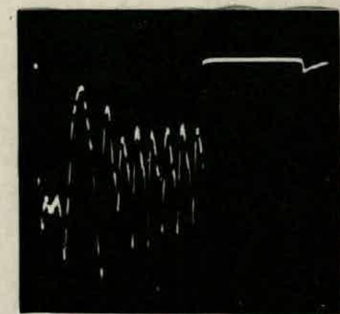

(f) x = 11.2 cm.
Second Minimum.

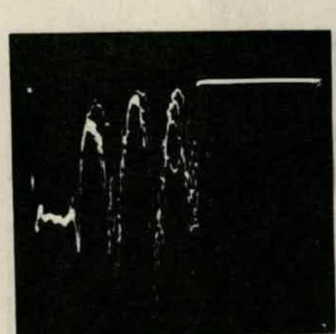

(g) x = 19 cm.
Positive Column.

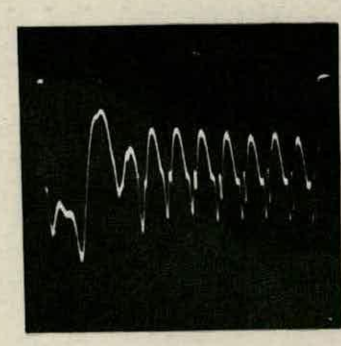

(h) x = 10 cm.
Expanded Time Scale.

Fig.7.2.2. Variation in light intensity along the axis of a pulsed discharge in helium at 10mm.Hg. pressure. (Tube 2, I = 10mA.).

have a period of approximately 50 μsec. and the phase advances by 360° in travelling 2 cm. towards the anode, corresponding to a phase velocity of approximately 400 metres/sec. towards the cathode. The number of cycles of oscillation present is constant along the length of the tube, which suggests that they are due to some form of standing wave pattern. These results are similar to those obtained by other research workers (Francis, 1956). The distance between the moving striations is approximately 2 cm. compared with 1 cm. for the fixed striations. This is consistent with the results obtained by Donahue and Dieke who found ℓ moving = 1 or 2 x ℓ stationary.

The electron density in the positive column is too low to allow accurate microwave measurements to be made but an indication that these oscillations are accompanied by large fluctuations in electron concentration is given by the v.s.w.r. probe output signal as shown in Figure 7.2.3.

The variation in electron concentration in the negative glow region during the rise of the current pulse is shown in Figure 7.2.4. along with the corresponding variation in light intensity, voltage and current.

The light intensity during the latter part of the current pulse is plotted as a function of peak current in Figure 7.2.5. and typical axial variations of light intensity and electron concentration are shown in Figure 7.2.6.

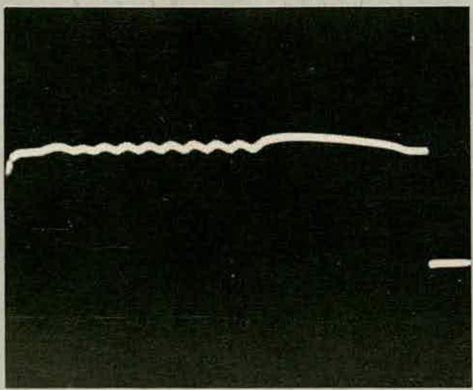

Fig. 7.2.3.

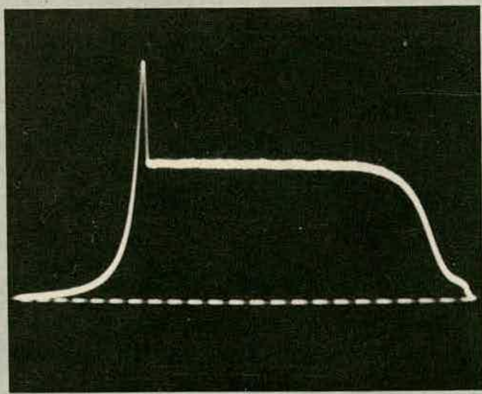

Fig. 7.2.10.

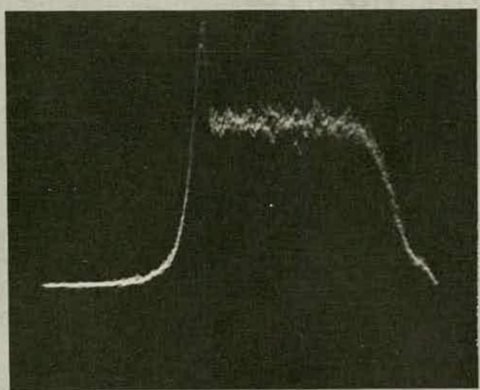

Fig. 7.2.12a.

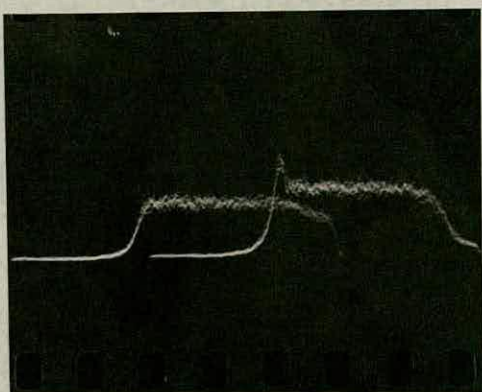

Fig. 7.2.12b.

(In Figures 7.2.10. and 7.2.12. time increases from right to left.)

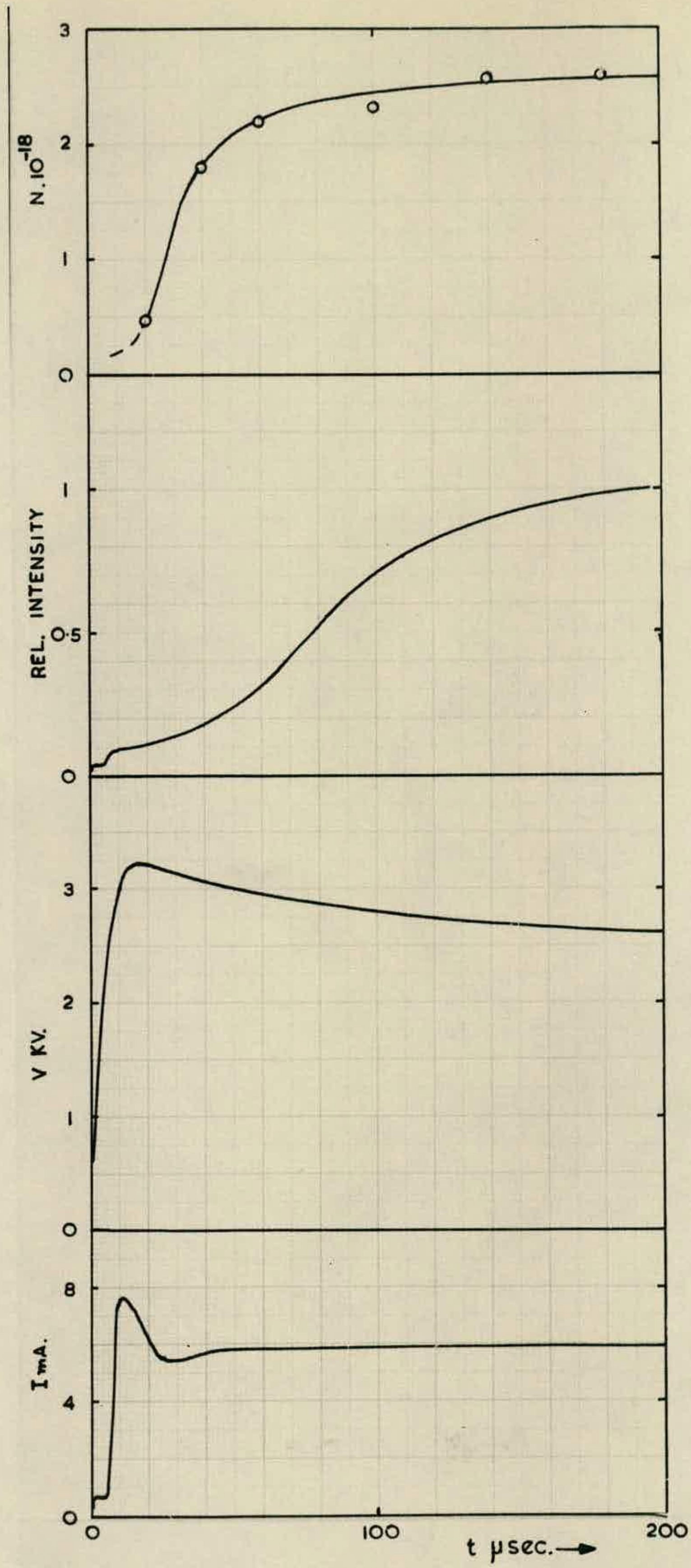

TUBE 4 X = 2 CM.

FIG. 7.2.4.

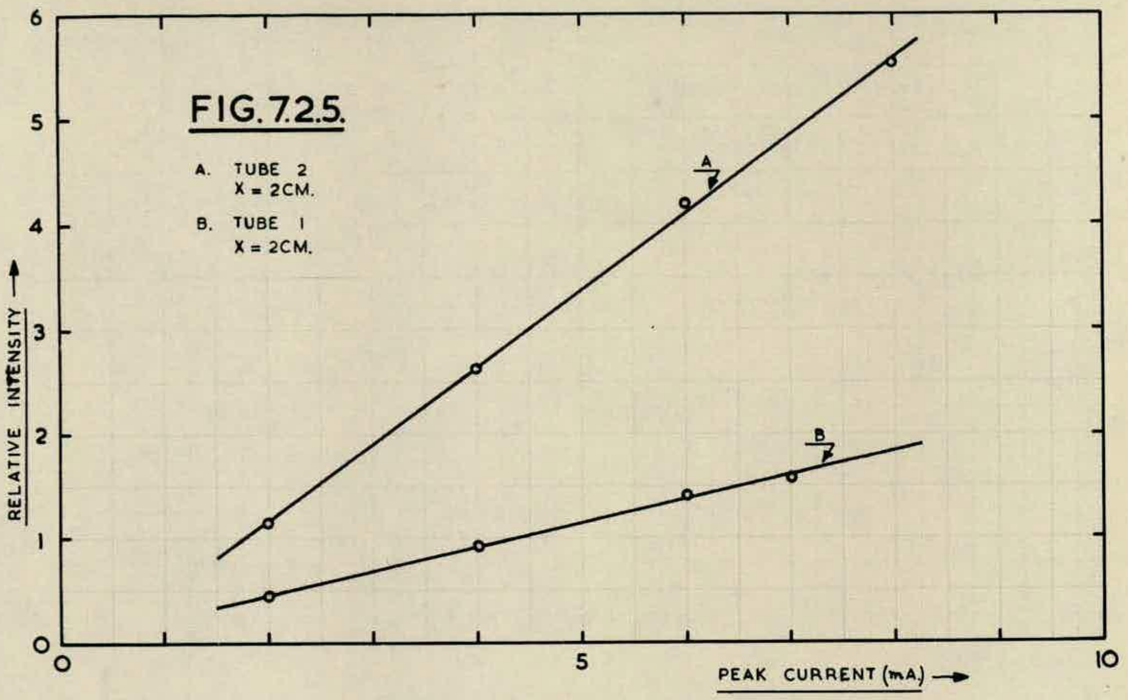
FIG. 7.2.5.
A. TUBE 2
X = 2CM.
B. TUBE 1
X = 2CM.
A
B
RELATIVE INTENSITY
PEAK CURRENT (mA.)
0
1
2
3
4
5
6
0
5
10

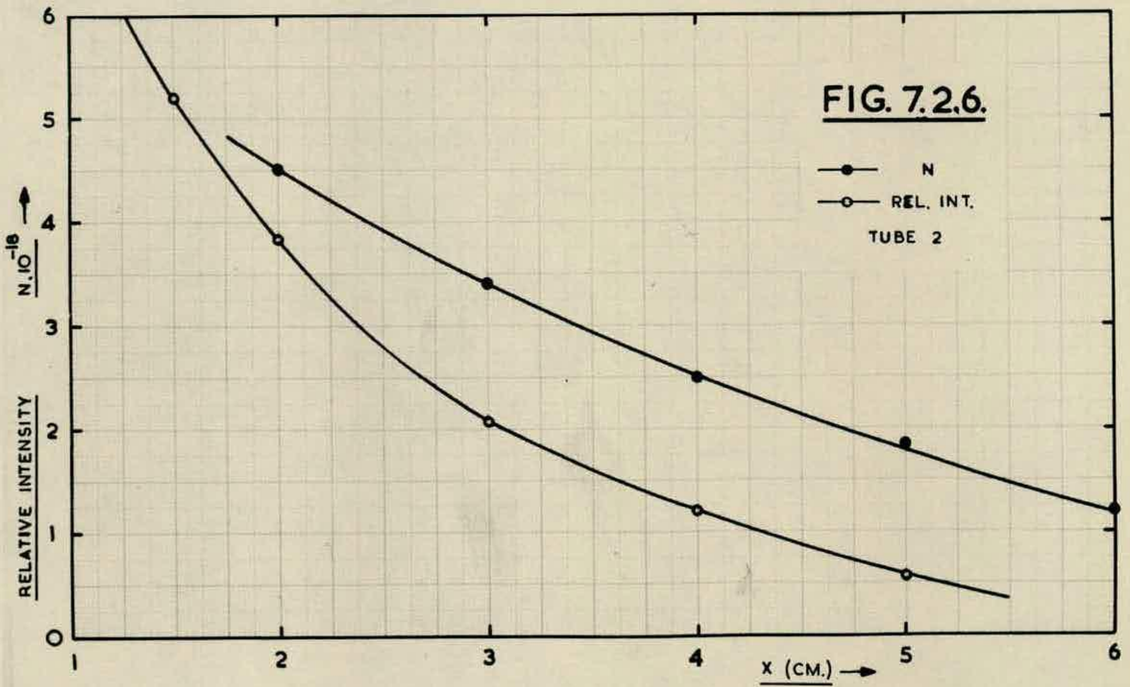
FIG. 7.2.6.
N
REL. INT.
TUBE 2
RELATIVE INTENSITY
N.10^-18
X (CM.)
0
1
2
3
4
5
6
1
2
3
4
5
6

At the end of the current pulse the electron concentration, collision frequency and electron temperature fall off as shown in Figures 7.2.7. - 7.2.9. but the light intensity rises to a maximum before falling to the value corresponding to the maintaining current. This afterglow is illustrated in Figure 7.2.10. The magnitude of the increase in light intensity depends upon the current and distance from the cathode, but it is of the order of 120%, 100% and 70% for pressures of 5, 10 and 15 mm.Hg. respectively. The corresponding times for the intensity to fall to its initial value being approximately 50, 28 and 17 μsec., so that the "length" of the afterglow is inversely proportional to pressure. The total light intensity during the afterglow is plotted on a log-log scale in Figure 7.2.11.

Some spectroscopic measurements in the range 3000°A - 6000°A have been made to determine the behaviour of the individual spectral lines during the period of the afterglow. A standard grating spectrometer was used with a slit width of approximately 1 mm., which was small enough to resolve the closest lines while giving a reasonable intensity. A 931-A photomultiplier tube was mounted in place of the eyepiece and the output from a 47K-Ω load resistor was fed to the oscilloscope through a simple R-C filter with an integrating time constant of 2 μsec. Due to the low light intensity the signal to noise ratio obtained was rather poor, but the results are sufficient to indicate

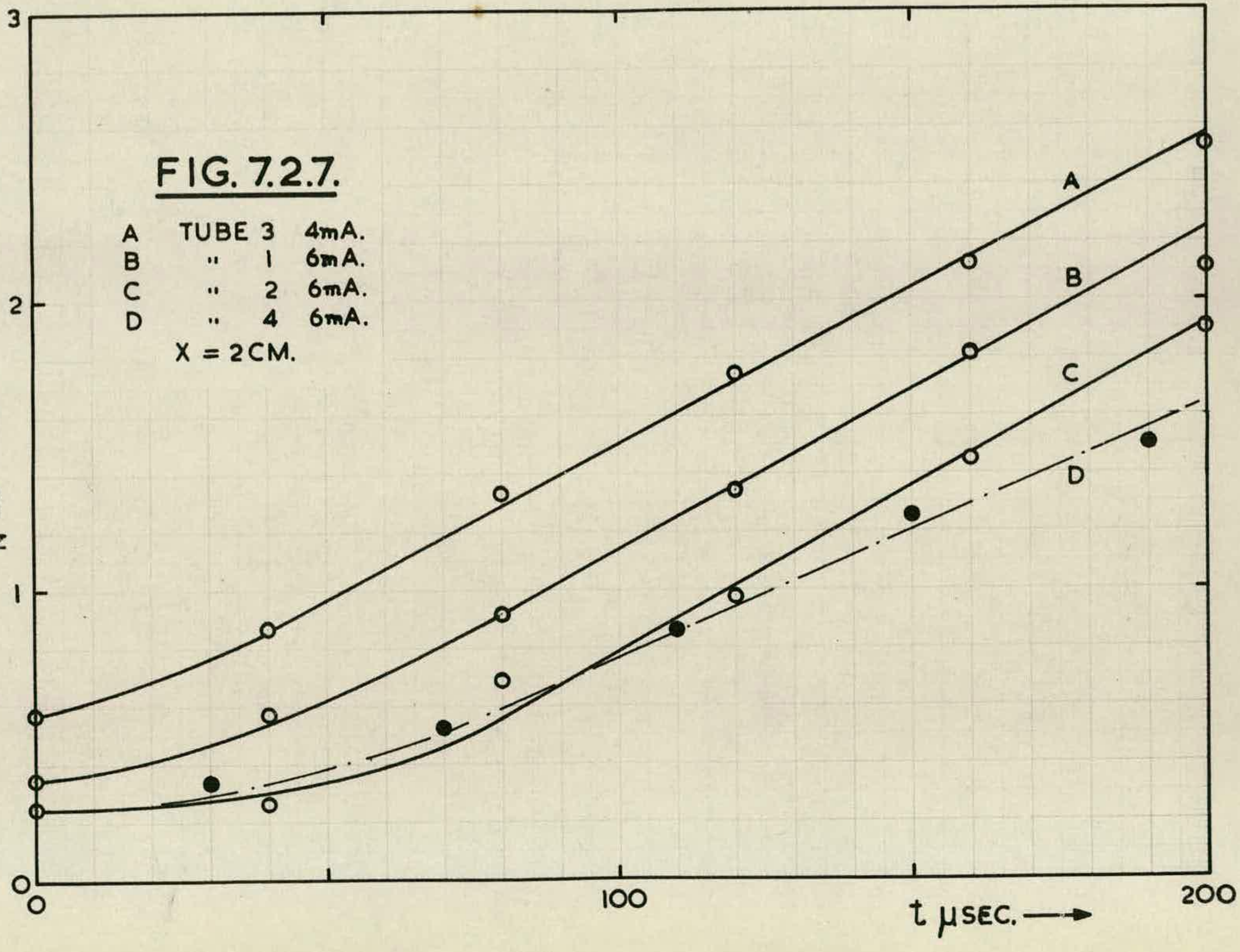
FIG. 7.2.7.
A TUBE 3 4mA.
B " 1 6mA.
C " 2 6mA.
D " 4 6mA.
X = 2CM.
A
B
C
D
$\frac{1}{N} \cdot 10^{18}$ →
t μSEC. →
0
100
200
0
1
2
3

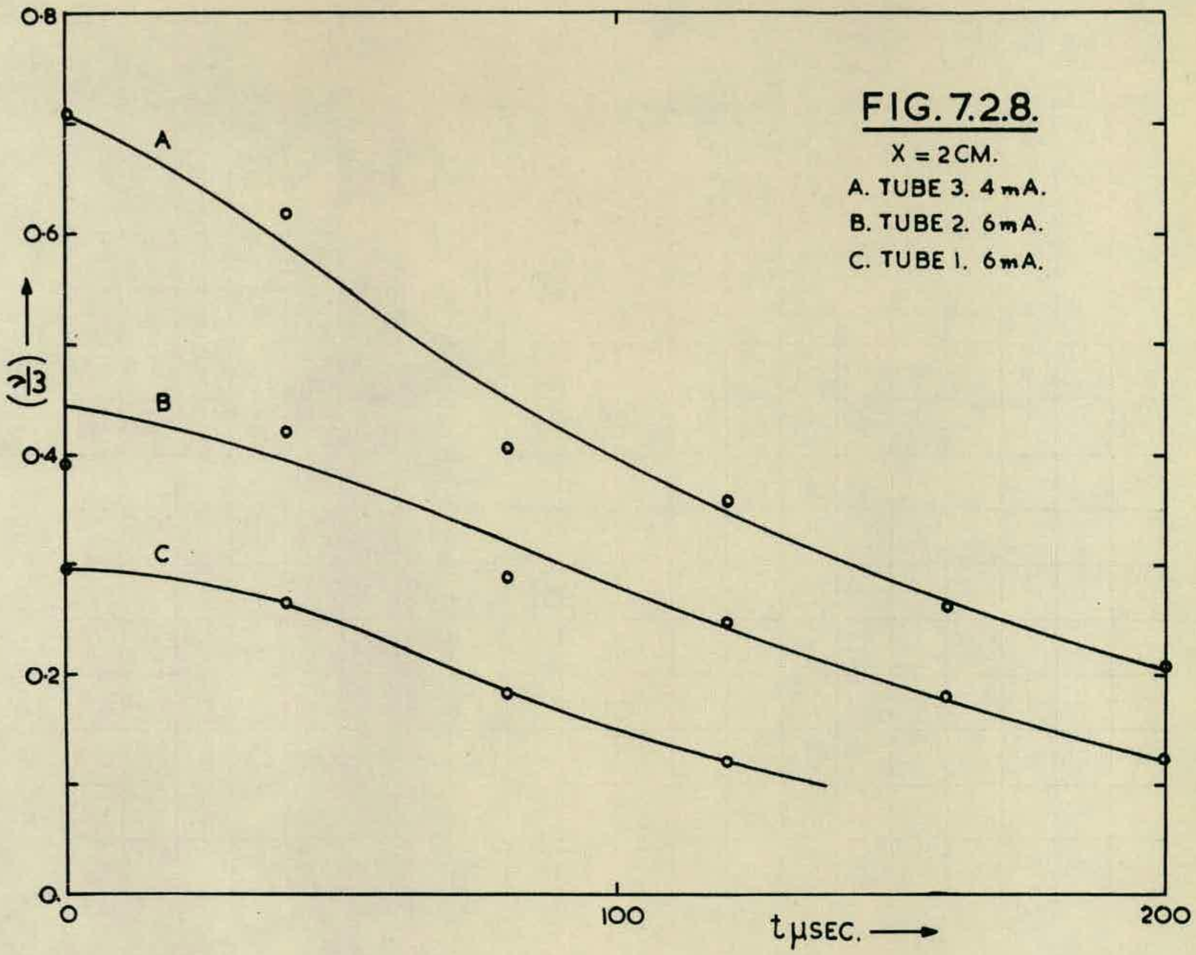

FIG. 7.2.8.

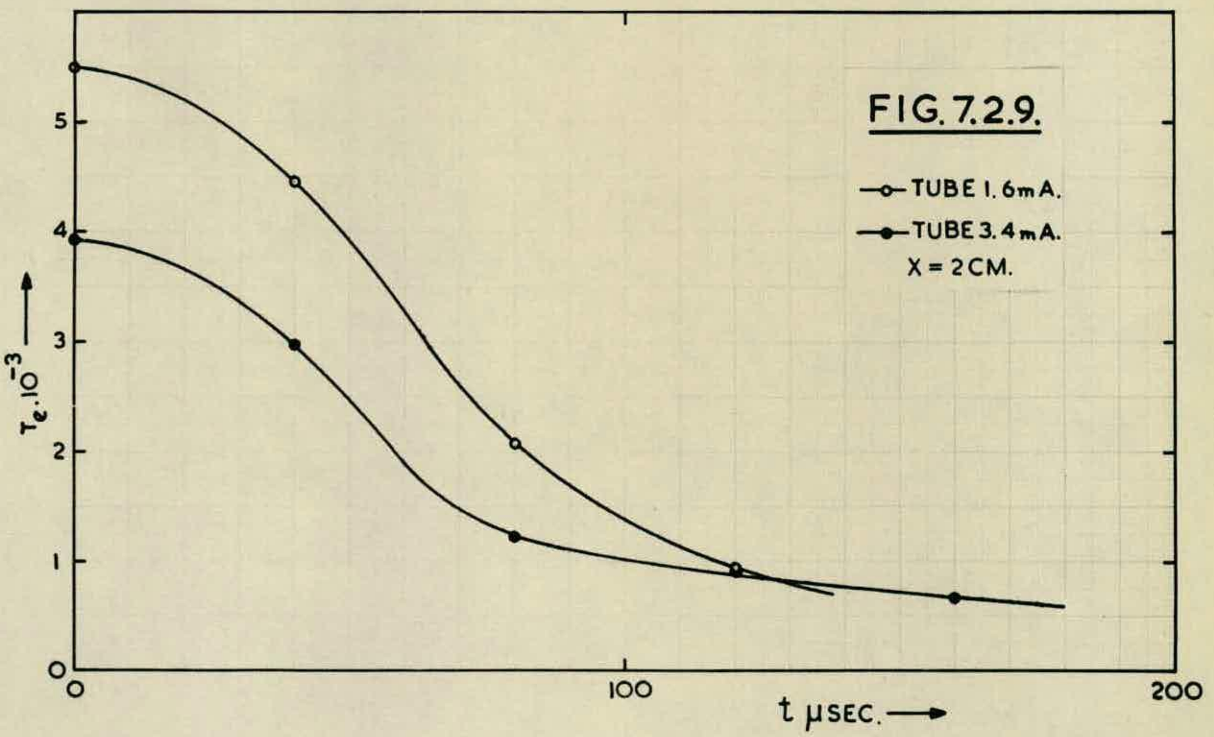

FIG. 7.2.9.

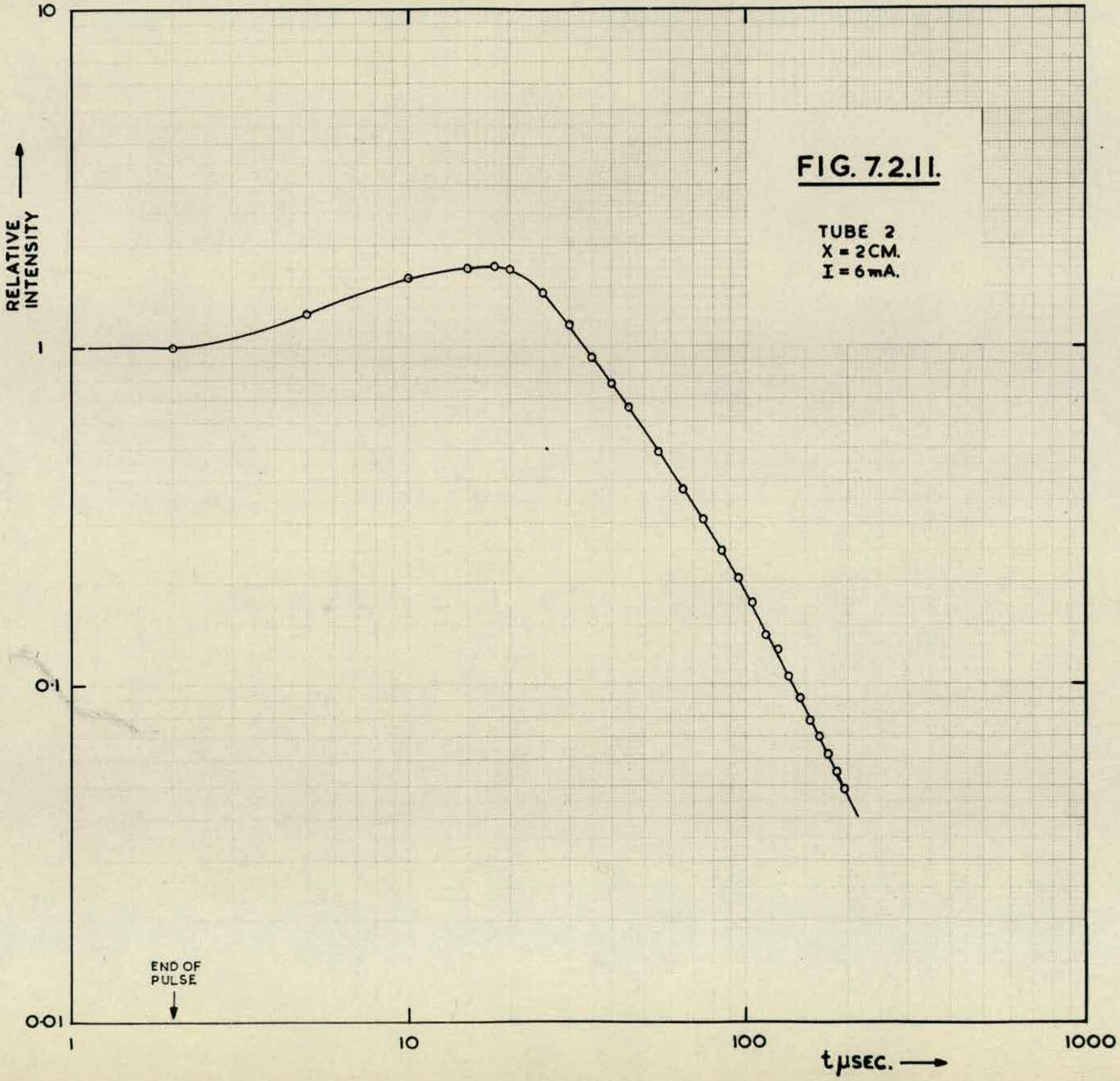
TUBE 2
X = 2CM.
I = 6mA.
RELATIVE INTENSITY
10
1
0·1
0·01
1
10
100
1000
t μsec.
END OF PULSE

FIG. 7.2.11.

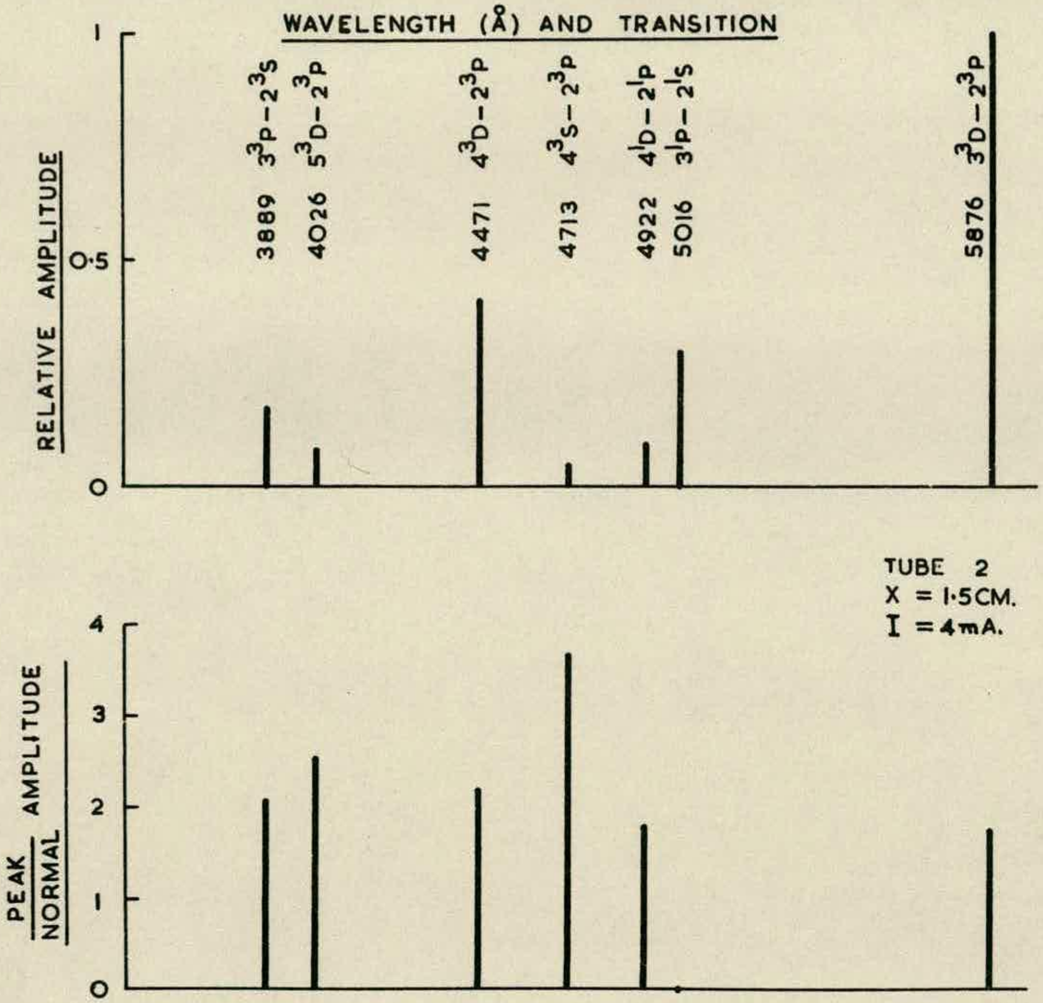
WAVELENGTH (Å) AND TRANSITION
RELATIVE AMPLITUDE
1
0.5
0
3889 $3^3P - 2^3S$
4026 $5^3D - 2^3P$
4471 $4^3D - 2^3P$
4713 $4^3S - 2^3P$
4922 $4^1D - 2^1P$
5016 $3^1P - 2^1S$
5876 $3^3D - 2^3P$
TUBE 2
X = 1·5 CM.
I = 4 mA.
PEAK / NORMAL AMPLITUDE
4
3
2
1
0

FIG. 7.2.13.

the time variation of the individual lines.
(Figure 7.2.12a).

Figure 7.2.13 gives the relative magnitude of the prominant spectral lines during the latter part of the current pulse, while the corresponding ratios of the maximum afterglow intensity to the intensity at the end of the current pulse are also given. (These results are approximate and take into account the spectral response of the photomultiplier tube.)

The 5016°A line shows no increase during the afterglow period and the intensity increases more rapidly at the start of the current pulse than in the case of the other lines studied. These effects are shown in Figure 7.2.12b.

In the positive column all the spectral line intensities tend to follow the current waveform and no afterglow can be detected.

7.3. Discussion of the results

In these experiments rectangular current pulses have been superimposed on the d.c. maintaining current through the discharge. However, the system bandwidth is finite and any change in discharge current must be preceded by a change in applied voltage. In attempting to force a step of current through the discharge the applied voltage will rise at the maximum rate possible, limited by the system bandwidth and in extreme cases by the maximum voltage available. On the other hand, the discharge current is determined by the average electron concentration and the electron drift velocity, neither of which can change instantaneously. The rise in current will therefore be delayed with respect to the applied voltage.

Considering the case for which results are shown in Figures 7.2.1. and 7.2.4., the initial voltage rise is 1 $\rightarrow$ 2kV. at 10 mm. Hg. pressure. For a 20 cm. tube the rise in E/p is therefore 5V cm^{-1} $(mm.Hg.)^{-1}$. Bradbury and Nielsen (Loeb, 1955b) give the corresponding rise in the steady state drift velocity as 5.10^{6} cm/sec. Under transient conditions the increase will be considerably less, say 10^{6} cm/sec. An estimate of the time required for a significant increase in electron concentration to occur can be obtained by considering the time for an electron to be accelerated through the ionisation potential of the gas ($\sim$ 24V). For $E \sim$ 50V/cm. this would require about 0.5 μsec., so that it would take several microseconds before any appreciable increase in current could occur.

In practice there is a small initial current rise on application of the voltage pulse which is probably due to the increase in drift velocity. This is followed after about 5 μsec. by a rapid increase to the peak pulse current (Figure 7.2.4.) This delay in the current waveform increases with gas pressure corresponding to a reduction in E/p

The cathode fall potential will be high and the electron concentration will not reach its final value until emission processes at the cathode reach a steady state. Cathode emission is controlled by the relatively heavy positive ions and the time required will therefore depend upon the positive ion mobility μ_+. Chanin and Biondi (1954) give μ_+ for helium $\sim 10\ cm^2/V.sec.$ Assuming the cathode dark space to be ~ 0.5 cm. across and taking $E \sim 1000V/cm.$ positive ions would take about 50 µsec. to cross the dark space to the cathode. In fact the electron concentration takes about 100 µsec. to reach a steady state (Figure 7.2.4.) and the tube voltage remains high during this period.

The light intensity, which will be due largely to direct excitation, will depend on both the electron concentration and electron temperature and it therefore lags behind the rise in electron concentration. The small initial rise in intensity corresponding to the initial rise in discharge current can be accounted for by the excitation produced by the increased electric field strength.

The oscillatory form of the current waveform indicates that large changes of dynamic impedance occur during the initial part of the pulse.

The increase in electron concentration and light intensity in the negative glow are therefore controlled by the cathode emission, while the fact that the final steady state current increase is due largely to an increase in electron concentration is verified by the linear intensity - v - current plot of Figure 7.2.5.

The axial variation of light intensity and electron concentration are similar, (Figure 7.2.6), although the variation in electron concentration is not so marked. This may be partly due to the different axial resolution of the two measurements, but it seems reasonable to assume that the electron concentration near the cathode exceeds $10^{19}/m^3$. The axial variation of collision frequency is not so great but there is a maximum near the cathode.

During the period of the current pulse the electron temperature will be high. This will also be the case under steady state condition with the maintaining current alone. However, immediately after the end of the current pulse there will be a large excess in the electron concentration. The electron temperature will fall towards the gas temperature and recombination will take place. The tube voltage required during this recombination period will be lower than the normal maintaining value due to the excess electron concentration. (See Figure 7.2.1.) Since the maintaining current is much less than the peak current it will have a negligible effect during the initial stages of recombination.

In addition to volume recombination ambipolar diffusion will also be present. Diffusion of this type is characterised by a time constant $T = \frac{L^2}{D_a}$

where L is a characteristic dimension of the containing vessel and D_a is the ambipolar diffusion constant. For helium Biondi and Brown (1949a) give $D_a = 540$ cm^2/sec at 1 mm. Hg. pressure. Taking $L \sim r \sim 0.3$ cm. and p = 5 mm.Hg. we find $T \sim 1$ m.sec. Since these measurement have been restricted to the first 200 μsec. after the end of the current pulse the effects of ambipolar diffusion will be small and volume recombination alone will be significant.

If recombination only were present the light intensity would be proportional to $^1/t^2$. In fact this is not so, the intensity rises to a maximum following the end of the current pulse (Figure 7.2.10) before falling to the value corresponding to the maintaining current, while the electron concentration tends to remain constant (Figure 7.2.7.) This effect is in some respects similar to the afterglow observed in recombining plasmas produced by high power microwave excitation, (Goldstein, 1955) although the magnitude of the effect in this case is much greater. Biondi has in fact observed an increase in the electron concentration following the removal of the excitation (Johnson et al, 1950).

There are several processes which might produce this afterglow effect. Firstly, the high temperature electrons must lose some of their energy to the gas before recombination occurs. Phelps et al (1951) estimate that in helium the electrons cool to within 10% of the gas temperature in a time 90/p μsec. It is evident from the results shown in Figure 7.2.9. that the electron temperature takes much longer to decay in these experiments.

The values of electron temperature calculated depend upon the value of Q_e, the collision cross section for electrons in helium. Von Engel (1955), Hirshfield and Brown (1958) and others give $Q_e = 20\ cm^{-1}(mm.Hg)^{-1}$ for energies up to several electron volts. This value leads to the results in Figure 7.2.9.

The initial values of electron temperature measured seem rather low, but as discussed earlier there are several possible sources of error, however, the results do seem to be of the correct order of magnitude at least for $t > 100\ \mu sec$ say. In passing it should be mentioned that the measured values of collision frequency (Figure 7.2.8.) decay in a similar manner to the electron temperature, and the collision frequency appears to be roughly proportional to gas pressure. It is evident that the decay of electron temperature alone is not sufficient to explain the large increase in light intensity during the period of recombination.

Goldstein (1955) has suggested that afterglow effects of the type observed can be explained on the assumption that metastable atoms in the decaying plasma are further excited to a short life radiating state, leading to the observed increase in intensity. As metastables in helium may have a lifetime in excess of

10^{-3} sec. (von Engel, 1955) this process may be significant in this case.

Spectroscopic examination of the individual line intensities in the range 3000 - 6000°A gave results of the type shown in Figure 7.2.13. Generally the weakest lines tend to show the greatest afterglow, while the $3^1P - 2^1S$ transition, which leads to metastables, shows no afterglow. Biondi (1960) has made measurements in the range 4500°A - 6000°A of the afterglow obtained from discharges excited by high power microwaves. He finds that all the lines first decrease in intensity for ~ 100 μsec. and then increase for several hundred microseconds, but the effect is of much lower intensity than in these experiments. According to Biondi the effect is due to metastables being raised to a radiating state when struck by energetic electrons, which are themselves produced by metastable - metastable ionising collisions.

Thus
$$He^m + He^m \rightarrow He^+ + He + e(\text{energetic})$$
$$He^m + e(\text{energetic}) \rightarrow He^* + e$$

The excited He^* then decay by emission of a quantum. At the same time the atomic ions are converted to molecular ions by three body collisions.

$$He^+ + 2He \rightarrow He_2^+ + He$$

The molecular ions then recombine dissociatively according to the mechanism proposed by Bates (1950)

$$He_2^+ + e \rightarrow He^* + He + \text{Kinetic Energy}$$

Biondi has verified that the metastables concerned are in the 2'S state (Loeb, 1955c). This would give rise to a line spectrum during the afterglow. Biondi and Johnson have found that at similar pressures the afterglow radiation consisted mainly of band spectra due to He_2^+, but only the line spectrum of atomic helium has been observed in these experiments.

According to Goldstein et al. (1953) the recombination coefficient shows a marked temperature dependence. It is therefore possible that the observed afterglow is caused partly by a large increase in the recombination coefficient due to a reduction in electron temperature, but the results of Figure 7.2.9. seem to indicate that the temperature decays only slightly during the initial afterglow. It may be that the reactions suggested by Biondi are sufficient to account for the effects observed. Certainly the presence of air as an impurity, which might destroy the metastables due to the Penning effect, removes all trace of the afterglow. The difference in the magnitude of the effect might well be due to the initial level of excitation. However, there remains the anomalous effects associated with the 5016°A line, which increases more rapidly at the onset of the current pulse and has no afterglow effect. It would be necessary to use more sensitive equipment to study accurately the time variation of the various line intensities over a wider range of wavelengths before any firm conclusions can be reached. It would be useful for example to examine the behaviour of other lines emitted by electrons in transition to the 2'S metastable state.

During the latter part of the afterglow (say 80 μsec after the end of the pulse for 10 mm.Hg. pressure) the light intensity decays as $^1/t^2$ (Figure 7.2.11.) and the electron concentration as $^1/t$ (Figure 7.2.7.) so that recombination is the dominant process. The electron temperature at this time may be of the order of 10^3 °K.

The recombination coefficient can be determined from the slope of the graphs in Figure 7.2.7., which gives $\alpha_{He} = 1.1 \times 10^{-8}$ cm^3/ion sec. for the tubes with molybdenum electrodes for pressures in the range 5 - 15 mm.Hg. Tube 4, which has tungsten electrodes, gives $\alpha_{He} = 0.88 \times 10^{-8}$ cm^3/ion sec. The difference may be due to the presence of the cathode material as an impurity. This result is in reasonable agreement with the values of 1.7×10^{-8} cm^3/ion sec. given by Biondi and Brown (1949b) and 0.95×10^{-8} cm^3/ion sec. given by Johnson et al (1950) for discharges excited by microwaves, although Sexton and Craggs (1958) have obtained a value of 6.8×10^{-8} cm^3/ion sec. from measurements at 3 cm. wavelength. The temperature measurements seem to suggest that for $T_e < 2.10^3$ °K the recombination coefficient is fairly constant (See Figures 7.2.7. and

7.2.9.)

Having obtained the electron concentration from microwave measurements it is possible to estimate the electric field in the negative glow region. The average current density for a 6mA pulse is approximately 14 mA/cm^2 and the electron density is $\sim 10^{12}/cm^3$. so that the electron drift velocity must be $\sim 10^5$ cm/sec.

According to the results of Bradbury and Nielsen this corresponds to $\frac{E}{p} \sim 0.1$, so that $E \sim 1V/cm.$, which is lower than might be expected. In the positive column where the electron concentration is lower by one or two orders of magnitude the electric field will be $10 \rightarrow 100V/cm$.

Chapter 8

Conclusions

It is obvious from the discussion given in Section 5.4. that microwave probe methods for studying ionised gases can be expected to yield fairly reliable values for the electron concentration even when the electron velocity distribution function is unknown. Although it is in many ways convenient that the microwave conductivity is relatively insensitive to the form of the velocity distribution function it does mean that microwave methods can yield little information about the distribution function. In some respects therefore microwave methods are complementary to conventional probe methods, which can give fairly reliable estimates of the velocity distribution function.

Values of collision frequency can be determined within perhaps 50% error even for an unknown distribution function and if the distribution function is known to be Maxwellian, as is often the case in a decaying plasma, the electron temperature can be obtained within perhaps 25% error using the dielectric post method of measurement.

The accuracy of the results given in the previous chapter is limited to some extent by the residual v.s.w.r. in the waveguide system. If a grade 1 v.s.w.r. indicator had been available a considerable improvement might have been obtained. For example, a common specification for a grade 1 instrument is the measurement of impedance to better than 0.5%, corresponding to an error in normalised susceptance of say 0.005 compared with a limiting value of 0.02 with the present equipment. An improvement in accuracy and sensitivity of half an order of magnitude would therefore be obtained.

The sensitivity of this dielectric post method would, however, still be considerably less than can be achieved using a discharge tube mounted in a high - Q resonant cavity, but it would be difficult to obtain the same time resolution using the cavity method. Sexton et al (1959) have made measurements of electron concentrations down to $10^{13}/m^3$., while the limiting sensitivity of the dielectric post method appears to be of the order of $10^{17}/m^3$. One of the restrictions to the sensitity is due to the possibility of leakage of microwave power along the axis of the discharge tube, thus limiting the diameter of tube which can be used.

The axial resolution obtained in these experiments was 1 cm. This could be improved by further reducing the narrow waveguide dimension and such a reduction would be necessary in order to study the electron concentration in the positive column where striations are present. One method of achieving this would have been to reduce the dimensions of the apparatus by operating at X-Band (3 cm.). This would have increased the maximum microwave field strength which could be used, but due to smaller waveguide cross section the microwave power level would have been reduced. The value of ϵ_r for given discharge parameters would also have been reduced so that a considerable reduction in sensitivity would have resulted from the use of a higher microwave frequency. Ambipolar diffusion would be much more important with smaller discharge tubes and it would no longer be possible to measure recombination coefficients with any accuracy. It therefore seems that S-Band is most suited for this particular form of microwave probe measurement.

The sealed discharge tubes described in Chapter 4 are suitable for long periods of operation. The use of the constant current pulse generator gives stable operation over a useful life of several hours with current pulses up to about 10 mA. amplitude. There seems to be little difference between molybdenum and tungsten as cathode materials as far as sputtering is concerned, although tungsten appears to be slightly better from this point of view.

The microwave results obtained are sufficient to give a qualitative picture of the behaviour of pulsed glow discharges in helium and the values of recombination coefficient and electron concentration obtained should be reliable. The values of electron temperature obtained appear to be rather low, but they should certainly be of the correct order or magnitude.

The use of light intensity and spectroscopic studies with the aid of a photomultiplier tube have been useful in studying the afterglow and the striations. A more detailed study with more sensitive equipment and over a wider range of wavelength would no doubt yield useful information about their origin and might help to explain the anomolous behaviour of the 5016°A line. It is unfortunate that more details of spectroscopic measurements have not been given by some authors describing microwave probe investigations of gas discharges. For example, little understanding appears to exist of the appearance of the band spectrum of He_2^+ in some experiments, while purely line spectra are obtained in others.

The microwave measurements described are restricted in that they refer only to the negative glow region of discharges in helium. The equipment and methods used could however be profitably applied to measurements in other regions and other gases. The use of the pulsed discharge is particularly attractive since it considerably extends the useful life of the discharge tubes and reduces cathode heating for large discharge currents.

Acknowledgements

This research was carried out in the Electronics Section of the Department of Engineering, University of Edinburgh, and the author is indebted to Professor R. N. Arnold for the provision of the necessary facilities.

Mr. W. E. J. Farvis, Senior Lecturer in Applied Electricity, supervised the project and has provided invaluable advice and assistance which is gratefully acknowledged.

Thanks are also due to the other members of staff for their assistance, to Mr. T. S. Broom for assembling the vacuum system and discharge tubes, to Miss M. C. Hunter for typing this thesis and to Mr. A. R. Lucas for his assistance with some of the photography.

The research was supported by an Admiralty contract and the author is indebted to C.V.D. and S.E.R.L. for financial and other assistance.

Bibliography

Bates, D.R. (1950), Phys. Rev., 78, 492

Biondi, M.A. (1960), private communication

Biondi, M.A. and Brown, S.C. (1949a), Phys.Rev., 75, 1700.

Biondi, M.A. and Brown, S.C. (1949b), Phys. Rev., 76, 1697.

Chanin, L.M. and Biondi, M.A., (1954), Phys. Rev., 94 910.

Chapman, S. and Cowling, T.G. (1952), The Mathematical Theory of Non-Uniform Gases, C.U.P.

Dingle, R.B., Arndt, D., and Roy, S.K. (1956), App. Sci. Res., B6, 144.

Donahue, T. and Dieke, G.H. (1951), Phys. Rev., 81, 248

Eccles, W.H. (1912), Proc. Roy. Soc., A87, 79

Fang, P. H. (1959), Phys. Rev., 113, 13

Francis, G. (1956), Handbuch der Physik, Vol. XXII Springer-Verlag, Berlin, 140.

Frank, N.H. (1943), Rad. Lab. Technical Report No.T.9., 32.

Frank, N.H. (1959), private communication

Goldstein, L. (1955), Advances in Electronics and Electron Physics, VII , Academic Press Inc., N.Y.

Goldstein, L., Anderson, J.M., and Clark, G.L. (1953), Phys. Rev., 90, 486.

Hirshfield, J.L., and Brown, S.C. (1958), J. App. Phys., 29, 1749.

Johnson, R.A., McClure, B.T. and Holt, R.B. (1950), Phys. Rev., 80, 376

Langmuir, I and Mott-Smith, H.M. (1923), Gen. Elect. Rev., 26, 731.

Lewin, L, (1951), Advanced Theory of Waveguides, Illife and Sons Limited, London, pp.23 - 36

Levy, R. (1959), Proc. I.E.E., Part C, 106, 193.

Loeb, L.B. (1955a), Basic Processes of Gaseous Electronics, Univ. of Calif. Press, Los Angeles, 367.

Loeb, L.B. (1955b), loc.cit. 232

Loeb, L.B. (1955c), loc.cit. 80

Marcuvitz, N. (1951a), Waveguide Handbook, Rad. Lab., Series No.10, McGraw Hill, N.Y., 19.

Marcuvitz, N. (1951b), loc.cit., 266

Margenau, H. (1946), Phys. Rev., 69, 508

Margenau, H. (1958), Phys. Rev., 109, 6.

Margenau, H. and Stillinger, D. (1959), J.App. Phys., 30, 1385

Montgomery, C.G., Dicke, R.H. and Purcell, E.M. (1948) Principles of Microwave Circuits. Rad. Lab.Series No. 8, McGraw Hill, N.Y., 389.

Moreno, T. (1948), Microwave Transmission Design Data. McGraw Hill, N.Y., 197

Phelps, A.V., Fundingsland, O.T., and Brown, S.C. (1951), Phys. Rev., 84, 559.

Prime, H.A. (1952), Aust. J. Sci. Res., A5, 607.

Pringle, D.H. and Farvis, W.E.J. (1955), Proc. Phys. Soc., B LXVII , 836

Scott, J.G. (1956), Postgraduate Diploma Thesis, Univ. of Edin., EDR/34

Sexton, M.C. and Craggs, J.D. (1958), J. Electronics and Control, IV , 493.

Sexton, M.C., Lennon, J.J. and Mulcahy, M.J. (1959), Brit. J. App. Phys., 10, 356.

Skolnik, M.J. and Puckett, H.R. (1955), J.App.Phys., 26, 74

Southworth, G.C., (1950), Principles and Application of Waveguide Transmission , D. Van Nostrand Co., Inc., N.Y. pp.269 - 274.

Torrey, H.C. and Whitmer, C.A. (1948), Crystal Rectifiers, Rad.Lab.Series No.15, McGraw Hill, N.Y., 334.

Von Engel, A. (1955), Ionized Gases, Clarendon Press, Oxford.

Watson, G.N. (1952), A Treatise on the Theory of Bessel Functions, C.U.P.

Waymouth, J.F. (1959), J.App. Phys., 30, 1404

APPENDIX A

Notes on the Production of the Gas Discharge Tubes

The construction of the electrodes is described in Section 4.1. The molybdenum electrodes were electrolytically cleaned using a phosphoric acid deplating bath, while caustic potash was used for the tungsten electrodes. Each of the electrode supporting rods was oxidised by heating to red heat in an air-gas flame and a bead of the appropriate sealing glass (C11 for molybdenum, C9 for tungsten) formed about 1.5 cm. from the end by collapsing a close fitting glass sleeve on to the rod. The electrodes were then electrolytically cleaned to remove the oxide formed during the beading process.

The pyrex sleeves fitted behind the electrodes, to reduce the tendency for the discharge to strike behind the cathode, consist of 4 cm. lengths of 6 mm. diameter tube. These sleeves have three small pyrex protrusions near each end to centralise them in the main tube (See Figure 4.1.1.) and the ends are ground flat.

The glass used in the construction of the tubes was thoroughly cleaned with chromic acid and distilled water before use.

The main section of the tubes is a 30 cm. length of 9 mm. external diameter x 7.5 mm. bore precision pyrex tube. After sealing off one end of the main tube the exhaust arm was added about 1 cm. from the closed end at right angles to the tube. One of the pyrex sleeves was then inserted and sealed into the closed end of the tube. The end was blown open and a tubular seal built up outside the tube. (Pyrex /C9/C11 for molybdenum electrodes and pyrex /C9 for tungsten). The first electrode was then inserted and sealed into the tube by collapsing the glass seal on to the bead previously formed on the supporting rod. During this sealing process nitrogen was circulated through the tube to prevent oxidation of the electrode.

The second electrode and pyrex sleeve were inserted into the tube and the other end sealed off. The procedure for making the metal to glass seal was then repeated and the second electrode sealed into position.

Finally a barium getter was fitted in the exhaust arm and a constriction formed for sealing off the tube. The tubes were given a preliminary test for leaks using a high frequency tester and sealed to the vacuum system for filling (See Figure 4.2.1.).

APPENDIX B

Computer Solution of Dielectric Post Equations

B.1. Evaluation of the constants

Referring to equation 6.2.5., we have

$$\beta \frac{J_1(\beta)}{J_0(\beta)} = \frac{1}{J_0^2(\alpha)} \cdot \frac{1}{\left[S_0 - \frac{\alpha^2}{4} + j\,\frac{2\lambda_g}{a\underset{\sim}{y}} \right]} + \alpha\,\frac{J_1(\alpha)}{J_0(\alpha)}$$

where

$$S_0 = \log_e\left(\frac{4a}{2\pi R}\right) - 2 + 2\sum_{\substack{n=2 \\ n\ \text{odd}}}^{\infty}\left[\frac{1}{\sqrt{n^2 - \left(\frac{2a}{\lambda_0}\right)^2}} - \frac{1}{n}\right]$$

and $\alpha = \dfrac{2\pi R}{\lambda_0}$, $\beta = \sqrt{\underset{\sim}{\epsilon_r}}\,.\,\alpha$.

In these experiments the bore of the discharge tube was 7.5 mm., so that R = 3.75 mm. The tube was mounted in W.G. No.10 which has internal dimensions a = 2.84", b = 1.34", and all measurements were made at a frequency of 3000 Mc/s (λ_0 = 10 cm.)

The wavelength in the guide is given by

$$\lambda_g = \frac{1}{\sqrt{\left[\frac{1}{\lambda_0^2} - \frac{1}{(2a)^2}\right]}} = 13.873\ \text{cm.}$$

Also

$$\alpha = 0.23562,\ J_0(\alpha) = 0.98617,\ J_1(\alpha) = 0.11699$$

$$\frac{\alpha^2}{4} = 0.013888\ ,\ \frac{2\lambda_g}{a} = 3.8464$$

$$\log_e\left(\frac{4a}{2\pi R}\right) = \log_e(12.246) = 2.50521$$

Evaluation of the series involved in S_0 for values of n up to n = 39 gave $\sum = 0.06273$

So that $S_o = 2.50521 - 2 + 2(0.06273) = 0.63067$

Substituting these values

$$\beta\frac{J_1(\beta)}{J_0(\beta)} = \frac{1}{(0.98617)^2} \cdot \frac{1}{\left[0.63067 - 0.01388 + j/\underset{\sim}{y}\, 3.8464\right]} + 0.23562 \cdot \frac{0.11699}{0.98617}$$

or

$$\beta\frac{J_1(\beta)}{J_0(\beta)} = \frac{0.26733}{0.16035 + j/\underset{\sim}{y}} + 0.02795$$

which is equation 6.2.6.

B.2. Derivation of equation 6.3.1.

The left hand side of equation 6.2.6. can be expanded as a Taylor series

$$f(z) = f(a) + (z-a)f'(a) + \cdots + \frac{1}{n!}(z-a)^n f^n(a) + \cdots$$

where $f(z) = \beta\dfrac{J_1(\beta)}{J_0(\beta)}$ and β is assumed to have the form $\beta = (l + jm)$ where l and m are real and positive and $l > m$

Note that $J_0(-z) = J_0(z)$, $J_1(-z) = -J_1(z)$

$$J_0'(z) = -J_1(z)$$

$$J_1'(z) = J_0(z) - \frac{1}{z}J_1(z)$$

Denoting $\dfrac{J_1(l)}{J_0(l)}$ by J , then

$$\frac{dJ}{dl} = \frac{d}{dl}\left(\frac{J_1(l)}{J_0(l)}\right) = \frac{J_0(l)J_1'(l) - J_1(l)J_0'(l)}{J_0^2(l)} = \left[1 - \frac{1}{l}J + J^2\right]$$

Thus $f(a) = \ell J$

$$f'(a) = J + \ell\left[1 - \tfrac{1}{\ell}J + J^2\right] = \left[\ell + \ell J^2\right]$$

$$f''(a) = 1 + J^2 + 2\ell J\left[1 - \tfrac{1}{\ell}J + J^2\right]$$

$$= \left[1 + 2\ell J - J^2 + 2\ell J^3\right]$$

Similarly

$$f'''(a) = \left[2\ell - 2J + \left(8\ell + \tfrac{2}{\ell}\right)J^2 - 6J^3 + 6\ell J^4\right]$$

$$f^{IV}(a) = \left[\left(16\ell + \tfrac{6}{\ell}\right)J - \left(28 + \tfrac{6}{\ell^2}\right)J^2 + \left(40\ell + \tfrac{22}{\ell}\right)J^3 - 36J^4 + 24\ell J^5\right]$$

As shown in section 6.3. ℓ is always negative. Taking this into account will reverse the sign of the odd order derivatives, leaving the others unchanged. Thus the expansion becomes

$$\beta\frac{J_1(\beta)}{J_0(\beta)} = \ell J - jm\left[\ell + \ell J^2\right]$$

$$- \frac{m^2}{2}\left[1 + 2\ell J - J^2 + 2\ell J^3\right]$$

$$+ j\frac{m^3}{6}\left[2\ell - 2J + \left(8\ell + \tfrac{2}{\ell}\right)J^2 - 6J^3 + 6\ell J^4\right]$$

$$+ \frac{m^4}{6}\left[\left(16\ell + \tfrac{6}{\ell}\right)J - \left(28 + \tfrac{6}{\ell^2}\right)J^2 + \left(40\ell + \tfrac{22}{\ell}\right)J^3\right.$$

$$\left.- 36J^4 + 24\ell J^5\right] + \cdots$$

In practice terms of order greater than m^4 are negligible. If $m > \ell$ the expansion involves Bessel functions of imaginary argument (see equations 6.3.4 and 6.3.5.)

B.3. Computer Programme and Table of Results.

An autocode programme has been prepared for the Ferranti-Pegasus digital computer and a copy of this programme is included.

For simplicity both forms of the expansion for $\beta \frac{J_1(\beta)}{J_0(\beta)}$ are computed (assuming $\ell > m$ and $m > \ell$), the correct solution being selected by inspection of the table of results.

It is convenient to refer to the larger of the two variables (ℓ and m) as the main variable and the smaller as the auxiliary variable.

The programme proceeds as follows:
A value is selected for the main variable (the argument of the Bessel functions) in the range $0 \rightarrow 1$ and the Bessel functions $J_0(\ell)$, $J_1(\ell)$, $I_0(m)$, $I_1(m)$ are calculated from the appropriate series expansions, neglecting terms of greater than seventh order. The ratios $\frac{J_1}{J_0}$ and $\frac{I_1}{I_0}$ are then printed out.

The various derivatives appearing in the series expansions for $\beta \frac{J_1(\beta)}{J_0(\beta)}$ are functions of the main variable and these ratios of Bessel functions and they can therefore be calculated.

A value for the auxialiary variable is then selected in the range $0 \rightarrow 0.2$ and $\beta \frac{J_1(\beta)}{J_0(\beta)}$ computed using both forms of the series expansion. The corresponding values of admittance given by equation 6.2.6. are then calculated and printed out. This process is repeated for all the required values of the main and auxiliary variables.

Since the constants associated with the dimensions of the discharge tube and waveguide mount appear only in this last stage of the calculation (the calculation of admittance from equation 6.2.6.) the programme could be easily modified to take into account different discharge tube dimensions.

The results are given below in the form of a table with five columns and a number of sections. The first column in each section is headed by the value of the main variable used in that section, followed by the values of the auxiliary variable. The conductance and susceptance calculated from the expansion in terms of $\frac{J_1(\ell)}{J_0(\ell)}$ are given in the next two columns, while the results obtained using the expansion in terms of $\frac{I_1(m)}{I_0(m)}$ are given in the fourth and fifth columns. In addition the appropriate values of $\frac{J_1(\ell)}{J_0(\ell)}$ and $\frac{I_1(m)}{I_0(m)}$ are printed at the top of each section.

Normally $m > \ell$, so for values of the main variable greater than 0.2 the results given in the last two columns will apply.

Although several improvements could be made to the programme they have not been included as the results computed by this method have proved sufficient for the present problem.

GAS DISCHARGE FORMULA WITH BESSEL FUNCTIONS OF COMPLEX ARGUMENT

l, m / m, l	$\frac{J_1(l)}{J_0(l)}$	$\frac{I_1(m)}{I_0(m)}$		
+0.010	+0.005000	+0.005000		
+0.000	+0.000000	-0.102661	+0.000000	-0.103023
+0.050	+0.001805	-0.107270	+0.001813	-0.098496
+0.100	+0.003588	-0.121039	+0.003649	-0.084860
+0.150	+0.005325	-0.143795	+0.005531	-0.061939
+0.200	+0.006996	-0.175254	+0.007485	-0.029441
+0.020	+0.010001	+0.009999		
+0.000	+0.000000	-0.102118	+0.000000	-0.103565
+0.050	+0.003612	-0.106820	+0.003625	-0.099042
+0.100	+0.007177	-0.120864	+0.007295	-0.085416
+0.150	+0.010650	-0.144074	+0.011059	-0.062514
+0.200	+0.013989	-0.176156	+0.014966	-0.030041
+0.030	+0.015002	+0.014998		
+0.000	+0.000000	-0.101213	+0.000000	-0.104470
+0.050	+0.005420	-0.106009	+0.005435	-0.099952
+0.100	+0.010769	-0.120333	+0.010938	-0.086343
+0.150	+0.015978	-0.144003	+0.016581	-0.063470
+0.200	+0.020983	-0.176718	+0.022438	-0.031040
+0.040	+0.020004	+0.019996		
+0.000	+0.000000	-0.099945	+0.000000	-0.105735
+0.050	+0.007230	-0.104836	+0.007242	-0.101225
+0.100	+0.014365	-0.119445	+0.014576	-0.087640
+0.150	+0.021311	-0.143582	+0.022095	-0.064809
+0.200	+0.027980	-0.176939	+0.029899	-0.032438
+0.050	+0.025008	+0.024992		
+0.000	+0.000000	-0.098314	+0.000000	-0.107360
+0.050	+0.009044	-0.103302	+0.009046	-0.102861
+0.100	+0.017967	-0.118200	+0.018206	-0.089307
+0.150	+0.026651	-0.142812	+0.027597	-0.066528
+0.200	+0.034985	-0.176819	+0.037344	-0.034234
+0.060	+0.030014	+0.029987		
+0.000	+0.000000	-0.096319	+0.000000	-0.109345
+0.050	+0.010863	-0.101406	+0.010845	-0.104858
+0.100	+0.021578	-0.116597	+0.021826	-0.091343
+0.150	+0.032002	-0.141691	+0.033085	-0.068628
+0.200	+0.042000	-0.176360	+0.044770	-0.036427

+0.070	+0.035021	+0.034979		
+0.000	+0.000000	-0.093959	+0.000000	-0.111689
+0.050	+0.012687	-0.099146	+0.012638	-0.107217
+0.100	+0.025199	-0.114635	+0.025436	-0.093745
+0.150	+0.037366	-0.140220	+0.038556	-0.071107
+0.200	+0.049030	-0.175560	+0.052171	-0.039016
+0.080	+0.040032	+0.039968		
+0.000	+0.000000	-0.091232	+0.000000	-0.114389
+0.050	+0.014517	-0.096521	+0.014426	-0.109934
+0.100	+0.028831	-0.112314	+0.029033	-0.096515
+0.150	+0.042746	-0.138398	+0.044007	-0.073964
+0.200	+0.056077	-0.174420	+0.059546	-0.041999
+0.090	+0.045046	+0.044954		
+0.000	+0.000000	-0.088138	+0.000000	-0.117446
+0.050	+0.016355	-0.093530	+0.016206	-0.113011
+0.100	+0.032478	-0.109633	+0.032615	-0.099649
+0.150	+0.048144	-0.136223	+0.049435	-0.077196
+0.200	+0.063145	-0.172938	+0.066888	-0.045375
+0.100	+0.050063	+0.049938		
+0.000	+0.000000	-0.084674	+0.000000	-0.120858
+0.050	+0.018201	-0.090172	+0.017978	-0.116443
+0.100	+0.036140	-0.106589	+0.036180	-0.103146
+0.150	+0.053564	-0.133695	+0.054838	-0.080803
+0.200	+0.070237	-0.171114	+0.074196	-0.049141
+0.120	+0.060108	+0.059892		
+0.000	+0.000000	-0.076632	+0.000000	-0.128737
+0.050	+0.021921	-0.082347	+0.021494	-0.124372
+0.100	+0.043518	-0.099410	+0.043255	-0.111223
+0.150	+0.064478	-0.127574	+0.065557	-0.089133
+0.200	+0.084511	-0.166438	+0.088691	-0.057835
+0.140	+0.070172	+0.069829		
+0.000	+0.000000	-0.067088	+0.000000	-0.138012
+0.050	+0.025685	-0.073029	+0.024967	-0.133704
+0.100	+0.050981	-0.090762	+0.050243	-0.120728
+0.150	+0.075511	-0.120024	+0.076143	-0.098934
+0.200	+0.098926	-0.160383	+0.103002	-0.068063
+0.160	+0.080257	+0.079745		
+0.000	+0.000000	-0.056024	+0.000000	-0.148664
+0.050	+0.029502	-0.062199	+0.028392	-0.144421
+0.100	+0.058545	-0.080629	+0.057131	-0.131643
+0.150	+0.086685	-0.111029	+0.086575	-0.110186
+0.200	+0.113512	-0.152939	+0.117100	-0.079802

+0.180	+0.090366	+0.089637		
+0.000	+0.000000	-0.043417	+0.000000	-0.160672
+0.050	+0.033380	-0.049836	+0.031761	-0.156502
+0.100	+0.066227	-0.068990	+0.063907	-0.143946
+0.150	+0.098025	-0.100574	+0.096833	-0.122865
+0.200	+0.128299	-0.144092	+0.130958	-0.093024
+0.200	+0.100503	+0.099503		
+0.000	+0.000000	-0.029239	+0.000000	-0.174013
+0.050	+0.037328	-0.035912	+0.035068	-0.169923
+0.100	+0.074043	-0.055821	+0.070557	-0.157611
+0.150	+0.109555	-0.088637	+0.106900	-0.136944
+0.200	+0.143318	-0.133827	+0.144551	-0.107700
+0.220	+0.110671	+0.109340		
+0.000	+0.000000	-0.013461	+0.000000	-0.188662
+0.050	+0.041354	-0.020400	+0.038308	-0.184659
+0.100	+0.082011	-0.041096	+0.077071	-0.172611
+0.150	+0.121300	-0.075195	+0.116756	-0.152393
+0.200	+0.158603	-0.122125	+0.157853	-0.123798
+0.240	+0.120872	+0.119144		
+0.000	+0.000000	+0.003950	+0.000000	-0.204590
+0.050	+0.045469	-0.003266	+0.041476	-0.200681
+0.100	+0.090150	-0.024784	+0.083438	-0.188917
+0.150	+0.133288	-0.060222	+0.126386	-0.169182
+0.200	+0.174186	-0.108964	+0.170843	-0.141283
+0.260	+0.131111	+0.128914		
+0.000	+0.000000	+0.023033	+0.000000	-0.221767
+0.050	+0.049682	+0.015527	+0.044566	-0.217959
+0.100	+0.098479	-0.006851	+0.089647	-0.206497
+0.150	+0.145546	-0.043689	+0.135773	-0.187276
+0.200	+0.190104	-0.094321	+0.183499	-0.160118
+0.280	+0.141390	+0.138646		
+0.000	+0.000000	+0.043829	+0.000000	-0.240163
+0.050	+0.054003	+0.036019	+0.047573	-0.236460
+0.100	+0.107020	+0.012740	+0.095689	-0.225318
+0.150	+0.158104	-0.025562	+0.144904	-0.206640
+0.200	+0.206392	-0.078168	+0.195801	-0.180262
+0.300	+0.151713	+0.148337		
+0.000	+0.000000	+0.066385	+0.000000	-0.259742
+0.050	+0.058445	+0.058256	+0.050494	-0.256150
+0.100	+0.115792	+0.034032	+0.101555	-0.245343
+0.150	+0.170993	-0.005804	+0.153764	-0.227234
+0.200	+0.223091	-0.060476	+0.207731	-0.201675

+0.320	+0.162084	+0.157986		
+0.000	+0.000000	+0.090751	+0.000000	-0.280470
+0.050	+0.063019	+0.082286	+0.053324	-0.276993
+0.100	+0.124821	+0.057070	+0.107237	-0.266535
+0.150	+0.184247	+0.015625	+0.162343	-0.249019
+0.200	+0.240241	-0.041210	+0.219273	-0.224311
+0.340	+0.172505	+0.167590		
+0.000	+0.000000	+0.116983	+0.000000	-0.302311
+0.050	+0.067737	+0.108166	+0.056060	-0.298953
+0.100	+0.134130	+0.081906	+0.112728	-0.288857
+0.150	+0.197900	+0.038769	+0.170629	-0.271953
+0.200	+0.257887	-0.020335	+0.230412	-0.248127
+0.360	+0.182980	+0.177146		
+0.000	+0.000000	+0.145143	+0.000000	-0.325224
+0.050	+0.072613	+0.135953	+0.058698	-0.321990
+0.100	+0.143746	+0.108593	+0.118023	-0.312266
+0.150	+0.211990	+0.063678	+0.178613	-0.295995
+0.200	+0.276074	+0.002190	+0.241137	-0.273076
+0.380	+0.193514	+0.186651		
+0.000	+0.000000	+0.175296	+0.000000	-0.349173
+0.050	+0.077663	+0.165714	+0.061237	-0.346064
+0.100	+0.153697	+0.137194	+0.123114	-0.336723
+0.150	+0.226557	+0.090403	+0.186287	-0.321099
+0.200	+0.294853	+0.026409	+0.251435	-0.299109
+0.400	+0.204110	+0.196104		
+0.000	+0.000000	+0.207518	+0.000000	-0.374115
+0.050	+0.082901	+0.197520	+0.063673	-0.371136
+0.100	+0.164014	+0.167774	+0.127999	-0.362185
+0.150	+0.241645	+0.119004	+0.193643	-0.347221
+0.200	+0.314277	+0.052370	+0.261298	-0.326178
+0.450	+0.230894	+0.219490		
+0.000	+0.000000	+0.297656	+0.000000	-0.440549
+0.050	+0.096937	+0.286507	+0.069304	-0.437900
+0.100	+0.191628	+0.253369	+0.139280	-0.429949
+0.150	+0.281956	+0.199138	+0.210612	-0.416678
+0.200	+0.366043	+0.125241	+0.284009	-0.398058
+0.500	+0.258153	+0.242500		
+0.000	+0.000000	+0.402687	+0.000000	-0.512277
+0.050	+0.112571	+0.390196	+0.074264	-0.509965
+0.100	+0.222334	+0.353108	+0.149206	-0.503033
+0.150	+0.326655	+0.292542	+0.225512	-0.491481
+0.200	+0.423227	+0.210267	+0.303892	-0.475318

+0.550	+0.285951	+0.265100		
+0.000	+0.000000	+0.524414	+0.000000	-0.588627
+0.050	+0.130187	+0.510340	+0.078549	-0.586652
+0.100	+0.256867	+0.468603	+0.157767	-0.580735
+0.150	+0.376770	+0.400612	+0.238333	-0.570896
+0.200	+0.487074	+0.308577	+0.320941	-0.557173
+0.600	+0.314363	+0.287263		
+0.000	+0.000000	+0.665077	+0.000000	-0.668930
+0.050	+0.150269	+0.649114	+0.082166	-0.667285
+0.100	+0.296150	+0.601843	+0.164981	-0.662361
+0.150	+0.433586	+0.525052	+0.249104	-0.654196
+0.200	+0.559124	+0.421530	+0.335205	-0.642854
+0.650	+0.343467	+0.308963		
+0.000	+0.000000	+0.827476	+0.000000	-0.752527
+0.050	+0.173437	+0.809230	+0.085134	-0.751199
+0.100	+0.341364	+0.755286	+0.170888	-0.747233
+0.150	+0.498728	+0.667944	+0.257891	-0.740678
+0.200	+0.641309	+0.550752	+0.346778	-0.731619
+0.700	+0.373349	+0.330177		
+0.000	+0.000000	+1.015133	+0.000000	-0.838784
+0.050	+0.200502	+0.994088	+0.087481	-0.837758
+0.100	+0.394041	+0.931991	+0.175547	-0.834700
+0.150	+0.574291	+0.831832	+0.264787	-0.829669
+0.200	+0.736086	+0.698184	+0.355796	-0.822766
+0.750	+0.404104	+0.350887		
+0.000	+0.000000	+1.232525	+0.000000	-0.927098
+0.050	+0.232540	+1.207995	+0.089243	-0.926355
+0.100	+0.456200	+1.135785	+0.179030	-0.924146
+0.150	+0.663009	+1.019842	+0.269906	-0.920539
+0.200	+0.846623	+0.866132	+0.362421	-0.915643
+0.800	+0.435835	+0.371075		
+0.000	+0.000000	+1.485410	+0.000000	-1.016907
+0.050	+0.271004	+1.456466	+0.090462	-1.016425
+0.100	+0.530556	+1.371502	+0.181422	-1.015000
+0.150	+0.768513	+1.235819	+0.273380	-1.012702
+0.200	+0.977066	+1.057321	+0.366835	-1.009651
+0.850	+0.468660	+0.390729		
+0.000	+0.000000	+1.781302	+0.000000	-1.107689
+0.050	+0.317905	+1.746659	+0.091182	-1.107444
+0.100	+0.620823	+1.645312	+0.182815	-1.106733
+0.150	+0.895710	+1.484520	+0.275350	-1.105627
+0.200	+1.132912	+1.274937	+0.369235	-1.104248

+0.900	+0.502709	+0.409837		
+0.000	+0.000000	+2.130181	+0.000000	-1.198969
+0.050	+0.376082	+2.088016	+0.091450	-1.198938
+0.100	+0.732201	+1.965176	+0.183303	-1.198869
+0.150	+1.051349	+1.771837	+0.275962	-1.198833
+0.200	+1.321566	+1.522646	+0.369824	-1.198950
+0.950	+0.538127	+0.428392		
+0.000	+0.000000	+2.545570	+0.000000	-1.290319
+0.050	+0.449655	+2.493220	+0.091314	-1.290478
+0.100	+0.872138	+2.341501	+0.182984	-1.290979
+0.150	+1.244911	+2.105073	+0.275364	-1.291891
+0.200	+1.553157	+1.804525	+0.368803	-1.293332
+1.000	+0.575080	+0.446389		
+0.000	+0.000000	+3.046243	+0.000000	-1.381358
+0.050	+0.544789	+2.979688	+0.090821	-1.381684
+0.100	+1.051598	+2.788079	+0.181953	-1.382685
+0.150	+1.490001	+2.493224	+0.273702	-1.384427
+0.200	+1.841760	+2.124814	+0.366371	-1.387023

AUTOCODE PROGRAMME TAPE

GAS DISCHARGE FORMULA WITH BESSEL FUNCTIONS OF COMPLEX ARGUMENT

```
J1.0

0)STOP
n1=1
n2=0
n3=0
n20=TAPEB5
v4=TAPEB3
1)v1=n1
v2=n2
v3=n3
v2=v1+v2
v3=v2+v3
v9=v3/100
v10=v9/2
v100=v10Xv10
v101=v100Xv10
v102=v100Xv100
v103=v100Xv101
v104=v101Xv101
v105=v101Xv102
v106=v102Xv102
v107=v102/4
v108=v104/36
v109=v106/576
v110=1-v100
v111=v110+v107
v112=v111-v108
v113=v112+v109
v114=1+v100
v115=v114+v107
v116=v115+v108
v117=v116+v109
v120=v101/2
v121=v103/12
v122=v105/144
v123=v10-v120
v124=v123+v121
v125=v124-v122
v126=v10+v120
v127=v126+v121
v128=v127+v122
Xv11=v125/v113
Xv130=v128/v117
PRINTv9,3083
PRINTv11,4186
PRINTv130,4386
Xv12=v11Xv11
v13=v12Xv11
v14=v12Xv12
v15=v12Xv13
v16=v12X3
v17=v14X3
v18=v14X36
v20=1+v12
v21=1-v12
v22=1+v16
v23=1+v17
v24=v11+v11
```

```
n4=0
2)v70=n4/100
PRINTv70,3143
v71=v70Xv70
v72=v71/2
v73=v70Xv71
v74=v73/6
v75=v71Xv71
v76=v75/24
v80=v72Xv35
v81=v76Xv66
v82=v32+v81
v83=v82-v80
v85=v70Xv33
v86=v74Xv47
v87=v85-v86
v172=v171Xv72
v184=v172-v170
v177=v176Xv76
v185=v184-v177
v179=v70Xv180
v178=v74Xv183
v186=v179+v178
v187=v83-v6
v188=v187Xv187
v189=v87Xv87
v190=v188+v189
v191=v187/v190
v192=v87/v190
v191=v4Xv191
v192=v4Xv192
v191=v191-v5
v193=v191Xv191
v194=v192Xv192
v195=v193+v194
v196=v191/v195
v197=v192/v195
PRINTv197,4126
PRINTv196,4086
v200=v185-v6
v201=v200Xv200
v202=v186Xv186
v203=v201+v202
v204=v200/v203
v205=v186/v203
v204=v4Xv204
v205=v4Xv205
v204=v204-v5
v206=v204Xv204
v207=v205Xv205
v208=v206+v207
v209=v204/v208
v210=v205/v208
PRINTv210,4126
PRINTv209,4086
n4=n4+n23
>2,n24≥n4

n1=n1+1
>1,n20≥n1
n1=n20
n2=n2+2
>1,n21≥n2
n2=n21
n3=n3+5
>1,n22≥n3

(>0)

*************

DATA TAPE

+10
+30
+60
+5
+20
+0.267333
+0.16034
+0.027954

*************
```

$v150=v130 \times v130$
$v151=v150 \times v130$
$v152=v150 \times v150$
$v153=v150 \times v151$
$v154=v150 \times 3$
$v155=v152 \times 3$
$v156=v152 \times 36$
$v160=1+v150$
$v161=1-v150$
$v162=1+v154$
$v163=1-v154$
$v164=1+v155$
$v165=v130+v130$
$v25=v24 \times v22$
$v26=v12 \times 28$
$v30=1/v9$
$v31=v30 \times v30$
$v32=v9 \times v11$
$v33=v9 \times v20$
$v34=v33+v33$
$v35=v21+v34$
$v40=v9 \times 2$
$v41=v40 \times v23$
$v42=v41-v25$
$v43=v9 \times 8$
$v44=v30+v30$
$v45=v43+v44$
$v46=v45 \times v12$
$v47=v46+v42$
$v50=v9 \times 16$
$v51=v30 \times 6$
$v52=v50+v51$
$v53=v52 \times v11$
$v54=v51 \times v30$
$v55=v54 \times v12$
$v56=v9 \times 40$
$v57=v30 \times 22$
$v58=v56+v57$
$v59=v58 \times v13$
$v60=v9 \times 24$
$v61=v60 \times v15$
$v62=v53-v26$
$v63=v62-v55$
$v64=v63+v59$
$v65=v64-v18$
$v66=v65+v61$
$v170=v130 \times v9$
$v171=v165 \times v161$
$v171=v171 \times v9$
$v171=v160-v171$
$v173=v50-v51$
$v173=v173 \times v130$
$v174=28-v54$
$v174=v174 \times v150$
$v175=v56-v57$
$v175=v175 \times v151$
$v176=v60 \times v153$
$v176=v176+v156$
$v176=v176-v175$
$v176=v176-v174$
$v176=v176+v173$
$v180=v161 \times v9$
$v181=v43-v44$
$v181=v181 \times v150$
$v182=v165 \times v163$
$v183=v164 \times v40$
$v183=v183-v182$
$v183=v183-v181$